Investigations on ECG Signals for Deriving Respiratory Signal and Sleep Apnea Detection

Doctoral Thesis

Submitted By

Hemant Sharma
Research Scholar
(College ID-2013REC9056)

Under Supervision of

Prof. Kamalesh Kumar Sharma
Dept. of ECE, MNIT, Jaipur

Department of Electronics & Communication Engineering
Malaviya National Institute of Technology, Jaipur, India
June 2017

Dedicated to My Parents and Wife

DECLARATION

I, **Hemant Sharma** declare that this thesis titled **"Investigations on ECG Signals for Deriving Respiratory Signal and Sleep Apnea Detection"** and the work presented in it is my own. The work has been carried out under the supervision of **Prof. Kamalesh Kumar Sharma**. I confirm that:

1. This work was done wholly or mainly while in candidature for a Ph.D. degree at MNIT Jaipur.
2. Where any part of this thesis has previously been submitted for a degree or any other qualification at MNIT Jaipur or any other institution, this has been clearly stated.
3. Where I have consulted the published work of others, this is clearly attributed.
4. Where I have quoted from the works of others, the source is always given. With the exception of such quotations, this thesis is entirely my own work.
5. I have acknowledged all main sources of help.
6. Where the thesis is based on work done by myself, jointly with others, I have made clear exactly what was done by others and what I have contributed myself.

Hemant Sharma
(2013REC9056)

ACKNOWLEDGEMENTS

There can't be any knowledge without a teacher, there won't be any salvation without a teacher, there won't be any realization of truth without a teacher, and there won't be any removal of flaws without a teacher. I was fortunate to be blessed with a shower of knowledge from my supervisor.

I would like to express my deep sense of gratitude to my supervisor, **Prof. Kamalesh Kumar Sharma** for his continuous and all way support and guidance in my research work. My sincere thanks to Prof. D. Boolchandani, DPGC Convenor, Department of Electronic & Communication Engineering, for providing facilities and encouragement to complete my research work.

I express my gratitude to DREC members, Dr. Mohammed Salim, Dr. Ghanshyam Singh, and Dr. Satyasai Jagannath Nanda for their constructive feedback in critically examining and reviewing my work. Further, I would like to acknowledge Dr. Om Lata Bhagat, All India Institute of Medical Sciences (AIIMS) Jodhpur, for inspiring me to investigate the ECG signals for the respiration monitoring. I also extend my deep sense of gratitude to Prof. Udaykumar R Yaragatti, Director, MNIT, Jaipur for strengthening the research environment of the institute by providing all necessary facilities to the research scholar.

Further, I would like to thank my colleagues Dinesh Saini, Dr. Shashikant Sharma, Shailendra Tripathi, Tangudu Bharat Kumar, and Abhijeet Sharma for the valuable feedbacks, technical discussions related to my research work during the duration of the engagement.

My heartiest gratitude to my parents for their consistent encouragement, moral support, and blessings during this period. I appreciate their patience with me during this period. I am grateful to my wife, Amita Sharma, for her endless support and understanding. I am also thankful to my niece Manvi (Guddan) for her cheerful company during this time.

Last but not the least I would like to thank God, the Almighty, for having made everything possible by giving me strength and courage to do this successfully.

(Hemant Sharma)

ABSTRACT

The functioning of the human heart is affected by several health problems including breathing disorders, cardiovascular problem, neurological disorders and other physiological conditions. The occurrences of these health complications disturb the electrical activities of the heart. As a consequence, any disturbance in the cardiac activities due to the health complications is reflected in the recorded electrocardiogram (ECG) signal of the patient. Thus, tracking beat-to-beat variations in the ECG characteristics can be used for the purpose of diagnosis of diseases. Therefore, several health-related problems can be detected by investigating the ECG signal alone. Respiration is one of the important physiological events in the patient which needs to be investigated to evaluate the patient deterioration. Adequate knowledge of the respiration can also benefit from the detection of sleep apnea which is a breathing disorder characterized by the repetitive events of complete or partial cessation of airflow due to the physical collapse of the upper airway of the patient. Conventional equipment for the respiration measurement and detection of sleep apnea problem consist of many limitations while using them for long-term monitoring and are not feasible to use in the home-based health monitoring devices. It is a well-known fact that the respiratory process yields changes in the characteristics of the ECG signal. Therefore, researchers are focused on investigating the ECG signal for deriving the respiratory signal and detection of sleep apnea problem in the patient. The use of the ECG-derived respiration (EDR) techniques reduces the need for an extra sensor for the respiration measurement. Similarly, detection of sleep apnea problem in the patient using the ECG signal reduces the need for specialized sleep laboratories for the apnea diagnosis. Thus, the use of the ECG signal for the estimation of respiration and detection of sleep apnea can benefit in the development of cost-effective home-based portable devices for routinely health monitoring of the patient.

The work in the thesis is mainly devoted to the development of efficient techniques for deriving the respiratory signal and detection of sleep apnea problem in the patient using single-lead ECG. The presence of BW noise in the ECG signal possesses serious challenge to the processing of such signals. Therefore, the development of an effective approach for the removal of BW from the ECG signal is also considered as a part of the research work.

In the present research work, first, an algorithm based on the Hilbert Vibration Decomposition (HVD) for the removal of BW from the ECG signal is presented. The HVD technique decomposes the non-stationary wideband signals into a sum of components with slowly varying amplitudes and frequencies, where the first component of decomposition represents the highest instantaneous amplitude component. In this work, it is proposed that

the first component (highest energy component) obtained using the HVD of the ECG signal corresponds to the BW signal in it. The performance of the proposed BW removal technique is evaluated using the correlation criterion and the signal-to-noise ratio. The simulations are performed using artificial BWs of different amplitudes added in the ECG recordings of the *MIT-BIH arrhythmia* database. Results demonstrated that the proposed technique for BW removal provided improved performance than the empirical mode decomposition with mathematical morphology (EMD-MM) technique. It is also observed that the proposed method for BW removal is computationally efficient and performs better under the condition of severe baseline distortion without affecting the actual morphology of the ECG signal.

The next aim of the thesis was focused on deriving the respiratory signal from single-lead ECG. For this purpose, two new EDR techniques are proposed here for a reliable estimation of the respiratory signal using single-lead ECG. The first EDR approach is based on the homomorphic filtering of the ECG signal. The proposed EDR technique mainly relies on the assumption that the ECG signal is generated from the convolution of the electrical activities of the heart and the transfer function of a linear time-invariant (LTI) system which is influenced by the respiratory process. The homomorphic filtering approach is used to deconvolve the components of the respiration and the heart activities. After that, the respiratory signal is obtained by the band-pass filtering of the cepstrum of ECG signal. The experiments are performed over the *Fantasia* dataset. The performance of the proposed EDR algorithms is assessed using the correlation coefficient, the magnitude squared coherence coefficient, and agreement in the respiratory rates computed from the derived and reference (recorded) respiratory signals. The performance results of the proposed EDR techniques are compared with the state-of-art methods based on the R-peak amplitude (RPA), respiratory sinus arrhythmia (RSA), and principal component analysis (PCA). Results confirm that the performance of the homomorphic filtering based EDR approach is observed to be better than the RPA and RSA methods, but significant improvements are not observed when compared with the PCA-based technique.

On the other hand, the second EDR approach is based on the decomposition of each QRS complex of ECG signal using the Hermite basis functions. We hypothesize that the respiration, which is a quasi-periodic signal, affects the energy in the QRS complexes and the distribution of energy along each component in the orthogonal signal expansion based on the Hermite basis functions of ECG signal also. Beat-to-beat variation in the QRS complexes of ECG signal caused by the respiration is monitored by computing the energy and the standard deviation of the Hermite coefficients for the estimation of the respiratory signal. The performance of the proposed EDR technique is evaluated over the entire *Fantasia* dataset. It is seen from the experimental results that the Hermite decomposition based EDR approach is observed to be outperforming the existing methods based on RSA, RPA, PCA, and homomorphic filtering. Upon investigating the young and elderly subjects

separately, the Hermite decomposition based EDR approach provided improved results than the PCA, and RPA methods for the young subjects, but outperformed the state-of-art methods for the elderly subjects. Experimental results confirm that the proposed EDR techniques can be utilized for continuous monitoring of the respiration using single-lead ECG.

The research work is extended to the detection of sleep apnea problem in the patient using single-lead ECG. For this purpose, two new techniques are proposed here to investigate the ECG recordings of different subjects to decide whether the recording belongs to the apnea category or the normal one. The first technique is based on the decomposition of each QRS complex of ECG signal in terms of the Hermite basis functions for the detection of sleep apnea. In the proposed technique, the coefficients of the Hermite expansion along with three features based on R–R time series (mean of R–R intervals, the standard deviation of R–R intervals) and energy in the error of the QRS approximation are used to discriminate the apnea and normal segments.The performance of the proposed sleep apnea detection technique is assessed over the *Apnea-ECG* dataset. The experimental results show that the proposed methodology provided effective performance which is comparable with the methods existing in the literature at reduced computational cost due to the lesser number of features selected for the classification.

The second approach for sleep apnea detection is based on the features extracted from the heart rate variability (HRV) and EDR signals. Here, the EDR signal used for the feature extraction is obtained using the EDR approach based on the Hermite basis functions. A number of time and frequency domain features are extracted from the HRV and EDR signals on the minute-by-minute basis. These features are then used as input to the classifiers for the classification of apnea and normal recordings. Upon investigating the performance of the proposed technique over the *Apnea*-ECG dataset, the independent test results show that all recording of the withheld (independent) set are successfully classified in the apnea and normal categories using the least-square support vector machine (LS-SVM) model. Upon examining the performance results, it is seen that the proposed approach based on the HRV and EDR signals for apnea detection provided better performance than the existing techniques in the literature. The performance results confirm that the proposed techniques can be utilized for detection of sleep apnea problem in the patient.

In summary, this thesis investigates single-lead ECG signal to develop efficient techniques for the removal of BW from ECG, EDR extraction and detection of the sleep apnea problem in the patient using single-lead ECG signal. In this thesis, we demonstrate the usability of the HVD technique for the removal of BW noise from ECG and the homomorphic filtering for estimating the respiration from ECG signal. The research work also emphasizes the

usefulness of the Hermite basis functions to single-lead ECG for a reliable estimation of the respiratory signal and sleep apnea detection. The simulation results confirm that the proposed techniques can be effectively applied for BW removal of ECG, respiration estimation, and sleep apnea detection using single-lead ECG.

CONTENTS

LIST OF FIGURES

LIST OF TABLES

LIST OF SYMBOLS

The symbols used in the text have been defined at appropriate places, however for easy reference, the list of principle symbols is given below.

Symbol	Explanation
g, s	Real-valued signal
x	ECG signal
A	Analytic signal representation
$\tilde{g}$	Hilbert transform of real-valued signal
a_k	Envelope of k^{th} component of HVD
ω	Instantaneous frequency
θ	Instantaneous phase
x'	Baseline corrected ECG
γ	Correlation Criterion
SNR	Signal-to-noise ratio
μ	Mean
$\otimes$	Convolution
$D(.)$	Characteristic function of homomorphic filtering
$D^{-1}(.)$	Inverse characteristic function of homomorphic filtering
$\hat{s}$	Complex Cepstrum
b	Scalar
C_{xy}	Magnitude squared coherence coefficient
C	Correlation coefficient
MAE	Mean absolute error
PE	Average percentage error
ρ_c	Concordance correlation coefficient
bpm_{EDR}	Respiratory rate of EDR signal
bpm_{ref}	Respiratory rate of reference (recorded) respiration
$\phi_{n,\sigma}$	n^{th} order Hermite basis function

c	Coefficient of Hermite expansion
H_n	n^{th} order Hermite polynomial
σ	Scaling parameter of Hermite basis functions
N	Total number of lower order Hermite basis functions
e_σ	Hermite expansion error
δ	Dirac delta function
xq	QRS complex of an ECG signal
λ	Standard deviation value of the N Hermite coefficients c
E	Energy value of the N Hermite coefficients c
ψ	Mean coefficient vector
E_e	Average value of energy of the Hermite expansion error e_σ
mRR	Mean of R-R intervals
sRR	Standard deviation of R-R intervals
Sn	Sensitivity of the classification
Sp	Specificity of the classification
Ac	Accuracy of the classification
AUC	Area under receiver operation characteristic curve
TP	True positive
FP	False positive
TN	True negative
FN	False negative
VD_j	Variance of the detailed coefficients at j^{th} level of the wavelet decomposition
KD_j	Kurtosis of the detailed coefficients at j^{th} level of the wavelet decomposition
f_{val}	Feature
υ	Standard deviation of the feature
R_{DFT}	EDR signal using Homomorphic filtering with DFT
R_{DCT}	EDR signal using Homomorphic filtering with DCT
R_{RSA}	EDR signal using RSA method
R_{Ramp}	EDR signal using RPA method

R_{PCA}	EDR signal using PCA technique
R_{HDSD}	EDR Estimated using Standard Deviation of Hermite Coefficients
R_{HDE}	EDR Estimated using Energy of Hermite Coefficients
R_{ref}	Reference (recorded) respiratory signal
R_{EDR}	EDR Signal

LIST OF ABBREVIATIONS

The abbreviations used in the text have been defined at appropriate places, however, for easy reference; the list of abbreviations is given below.

Abbreviation	Explanation
ECG	Electrocardiogram
EDR	ECG-Derived Respiration
PSG	Polysomnography
EEG	Electroencephalogram
EOG	Electrooculogram
EMG	Electromyogram
HRV	Heart Rate Variability
RSA	Respiratory Sinus Arrhythmia
OSAS	Obstructive Sleep Apnea Syndrome
BW	Baseline Wander
EMD	Empirical Mode Decomposition
IMF	Intrinsic Mode Function
DWT	Discrete Wavelet Transform
PCA	Principal Component Analysis
KPCA	Kernel Principal Component Analysis
RPA	R-Peak Amplitude
HVD	Hilbert Vibration Decomposition
CVS	Cardiovascular System
SA	Sinoatrial Node
AV	Atrioventricular
CNS	Central Nervous System
ANS	Autonomic Nervous System
ULF	Ultra Low Frequency
VLF	Very Low Frequency
LF	Low Frequency
HF	High Frequency
AHI	Apnea-Hypopnea Index
IF	Instantaneous Frequency

SNR	Signal to Noise Ratio
EMD-MM	Empirical Mode Decomposition – Mathematical Morphology
LTI	Linear Time Invariant
DFT	Discrete Fourier Transform
IDFT	Inverse Discrete Fourier Transform
DCT	Discrete Cosine Transform
IDCT	Inverse Discrete Cosine Transform
FIR	Finite Impulse Response
FFT	Fast Fourier Transform
MAE	Mean Absolute Error
PE	Average Percentage Error
BPM	Breaths Per Minute
HD	Hermite Decomposition
SSE	Summed Square Error
SVM	Support Vector Machine
LS-SVM	Least Square Support Vector Machine
KNN	K Nearest Neighbors
MLPNN	Multilayer Perceptron Neural Network
ROC	Receiver Operating Characteristic
RBF	Radial Basis Function
R_{ref}	Reference (Recorded) Respiratory Signal
R_{RSA}	EDR using RSA Method
R_{Ramp}	EDR using RPA Method
R_{PCA}	EDR using PCA Technique
R_{DFT}	EDR using Homomorphic Filtering with DFT
R_{DCT}	EDR using Homomorphic Filtering with DCT
R_{HDSD}	EDR Estimated using Standard Deviation of Hermite Coefficients
R_{HDE}	EDR Estimated using Energy of Hermite Coefficients

CHAPTER – 1

INTRODUCTION

The functioning of the human heart is affected by several health problems including breathing disorders, cardiovascular problem, neurological disorders and several other physiological issues. The symptoms of these health problems also affect electrical activities of the heart. These variations in the functioning of the heart are reflected in the recorded electrocardiogram (ECG) signal. As a result, monitoring the ECG characteristics provide useful information about several health problems. Therefore, many health-related problems can be detected by analysing the ECG signal alone.

Respiration is one of the important physiological events in the patient which needs to be investigated to evaluate the patient deterioration [1]. A reliable measurement of the respiration is essential for the diagnosis of cardiovascular as well as breathing related problems. In clinical practice, the use of the respiratory measures can be found for monitoring the sleep apnea, stress, acute respiratory dysfunction, cardiac arrhythmia and several other cardiovascular diseases [1-2]. The respiratory rate is one of the human vital marks to measure sickness and is also used in deciding the anaerobic point during the sports training [3-4]. For MRI scanning of the thorax and heart region, it advantageous to have knowledge of the respiratory rate for the synchronization and compensation of MRI scans [5]. In addition to that, the proper knowledge of the respiration can benefit in the postoperative care where simultaneous monitoring of the heart activities and the respiration of the patient is needed [6]. Therefore, a reliable measurement of the respiratory information is of great interest in the clinical evaluations.

In clinical practice, the respiration is acquired using some dedicated equipment such as the inductive plethysmograph, thermistor, transthoracic inductance, strain gauge, pneumatic respiration, pulse oximetry, and whole body plethysmography [7]. These respiration measurement techniques are further divided into two categories: direct methods and indirect methods. In the category of direct methods, a sensor device is directly integrated to the airway to measure some characteristics of the inhale and exhale air. For example, the thermistor and carbon dioxide sensors are employed at the airway to measure temperature changes and carbon dioxide level in the inhale and exhale air [8]. On the other hand, the indirect methods measure muscles motions, thoracic volume, and tissue movements to obtain the respiratory pattern. In this category, for example, the inductive plethysmograph contains the coils that are placed around the thorax and the abdomen, measures changes in

the coil impedance caused by movements in the chest as well as abdomen due to the respiration.

Both the direct and indirect methods have their advantages as well as disadvantages in the cases where long-term monitoring of the respiration is required such as sleep apnea screening and stress testing. Also, the availability of these kinds of equipment to the general population is also a matter of consideration. Therefore, researchers are focused towards acquiring the respiratory signal non-invasively using the ECG signals. It is exciting to specify that the respiration process changes the R-R intervals as well as the morphology of ECG signal. This leads to developing the concept of obtaining the respiratory signal by extracting the respiratory-induced changes in the ECG signal [7]. The respiratory signal derived from the ECG signal is called ECG-derived respiration (EDR). The idea of deriving the respiratory signal from ECG reduces the need for an extra sensor for the respiratory measurement. Consequently, the respiratory signal derived from ECG helps in reducing the cost and complexity of the home-based healthcare systems. Recently, the quality the respiration signals derived from the ECG and photoplethysmograph (PPG) signals is investigated in [160-161], and it is claimed that the ECG signal provides a better quality of the respiratory signal as compared to the PPG. Therefore, the ECG signal should be used for a reliable estimation of the respiratory signal. Many techniques have been developed to get the efficient estimation of the respiration using single-lead ECG. Nevertheless, further research work needs to be carried out to get a reliable estimation of the respiratory signal from single-lead ECG for the real-time applications.

Further, the problem of sleep apnea is associated with abnormalities in the breathing pattern of the patient. Sleep apnea is defined as the repetitive episodes of complete or partial pause in the airflow due to the physical collapse of the upper airway for the short duration of time during sleep [9]. Sleep apnea is a well-recognized and widespread problem in both men and women, specifically adults, causing medical morbidity and mortality [10]. In earlier studies, it is found that the recurrent episodes of sleep apnea cause several health consequences. If the apnea problem is untreated for a long duration, it leads to some serious cardiovascular and neurological disorders [10-11]. Hence the problem of sleep apnea needs to be detected at an early stage.

In clinical practice, a subject having apnea or hypopnea is diagnosed using the overnight polysomnography (PSG). In the PSG process, 16 different physiological signals, comprising ECG, electroencephalogram (EEG), respiration, electrooculogram (EOG), electromyogram (EMG), oxyhemoglobin saturation, are simultaneously acquired from the patient [10]. Next, the patterns of these 16 physiological recordings are studied, and the decision is made whether a suspect is to be considered in the apnea category or the normal one. Despite the

fact that the PSG method is a popular tool for the diagnosis of sleep apnea, it happens to be time-consuming, very expensive, and uncomfortable for the patients. To perform the PSG technique, a well-established sleep laboratory is required. Due to less availability of sleep laboratories, most of the population suffering from the apnea problem remains undiagnosed. Therefore, an alternate method for the apnea detection is required which can be implemented with a fewer number of physiological signal as possible and can be applied in the home-based health monitoring devices. Hence, researchers are focusing toward the use of the lesser number of physiological signals (such as ECG, oronasal airflow) as possible and analyse them using sophisticated signal processing techniques for the automated detection of apnea problem. Based on early results, it is proved that the occurrence of apnea episodes influences the Heart rate variability (HRV) characteristics as well as the morphology of ECG beats. These variations in the ECG signal due to the sleep apnea episodes allow us to use the ECG signal for apnea detection. Several methodologies have been proposed by the researchers to classify the apnea patients from the normal one using single-lead ECG signal. In spite of that, a lot more work needs to be done to get effective performance results for apnea detection for the real-time application.

In this thesis, the development of various efficient techniques for deriving the respiratory single (EDR) and detection of the sleep apnea problem in the patient using single-lead ECG recordings are attempted. In addition to that, the ECG recordings are affected by the low-frequency noises particularly the baseline wander (BW) caused by the muscle movements, variations in the electrode positions, and the respiratory process [90]. Hence, the removal of BW from the ECG signal is required for better analysis of ECG. The frequency of both the BW noise in ECG and the respiratory signal of a healthy person vary up to 0.5 Hz. Upon deriving the respiratory signal from the ECG signal which is influenced by BW noise, the part of BW noise is reflected in the EDR signal. To suppress the effect of BW noise in the EDR, the ECG signals need to be pre-processed for BW removal before analysing them for the respiration estimation and detection of the sleep apnea problem. Therefore, the development of an effective approach for BW removal from the ECG signal is also considered as a part of the research work.

1.1 MOTIVATION FOR THE PRESENT WORK

Evolution of the ECG signal processing techniques for various applications has enhanced the development of low-cost home-based healthcare equipment. This has subsequently providing effective automated diagnosis tools that resulted in reducing the valuation time as well as human efforts in the clinical practice. Therefore, much of the attention has been concentrated towards analysis of ECG signals for the diagnosis of diseases as well as

monitoring routinely health conditions. In this context, this thesis mainly investigates the ECG signal for a reliable estimation of the respiration and detection of sleep apnea problem in the patients. As the removal of BW noise in the ECG signal is essential prior to the EDR extraction, the research work is also focused on providing an efficient solution for BW removal of the ECG signal. The existing methods in the literature to investigate the ECG signal for addressing the problems as mentioned above have certain limitations in their practical implementation. In addition to that, the development of efficient algorithms to get improved performance than the existing approaches for the EDR extraction and sleep apnea detection using single-lead ECG motivates us for making more efforts in these areas. The subsequent paragraphs highlight the research gaps of the existing work related to BW removal, EDR extraction, and sleep apnea detection using single-lead ECG.

- Removal of the BW noise from ECG signal is desirable for better clinical interventions. Several techniques have been developed by the researchers for the removal of BW from the ECG signals. The existing methods for BW removal, however, possess certain limitations in practical implementation. Filtering of the ECG signal using a high pass filter (cut-off frequency 0.7 Hz) is a classical method to remove BW from the ECG [90]. This filtering also removes the overlapping low-frequency ECG components with the noise, and that affects the beat morphology (mainly ST-segments) [91]. Therefore, BW removal from ECG based on the high-pass filter can distort the waveform which can lead wrong interpretation of the ECG characteristics. Another method based on the cubic spline is also used for removal of the artifacts from ECG signal [92]. However, this approach primarily assumes that the PR interval of ECG beat is well-defined and its location is recognizable for normal beats [91]. But, this assumption may not be valid in the case of presence of other types of noises in the ECG signal such as muscles artifacts, electrode movements, etc. [96]. Recently, the empirical mode decomposition (EMD) method is found as a popular tool for the removal of BW from the ECG signal [89]. In the EMD technique, the higher-order intrinsic mode functions (IMFs) are filtered through a low-pass filter to estimate the BW noise of ECG signal [89]. However, in the EMD-based approach, the number of IMFs to be low-pass filtered to obtain the BW noise is selected by trial basis [89]. The EMD based technique for BW removal also requires effective filter design. As the computational cost of the EMD technique is higher, it is less suitable to process the long segments of data. Therefore, a technique needs to be developed which can be easily applied to process the ECG signal for BW removal at reduced computational cost.
- As discussed earlier, there are several direct and indirect methods available to measure the respiration in the clinical practice. These methods can be implemented for

continuous monitoring of the respiration, but shows some drawbacks in the cases where the long-time monitoring of the respiration is required such as sleep apnea detection and stress testing. Use of the direct methods for monitoring the respiration benefits of more accurate results, but is less comfortable for the patient in the circumstances of long-time monitoring. Also, in the case of direct methods, the measurement devices interfere with the natural breathing of the patient [13]. However, the indirect methods are less obtrusive for continuous measurements, but are very sensitive to the muscles and thoracic movements. Also, the aortic blood flow can also produce the similar variations caused by the respiration process [6], [14]. Due to these limitations of direct and indirect methods, considerable attention is being focused on the development of the respiration measurement techniques using single-lead ECG signals. Several methods have been proposed by the researchers to get a reliable estimation of the respiration using the ECG signal [15-29]. These EDR techniques are broadly classified into two categories: analysis of the beat morphology of ECG and RSA, and filtering of the ECG signal in the respiratory band. The existing EDR methods in the literature have many limitations. For example, as the age of subject increases, the effect of RSA is appear to be less. Hence, the EDR based on the RSA methods performs poorly upon analysing the elderly population [16]. In the filtering based EDR techniques, any variations in the respiration are not reflected in the shape of the EDR signal, and the derived signal in the output is obtained as a smooth waveform [24]. Other some complex EDR methods based on beat-morphology extract the changes in QRS area [4], or rotation in the electric axis caused by the respiration [23]. Recently, the principal component analysis (PCA) technique has been employed to evaluate respiratory-induced beat-to-beat fluctuation in the ECG signal [26-27]. Although, the use of the PCA as EDR technique is based on the assumption of linearity between the respiratory signal and the ECG signal [27], but this assumption may not always be true for a real-time analysis. Later, an improved algorithm based on the Kernel PCA (KPCA) for deriving the respiratory signal using single-lead ECG is presented [27]. However, it was claimed that the KPCA technique provided better results than the PCA and R-peak amplitude (RPA) methods, but it is less suitable for the long segments of data due to the higher computational cost [27]. These limitations of the existing approaches encourage the development of such an EDR technique which should be viable and provide higher resemblance between the recorded and derived respirations at reduced computational cost. Based on the literature, most of the morphological variations in the ECG signal are caused by the muscles movement and the respiration [47]. Though, the RPA method monitors beat-to-beat amplitude of the QRS complexes of ECG to extract the respiratory pattern. But, the use of the entire QRS complex morphology for the estimation of respiratory signal can benefit in terms of better

resemblance of the EDR with the actual respiration pattern. Therefore, in this thesis, the development of effective EDR technique is attempted.

- The problem of sleep apnea is diagnosed using the PSG technique. The PSG is a 'gold standard' tool for the diagnosis of apnea, but has certain limitations. Also, the PSG is performed in the sleep laboratory with proper nursing for whole night which makes this process non-feasible due to limited availability of sleep laboratories. As a result, most of the apnea population remain undiagnosed [10]. As substitutes of the PSG technique, several methods have been established for apnea detection using single-lead ECG [30-53]. Most of the apnea detection approaches in the literature are mainly based on the time and frequency domain features extracted from the HRV and EDR signals. Previously, it was reported that changes in the morphology of the ECG signal is associated with sleep apnea [47]. In [47], it is also claimed that the sleep apnea detection algorithms based on features related to the morphological changes in ECG perform better than that one based on the spectral analysis of HRV. Variations in the QRS complex morphology of ECG due to the apnea episodes are also reported in [54]. Nevertheless, most of the algorithms concentrated towards use of the R-peak amplitude to get the respiratory related efforts, but the use of the entire QRS complex morphology to acquire the information of the apnea episodes is seen to be limited in the literature. Therefore, those features which extract the morphological changes in the QRS complexes of ECG signal caused by the apnea need to be exploited for sleep apnea detection. Additionally, the time and frequency domain features of the EDR signal (obtained using the QRS complex morphology) and HRV can also be utilized to get an efficient classification between the apnea and normal subjects.

1.2 PROBLEMS ADDRESSED IN THE THESIS

As mentioned previously that many techniques have been developed in the literature to track the respiratory influence in the ECG signal for the purpose of the accurate estimation of respiration. Despite the fact that the shape of the EDR signal obtained using the filtering approach poorly matches to the shape of the actual (reference) respiratory signal, the filtering methods do not require prior knowledge of any fiducial point (R-peaks) in the ECG signal to get the EDR signal. Hence, a suitable method (EDR) based on the filtering of ECG can provide informative measures of the respiration in the case where detection of the R-peak positions in ECG signal is difficult due to noise/artifacts. Also, most of the morphological variations in the ECG beats are caused by the respiration or the body movement. Variation in the morphology of the QRS complexes of ECG signal due to the respiration is reported in the literature. Therefore, instead of using only the amplitude of the

QRS complex of ECG signal, the entire QRS complex morphology needs to be investigated to get a reliable estimation of the respiration.

Additionally, the occurrence of sleep apnea episode also affects the QRS complex morphology of the ECG signal as reported in the literature. Hence, variations in the morphology of the QRS complex due to the sleep apnea episodes can be analysed to detect the sleep apnea problem in the patient. Also, the performance of different types of classifiers needs to be evaluated to get the suitable classifier for the apnea detection problem. Use of the HRV and the EDR signal, obtained by monitoring the morphological variation in the QRS complex of ECG signal, can be used to develop efficient apnea detection technique to get the improved performance than the existing approaches.

The problems addressed in the thesis are described as follows.

1. Development of an algorithm for the removal of BW noise from the ECG signal.
2. Development of the technique for obtaining the respiratory-induced changes in the ECG signal for deriving the respiratory signal.
3. Development of the methodology to detect the sleep apnea patient using single-lead ECG.

The first goal of this thesis comprises the pre-processing step of the ECG signal to eliminate the BW noise which is the main source of low-frequency noise in the ECG signal. Removal of BW from the ECG is an important issue to address in this work as it may lead to miss-detection of the R-peak position which is used as a fiducial point in the ECG to analyse the QRS complex as well as the HRV pattern. Additionally, the presence of the low-frequency BW in the ECG signal can cause the distortion in the derived respiratory signal particularly in the case of the filtering based EDR techniques. Therefore, removal of the BW noise from ECG is an essential step for both the EDR extraction and detection of sleep apnea problem.

The next aim of the thesis is to estimate the respiratory signal from single-lead ECG signal. For this purpose, the development of EDR algorithms based on the homomorphic filtering and tracking the respiratory-induced morphological variations in the QRS complex of ECG signal is attempted in this thesis. The experimental results of the EDR methods will be compared with the state of art techniques to evaluate a significant contribution of our research work.

The last goal of the thesis comprises the development of an improved approach using single-lead ECG recordings to discriminate the subject suffering to sleep apnea from the normal one. Here, the apnea classification algorithm is mainly developed by extracting information related to the morphological variations in the QRS complexes of ECG signal caused by the apnea episodes. The use of the HRV and the EDR signal (obtained from the

QRS complex morphology) is also exploited to achieve improved performance than the existing approaches. The classification will be performed over the independent dataset, and the performance of the proposed approaches will be compared with the existing techniques to evaluate their effectiveness.

1.3 ORGANISATION OF THE THESIS

The thesis starts with the introduction of ECG-based respiration estimation and sleep apnea detection. The research gap outline helps to understand the motivation for research in the present field, and analyses the issues present in the existing techniques for BW removal, EDR extraction and detection of sleep apnea problem in the patient using single-lead ECG. It further summarizes the contribution of the thesis. The thesis consists of six chapters including one entitled 'Introduction'. The remaining chapters of the thesis are structured as follows.

Chapter 2 comprises a brief overview of the human cardiovascular system and its two parts namely the heart and the vascular system. A detailed review of the functioning of the human heart, generation of the ECG signal, respiratory process, HRV, and RSA is also presented. This chapter also highlights the main sources of noise in the ECG, and the respiratory-induced variations in the ECG signal for the applications of EDR extraction, and sleep apnea detection. The detailed literature review of the existing techniques for BW removal, estimation of the respiration and detection of sleep apnea using single-lead ECG is presented, and various research gaps are highlighted.

Chapter 3 presents a new approach based on the Hilbert vibration decomposition (HVD) for the removal of BW from the ECG signal. A detailed review of the HVD technique is presented. Then, the proposed methodology for the removal of BW in the ECG signal using the HVD is described. The data from *MIT-BIH arrhythmia* database are used to evaluate the performance of the proposed BW removal technique. An artificial BW signal is added in the ECG recordings to measure the actual performance of the proposed technique. The performance results of the proposed methodology are compared with the EMD based technique for BW removal from ECG.

Chapter 4 is devoted to the extraction of respiratory induced variations in the ECG signal for estimation of the respiratory signal. To derive the respiratory signal from ECG, two new EDR algorithms are presented in this chapter. In the first EDR technique, the homomorphic filtering is applied to the ECG signal to get the cepstrum. Next, a band-pass filter is applied to the cepstrum of ECG signal to obtain the respiratory signal in the output. On the other hand, the second EDR methodology is based on monitoring of the respiratory induced morphological variations in the QRS complexes of ECG using the lower order Hermite basis

functions. The performance of the proposed EDR algorithms is compared with the state-of-art methods based on the PCA, RPA, and RSA over the *Fantasia* dataset, available at PhysioNet. The advantages and limitations of the proposed EDR methods are also discussed at the end of the chapter.

Chapter 5 deals with the problem of classification between the apnea and normal subjects based on the ECG recordings. In this chapter, two different algorithms for sleep apnea detection are presented. First, a technique based on the lower order Hermite basis functions for detection of the sleep apnea episodes is presented. The second technique for apnea detection is based on the time and frequency domain features derived from the HRV and the EDR signal. The experiments are performed over the *Apnea-ECG* dataset, available at PhysioNet. Classification results of the proposed techniques are discussed and compared with the existing work in the literature.

Chapter 6 concludes some major outcomes of the thesis. A summary of all results shown in Chapter 3-5 of the thesis is also presented. Finally, the future scope of the work is mentioned at the end of the chapter.

CHAPTER – 2

LITERATURE REVIEW

Nowadays, the trend of using the home-based healthcare devices for routine monitoring of the health conditions is increasing. This has subsequently encouraged the development of such non-invasive techniques that use the lesser number of physiological signals for the clinical interventions. The use of the lesser number of physiological signals for the diagnosis purpose makes the healthcare system cost-effective and less complex to evaluate the health conditions of the patient. Use of the ECG signals for the automatic diagnosis of several health related issues in the patient is widespread and efficient due to non-invasive measurement of the ECG signals. It is a well-known fact that the respiration process causes variations in the ECG signal which can be acquired to get the information related to the respiratory measures and breathing abnormalities in the patient. Therefore, the main focus of the research in the thesis is given to investigate the ECG signal for the estimation of the respiratory signal, and detection of the sleep apnea problem in the patient. As the BW noise is essential to remove from the ECG signal before the EDR extraction and sleep apnea detection, the development of efficient BW removal technique is also attempted in this thesis.

Before discussing the contribution of the research work, it is desirable to understand the basic physiological background associated with the respiratory process and sleep apnea problem. Therefore, this chapter provides the basic physiological principles of the cardiovascular system and the respiration process including the basic anatomy and functioning of the human heart, electric activities of the heart, and characteristics of the ECG signal. A brief description of some of the commonly used signals derived from the ECG signal is also embedded in this chapter. This chapter also highlights the main sources of noise in the ECG and the respiratory-induced variations in the ECG characteristics. Subsequently, a detailed overview of the obstructive sleep apnea (OSA), epidemiology of OSA, and its effect on the ECG and respiratory signals is mentioned Section 2.4. Details of the existing methods related to the BW removal, EDR extraction, and sleep apnea detection using the ECG signal are provided in successive sections for the better understanding of the contribution of work.

2.1 PHYSIOLOGICAL OVERVIEW

2.1.1. Cardiovascular System

Cardiovascular system (CVS) in the human is mainly made of the heart and the blood vessels [138]. In the CVS, the heart acts as a pump device and the blood vessels are filled with blood carrying it to the body organs [138]. Hence, the CVS is a closed system and is also referred as the circulatory system. As the name implies, the blood is pumped through the heart and circulated in the closed loop through the blood vessels. The main job of the CVS is to carry oxygen and nutrients to the body tissues and deduction of unwanted products (metabolic wastes) from the tissues [138]. Additionally, the circulatory system provides cell-to-cell communication and capability of intercept of outside attackers to defend the body [102]. A detailed description of the vascular system and the human heart is provided in subsequent paragraphs. In this section, introduction about the CVS is mainly based on [102] and [138].

Heart

The heart is one of the most powerful organs in the human body, and it looks roughly like a closed fist of a person. It located in the mid area of the thorax and positioned somewhat left of the breastbone [138]. The interior of the Heart is made of four chambers: right atrium, right ventricle, left atrium and left ventricle. In general, the right atrium and the right ventricle are described as the right heart, and the left atrium and the left ventricle are commonly referred as the left heart. The left and right chambers of the heart are divided by a heart wall known as the septum. The role of these four chambers of the heart is described in detail as follows [138].

- *Right atrium:* It is one of the receiver chambers of the heart which receives deoxygenated blood from the veins. This deoxygenated blood is then pumped into the right ventricle.
- *Right Ventricle:* It is one of the pumping chambers of the heart. The role of the right ventricle is to receive blood from the right atrium and then pumps that blood to the lungs for the gas exchange.
- *Left atrium:* It receives oxygenated blood from the lungs by relaxing, and pumps blood to the lower chamber (left ventricle) by contraction.
- *Left Ventricle:* It is the strongest chamber of the heart. The function of the left ventricle is to deliver or pump the oxygenated blood received from the left atrium to the arteries for the circulation. The blood pressure in the body is mainly related to the contraction and relaxation activity of the left ventricle.

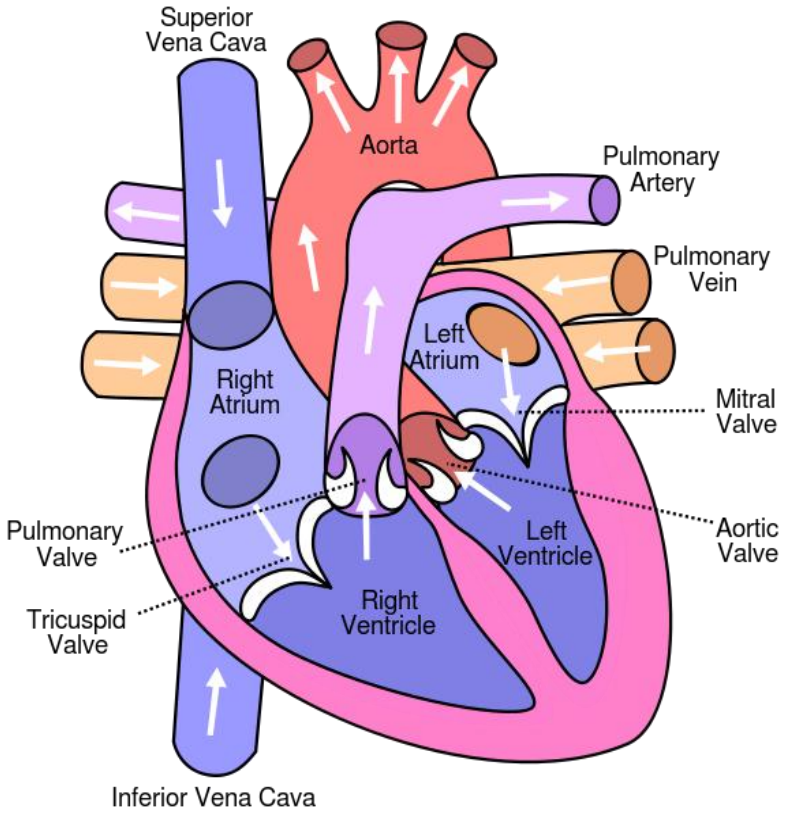

Fig. 2.1 The human heart, showing the lower and upper chambers and corresponding valves [140].

The internal structure of the heart and its blood receiving and pumping process is depicted in Fig. 2.1. It is clearly indicated that the upper chambers of the heart (atriums) are the blood receiver chambers and the lower chambers of the heart (ventricles) are the pumping chambers as shown in Fig. 2.1. In Fig. 2.1, the direction of the arrows indicates the direction of blood flow in the heart.

Vascular System

The vascular system is responsible for the proper circulation of the blood in the body, and it consists of three types of blood vessels: artery, veins, and capillaries [138]. The role of the arteries vessels is to transport oxygenated blood pumped by the heart to the body [138]. In other words, the arteries (except the pulmonary arteries) take the oxygenated blood away from the heart. The vein vessel transports blood with CO_2 or deoxygenated blood to the heart. Also, all the veins (except the pulmonary veins) convey deoxygenated blood. The role of capillaries is to transport the blood from small arteries to the small veins [138]. A general representation of both the vein and arteries connected with the body organs in the human cardiovascular system is shown in Fig. 2.2. In Fig. 2.2, the oxygenated blood is carried by the arteries (in red color), and the deoxygenated blood is carried by the veins towards the heart (in blue color).

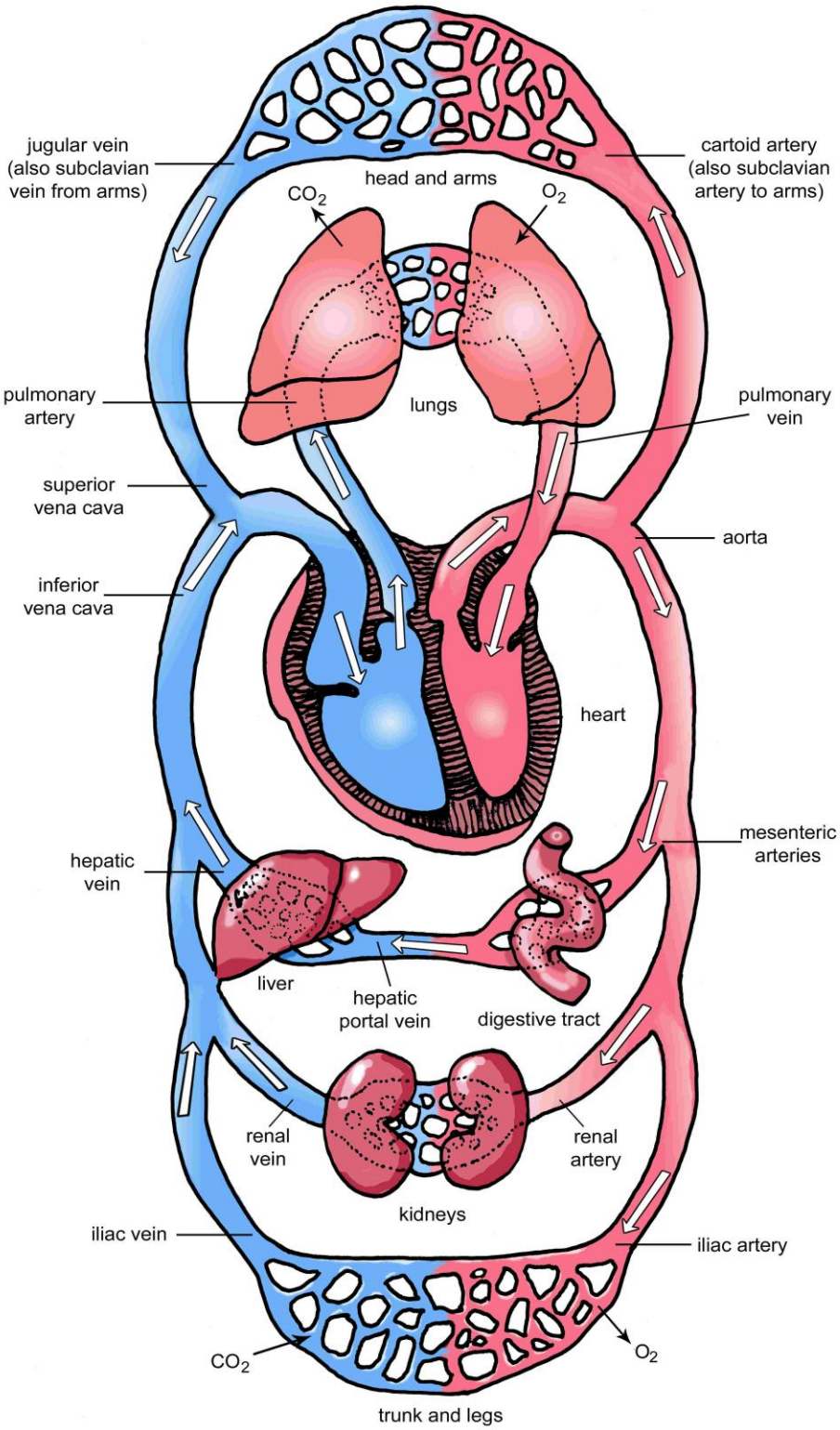

Fig. 2.2 The human cardiovascular system. The oxygenated blood transported by arteries is shown by red color, and deoxygenated blood carried by veins is indicated by blue color [102]

In the CVS, the circulation is divided into two categories, namely the systemic and pulmonary circulations [102]. These circulations are carried out the left and right parts of the heart. The right part of the heart pumps the deoxygenated blood (carried by the systemic

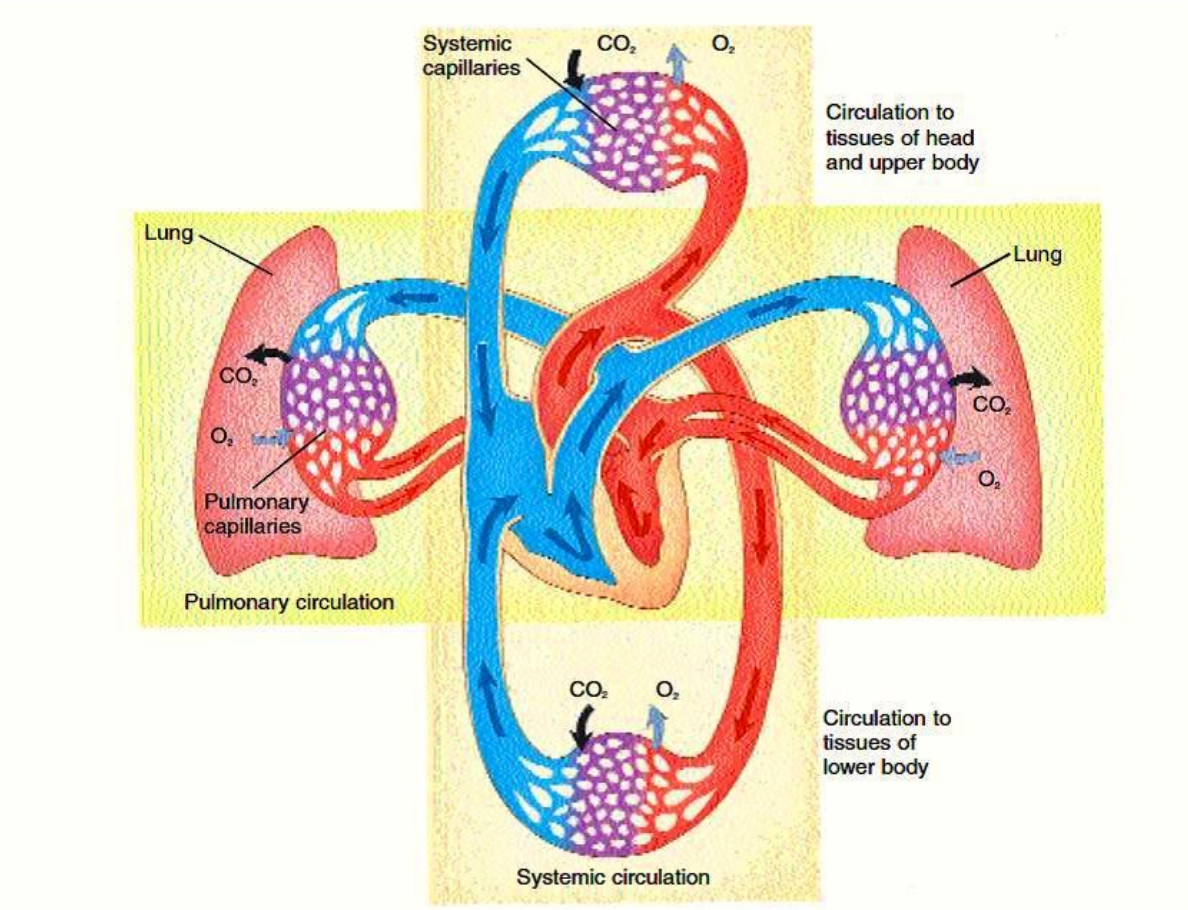

Fig. 2.3 The systemic and pulmonary circulations. Red represents oxygenated blood, and blue represents deoxygenated blood [139]

veins into the heart) into the pulmonary circulation for the release of CO_2 in the lungs. On the other hand, the oxygenated blood from the lungs enters into the left heart through the pulmonary circulation and then pumped back to the systemic arteries for the circulation in the body [139]. The process of systemic and pulmonary circulations is shown in Fig. 2.3 where the direction of the arrows indicates the direction of blood flow in the veins and the arteries.

2.1.2. Functioning of Human Heart

The heart conduction system is responsible for contraction and relaxation of contractile cells of the heart. The heart conduction system is constituted of four structures namely, the sinoatrial node, atrioventricular node, Purkinje fibers, and atrioventricular bundle (bundle of His) [138]. Special types of muscles (modified muscles) construct these cardiac structures which differ in functioning with the ordinary cardiac muscles. The specialty of the ordinary cardiac muscles is the capability of contraction, but can also conduct impulses [138]. On the other hand, the modified muscles can only conduct the impulses generated by the sinoatrial node [138].

- *Sinoatrial node (SA)*: It is also called sinus node and is made up of a group of cells which are located in the upper part of the right atrium wall (or right upper chamber of the heart) as shown in Fig. 2.4. The sinus node is the natural pacemaker of the heart, and it generates the electrical impulses (action potential) to activate contractions of the cardiac tissues. The rate of generation of electrical impulses is commonly referred as the heart rate and is controlled by the nerves innervation to the SA node.
- *Atrioventricular (AV) node*: The AV node is one of the structures of the conduction system of the heart. It is an area of specialized cardiac tissue and lies in the region between the atria and ventricles as shown in Fig. 2.4. An electrical impulse is generated by the SA node is spread out through the atriums and propagates through conduction systems towards ventricles. However, it is vitally needed to have some delay between the atrial depolarization and the ventricles depolarization to ensure that the atriums have completely delivered their blood to the ventricles before the ventricle contraction. Therefore, the main role of the AV node is to delay the action potential (excitation waveform) generated by the sinoatrial node so that continuous pumping of blood is maintained.
- *Bundle of His*: This structure of the heart conduction system is made of extraordinary cardiac muscle fibers which carry the action potential (electrical impulse), available at the AV node, through two branches to both the interventricular septum.
- *Purkinje fibers:* These fibers are situated at the inner wall of the ventricles as depicted in Fig. 2.4. The Purkinje fibers are specialized conducting (electrical excitation) fibers and have the role of providing synchronized contraction of both the ventricles to have normal conduction of the heart. These fibers play a critical role to maintain a regular heart rhythm in the human.

For maintaining the cardiac cycles, the electrical excitation must propagate through the conduction system. The SA node first fires the action potential, and then this action potential starts spreading through the atria region which results in contraction of the atriums. The process of depolarization becomes slower across the atria region needed for the complete ejection of the atria blood into the ventricles, and this delay in depolarization is controlled by the AV node [138]. The action potential at the AV node is then started moving down to both the interventricular septum through the bundle of His as shown in Fig. 2.4. Next, this action potential travels along with the bundles of Purkinje fibers located on both the left and right sides. These Purkinje fibers conduct the action potential very speedily (4 m/s) outward to the contractile cells in the apex of ventricles [138]. The rapidly spread of the action potential in the apex of the ventricles results in simultaneous

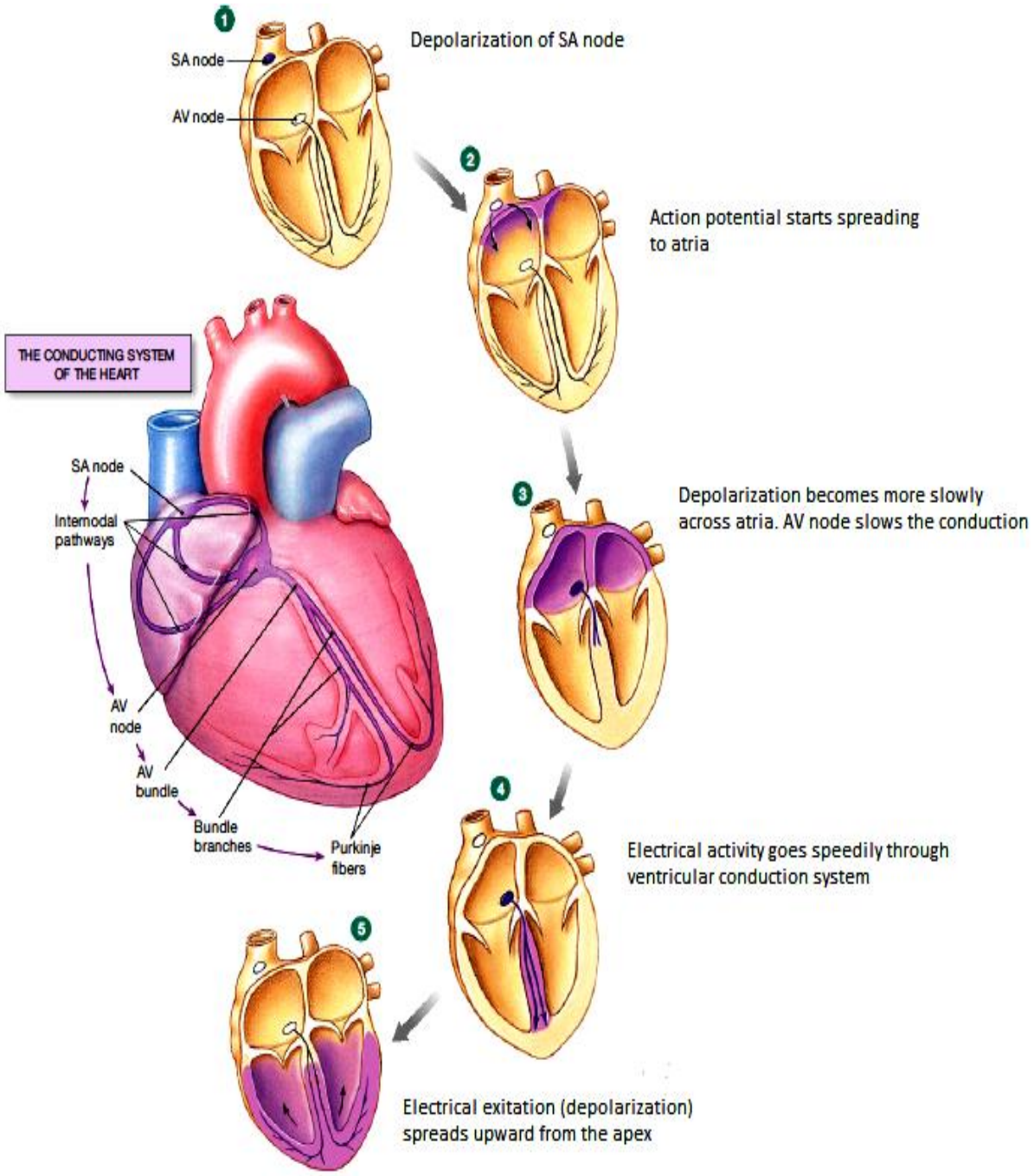

Fig. 2.4 Heart conduction system [138]

contraction of all contractile cells. Therefore, the contraction and relaxation of the atria and the ventricles are all started from the SA node, and the rhythm of the SA node for firing the action potential for the depolarization process is controlled by the autonomic nervous system [102].

2.1.3. Electrocardiogram

The contraction and relaxation of the atriums and ventricles are based on the action potential generated by the SA node and spread of it through the conduction pathway [138]. This

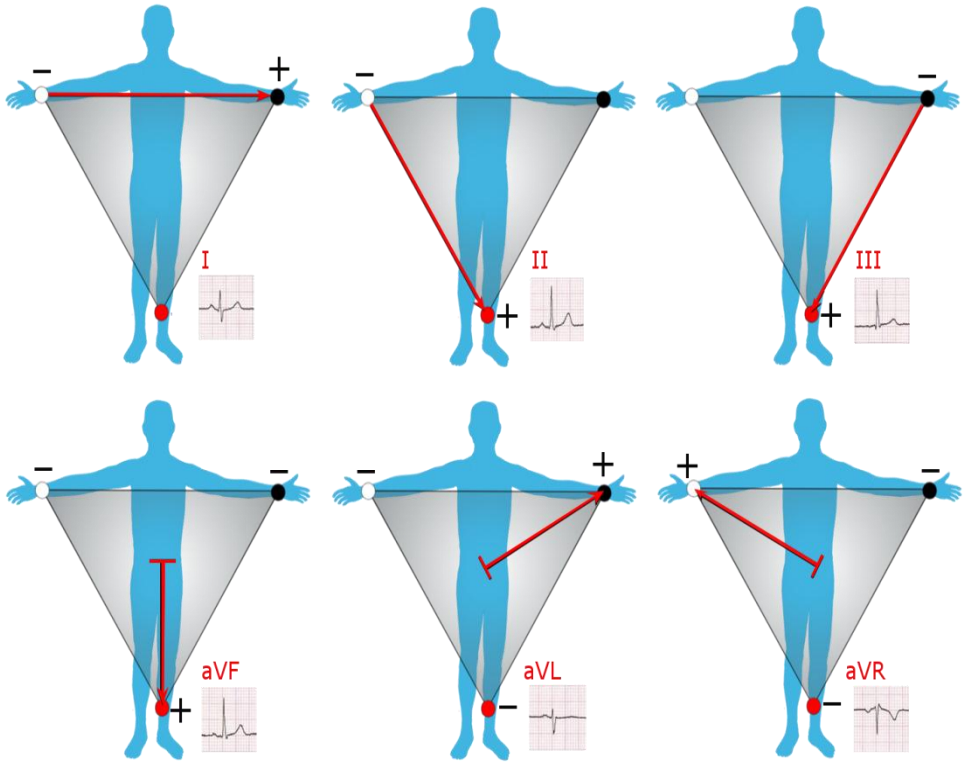

Fig. 2.5 The Einthoven's triangle [141]

process of conduction of the action potential through the conduction pathway creates the electrical potential difference which can be recorded and analyzed to evaluate the rhythmic disturbances for clinical diagnosis [138]. For this purpose, some electrodes are placed at specific locations on the skin around the heart to measure its electrical activities during relaxation and contraction. The recorded waveform, which characterized the electrical activities of the heart, is called electrocardiogram (ECG). The ECG contains useful information about the heart rhythms.

Walter Einthoven, the father of the modern ECG, first described the Einthoven's triangle for ECG measurements. It is a hypothetical triangle formed around the heart with the electrodes placed on both the arms and the left leg [138] as shown in Fig. 2.5. Three sides of this triangle are known as the 'leads'. Each side of the triangle is formed by the pair of two electrodes [138]. In this way, three pairs of electrodes correspond to three sides of the triangle and therefore are denoted as lead I, II, and III as shown in Fig. 2.5.

In ECG, the heart electrical activities are recorded by one lead at a time. In the recording process, one electrode acts as the positive electrode of a particular lead whereas the second one behaves as the negative electrode of that lead [138]. For example, during the lead II recording (recorded using the left leg and the right arm electrode pair as shown in Fig. 2.5),

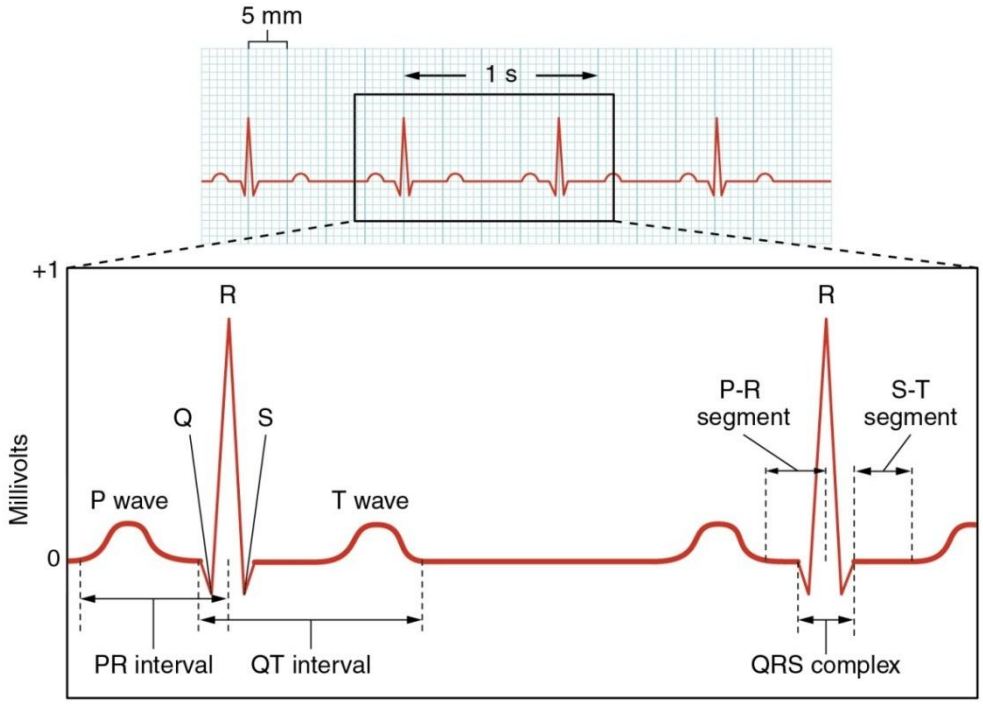

Fig. 2.6 Characteristics of an ECG signal [138]

the left leg electrode acts as the positive electrode, and the right arm electrode serves as the negative electrode, but the left arm electrode remains inactive [138].

Furthermore, three augmented limb leads, denoted as aVR, aVL, and aVF, are also formed using the leads I, II, and III as depicted in Fig. 2.5. These augmented limb leads essentially used for determining the electric axis of the heart in the vertical plane [142]. On the other hand, six more leads known as precordial leads (V_1, V_2, V_3, V_4, V_5, and V_6) are also employed around the heart to fetch the information in the transverse plane of the heart [141-142].

The ECG record demonstrates the addition of the electrical potential produced by all contractile cells of the Heart. This electrical potential varies according to the relaxation and contraction or depolarization and repolarization states of the atria and ventricle muscles. Single contraction and relaxation phase of the heart is recognized as the cardiac cycle. Fig. 2.6 depicts a typical ECG waveform obtained from lead I. A single cycle of an ECG trace can be described by combination of different waves, namely P, Q, R, S, and T. In the ECG trace, the three waveforms namely Q, R, and S combine forms the QRS complex as depicted in Fig. 2.6.

Further describing the ECG waves, the P wave in the ECG trace is caused by the depolarization of the atria region in the Heart (see Fig. 2.7). The action potential now travels through the AV bundle produces the Q wave below the baseline [138]. This electrical signal

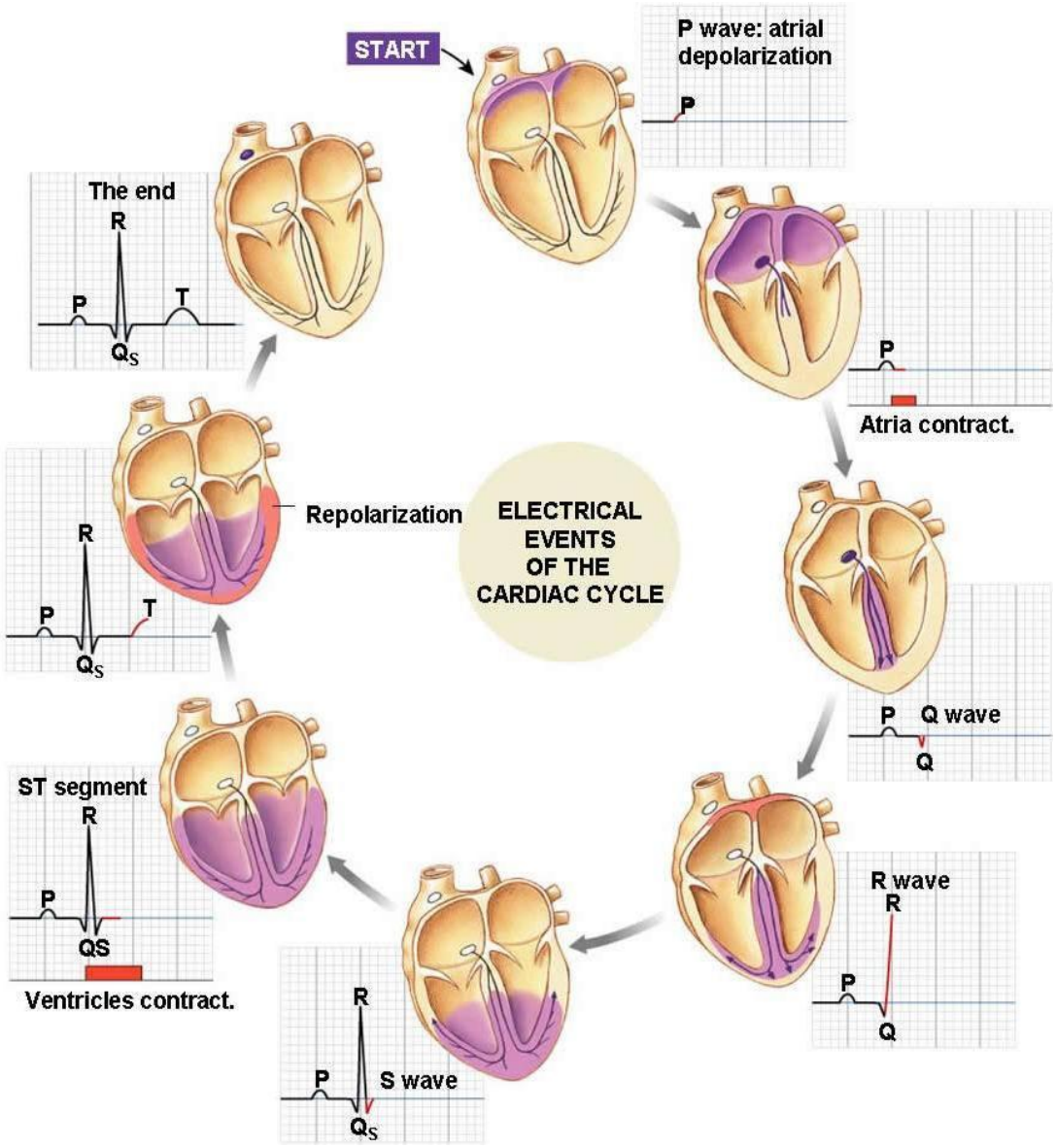

Fig. 2.7 ECG traces corresponding to depolarization and repolarization of the atria and ventricles of the heart [138].

then moves towards both the left and right ventricle septum giving rise in the amplitude of recorded potential, and hence R wave appears [138]. Now, the action potential spreads upward speedily from the apex producing the Q wave. Lastly, repolarization of the contractile cells of the ventricles is presented by the T wave. Here, the atrial repolarization is not depicted separately, but it contributes in the QRS complex [138].

2.1.4. Respiratory System

Respiration system is a biological process in the human body. The word respiration can be defined in two ways namely, cellular respiration and external respiration [138]. In cellular

respiration, the oxygen molecules react with the organic particles producing CO_2, water, and energy, and this process is also defined as the intracellular reaction as shown in Fig. 2.8 [138]. On the other hand, the external respiration consists of structures and organs responsible for the gas exchange between the environment and the body cells (see Fig. 2.8). The external respiration can be split into four collective processes as follows [138].

1) Exchanges of gas between the lungs and environment. This procedure is also called as ventilation or breathing. In the ventilation process, the passing of air from the atmosphere to the lungs is referred as inspiration (inhalation), and the passing of air from the lungs to the atmosphere is referred as expiration (exhalation). A single breathing (or respiratory) cycle involves of an inspiration tailed by expiration.
2) Transfer of the oxygen and CO_2 between the lungs and the blood.
3) Transport of the oxygen and CO_2 by the blood.
4) Exchange of oxygen and CO_2 between the blood and the cells.

As discussed previously, the oxygen in the body cells is transported by the cardiovascular or circulatory system and blood. Hence, the coordination between the external respiration

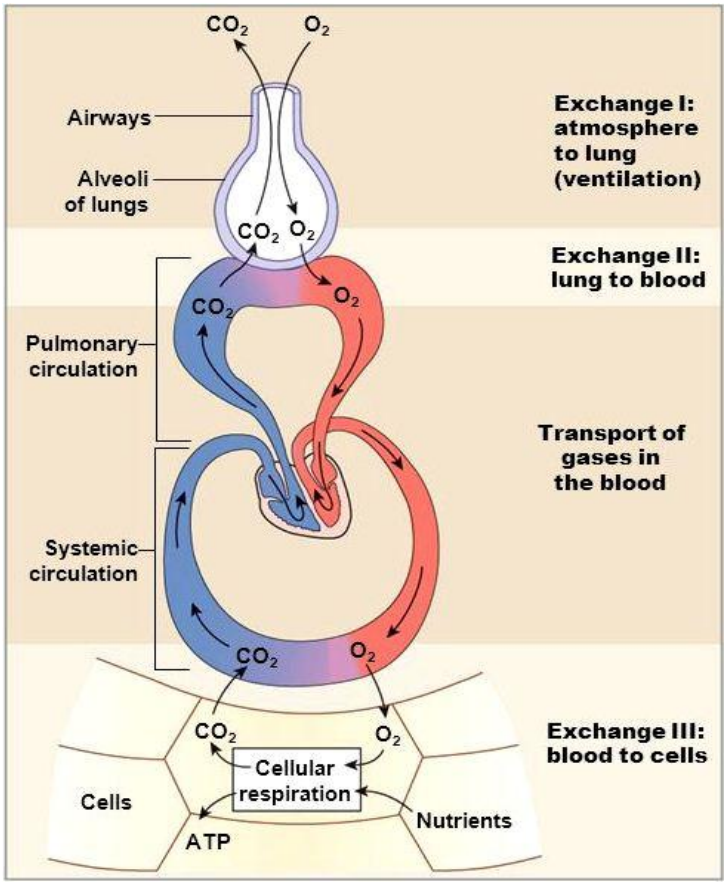

Fig. 2.8 Demonstration of external and cellular respiration systems in the human body [138]

and the circulatory system is required [138]. Structures involved in the ventilation and gas exchange process of the respiration system are described as follows [138].

- The airway or conducting system. It is the link between the outside environment and interchange surface of the lungs.
- The alveoli. These structures consist of chains of interconnected capillaries and sacs that combine form the gas exchange surface. On this exchange surface, oxygen of the air from inspiration transfers to the blood, and CO_2 of the blood moves to the air that will be taken outside the body during exhalation.
- The chest cavity or thorax, and abdomen. These consist of the bones and muscles needed to support the ventilation.

Besides, breathing is the unconscious rhythmic process in the body. The cardiac and skeletal muscles that usually start the inspiration and expiration process are not able to contract spontaneously and therefore controlled through the central nervous system (CNS) [138].

2.1.5. Heart Rate Variability

It is evident from the physiological background that the heart rate does not remain constant [102]. Based on the body demand, the rhythm of SA node in the heart is controlled by the sympathetic and parasympathetic nervous system [102]. Sympathetic and parasympathetic nerves carry the motor signals from the brain to the heart, and reflective functions of the heart to the brain [138]. Parasympathetic nerves slow down the heart rate by unleashing the acetylcholine, whereas the sympathetic nerves force to heart contract rapidly by discharging epinephrine and norepinephrine from the nerve and the adrenal glands [138]. For example, during the sports activities, the heart rate is usually higher as compared with the resting condition. This increase in the heart rate is based on the fact that during exercise body requires more oxygen and hence the heart rate is raised to supply more blood to fulfill body's demand. Hence, variation in the heart rate is termed as heart rate variability (HRV) [102]. For the clinical purpose, analysis of the HRV pattern can provide a significant information related to the abnormalities in the heart functioning. Patients suffering from the myocardial infarction are observed to be having a lack of variability in the heart rate which is the main cause of mortality [144], and this observation is found to be one of the most significant outcomes from the HRV analysis. Also, a decrease in the vagal tone causes the decrease in HRV [145].

The HRV from any ECG can be obtained by first detecting the positions of R-peaks of the QRS complexes of ECG signal [34]. Detection of the positions of R-peaks in the ECG signal is carried out by the specialized algorithm. For this purpose, one of the most popular algorithms known as the Pan-Tompkins algorithm [116] is used throughout this study. For

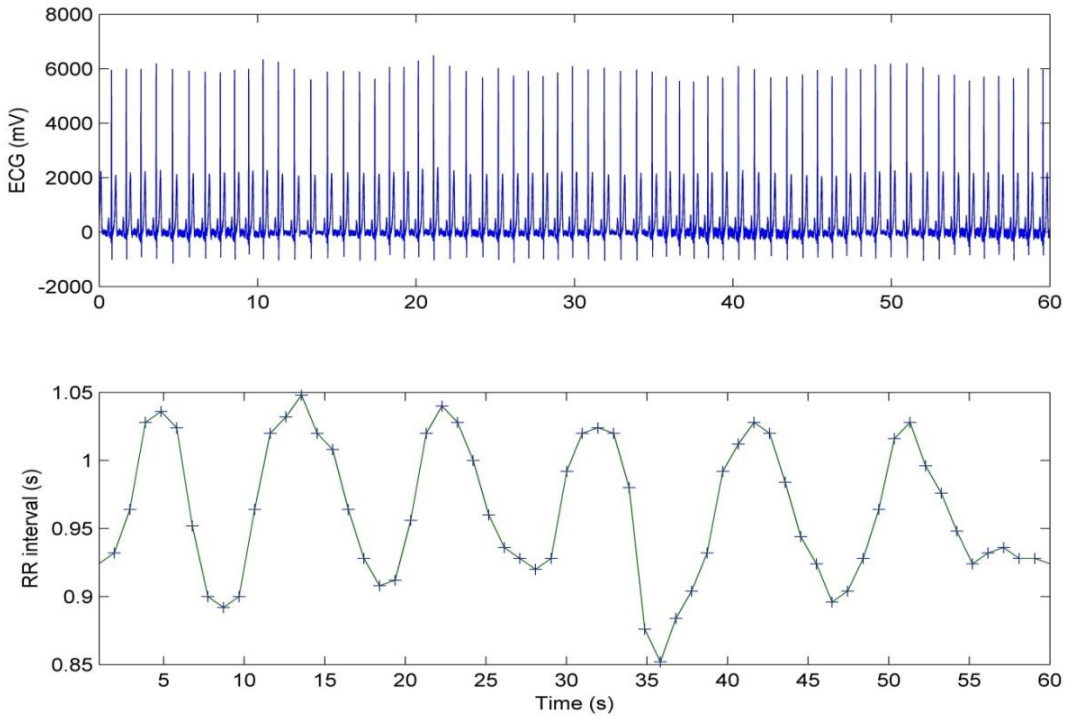

Fig. 2.9 The ECG signal (top panel) and corresponding RR interval time series, or tachogram (down panel). ['+' sign indicates detected R-peaks]

computation of HRV, RR intervals need to be computed after detection the positions of R peaks. An RR interval is defined as the duration between two successive R-peaks in the ECG signal. If RR intervals are plotted against time constitutes the tachogram which presents the basic signal to analyze the HRV [102]. An example in presented in Fig. 2.9 containing the ECG signal and corresponding R-R interval time series. The RR intervals can be further preprocessed to obtain normal-to-normal (NN) intervals [102].

The HRV (tachogram) signal can be characterized using many time and frequency domain measures [143], [146]. These measures of HRV can be further exploited for clinical applications. Some of the common HRV measures that are most significant for the clinical purpose, and are standardized by the Task Force of the European Society of Cardiology, and The North American Society of Pacing and Electrophysiology [147] are described in the subsequent paragraphs.

Time Domain Measures of HRV

Some of the most common time domain HRV measures are:

- mean N-N interval (meanNN)
- the standard deviation (SD) of the NN intervals (SDNN)
- difference between the longest and shortest NN intervals (diffNN)

- square root value of the mean computed for the squared differences between succeeding NN intervals (RMSSD)
- SD value of the squared differences between succeeding NN intervals (SDSD)
- Percentage of the differences of succeeding NN intervals more than 50 ms (pNN50).

In the above described time domain HRV measures, last three measures refer to the spectral power of the high-frequency components of HRV and hence associated with the parasympathetic activity of autonomic nervous system (ANS) [102].

Spectral Analysis of HRV

Apart from the time domain, spectral domain analysis of the tachogram also provides information related to the sympathetic and parasympathetic activities of ANS. For this purpose, the frequency spectrum of the HRV is analyzed mainly in four frequency bands [143]:

- Ultra low frequency (ULF) band: 0 – 0.003 Hz
- Very low frequency (VLF) band: 0.003 – 0.04 Hz
- Low frequency (LF) band: 0.04 – 0.15 Hz
- High frequency (HF) band: 0.15 – 0.4 Hz.

For each frequency band, power is computed by integrating power spectral density curve (PSD) in the predefined frequency band as described above and then normalized it with the total power computed in the band of 0 – 0.4 Hz. In HRV, ULF band consists of information linked to circadian rhythm, but variations in the VLF band and its physiological association is still unclear [102]. The LF band in HRV reflects information related to the sympathetic and parasympathetic modulations [148-149]. It is also investigated that the Mayer waves (caused by oscillations of arterial pressure) also have an impact on the LF band power of HRV [150]. The HF band power of HRV depends on the cardiac vagal activity. One of the important measures of the HRV is the ratio between LF to HF powers which describes the sympathovagal balance. However, this explanation has been questioned in different studies [151-152].

2.1.6. Respiratory Sinus Arrhythmia

The relation between respiration and variation in the heart beat intervals in the resting humans is understood by the phenomenon known as the respiratory sinus arrhythmia (RSA) [55]. The RSA is described by the concomitant variations (modulation) in the heart beat intervals of ECG synchronized with the respiratory efforts as displayed in Fig. 2.10. In this modulation, the heart rate increases during inspiration followed by a decline during expiration. Earlier studies have revealed that the mechanism of RSA is linked with the modulation of cardiac vagal efferent activity by the central respiratory drive [56-58]. Also,

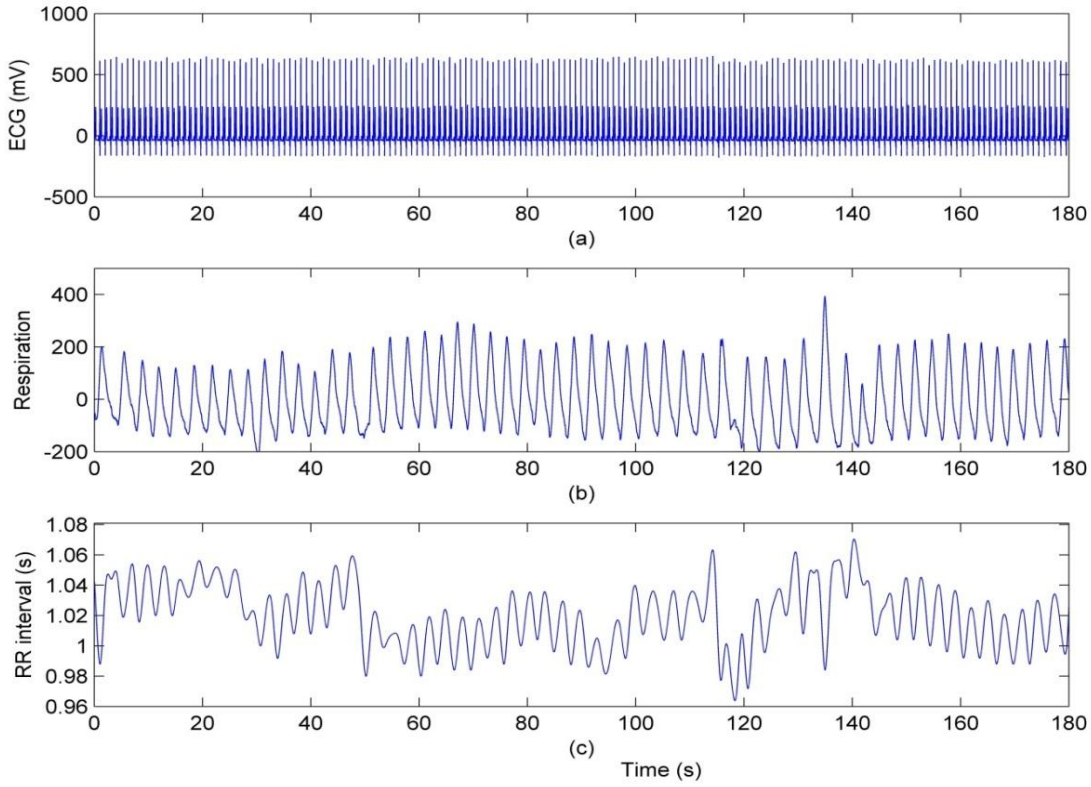

Fig. 2.10 Simultaneously recorded ECG and respiratory signals, and RR interval time series (tachogram). (a) ECG; (b) Respiration; and (c) RR interval time series (tachogram). The RR time series is modulated according to the respiratory cycles that indicate the presence of RSA component.

increase in the degree of RSA is associated with the increase in the cardiac vagal activity [59-60]. It is also observed that most of the RSA at resting state is associated with variations in the vagal tone induced by the central respiratory drive [102]. The magnitude of RSA is determined by analyzing the high-frequency component of HRV and is commonly utilized for assessing the vagal cardiac modulation [61-63]. It is largely debated whether the RSA reflects an active physiological character or simply throw back a passive cardiovascular response in the case of the respiration as input [64-65]. Thus, the mechanism by which the RSA is associated remains unclear. Nevertheless, RSA is utilized as an index to quantify the cardiac vagal efferent activity, and other clinical practices including stress, and cardiovascular problems [153].

The physiological importance of RSA is assessed by both the time and frequency domain methods. The time domain approach consists of a peak-valley method that evaluates the RSA in terms of the difference between the longest and shortest RR intervals during inspiration and expiration [154]. On the other hand, the degree of RSA can be quantified by evaluating the power in the HF band of the tachogram (HRV) [154]. It can be observed that the respiratory frequency lies in HF band of HRV when the subject remains in the resting

state. Moreover, the degree of RSA in HRV varies according to the age of the subject. The magnitude of RSA in HRV decreases as the age of the subject increases which is the main drawback of RSA method when using it for the respiratory related measures [16].

2.2 Sources of Noise in ECG

The ECG is easily recordable physiological signal which constitutes symptoms of various types of health problem.in the body. Therefore, it is being used in the development of home-based portable healthcare devices for routinely monitoring of health. The ECG recordings are easily affected by several types of noises caused by the muscle movements, variations in the electrode positions, and the respiratory process [90]. Nowadays, the ECG signals are transmitted at long distance using different telecommunication platforms for health monitoring of the patients at the long distance. Therefore, the ECG recordings are easily corrupted by several types of noises including low and high-frequency artifacts that make its interpretations difficult to the clinician. In this section, we discuss various sources of noise that affect the ECG recording. The spectrum of the BW noise coincides with that of the respiration. As a consequence, the presence of BW in the ECG recordings can affect the respiratory signal estimated from the ECG. Therefore, in this thesis, we mainly focused on the BW artifact present in the ECG recordings. An overview of several developed techniques for BW removal from the ECG signal is also embedded in this section.

2.2.1. Baseline Wander and Powerline Interference

Baseline Wander

Baseline wander (BW) is a common artifact exists in the ECG signal and is also one of the major sources of low-frequency noise in the ECG recordings [66]. The BW noise in the ECG recordings mainly arises due to the respiration [66]. Movements of the skeletal muscles and the electrodes employed for the recording of the heart activities also cause this kind of artifacts in the ECG signal [67]. In addition to that, this sort of artifact can be caused by changes in temperature and bias in the instrumentation amplifiers [68]. However, the BW component in ECG signal lies in the range of 0 to 0.5 Hz, but this range could be larger in the case when the ECG is recorded during physical exercise [69-71]. BW in the ECG affects the clinical interpretation of ECG signal resulting in bias the estimation of the terms. For example, studying of the ST segment is difficult while having BW in the ECG signal, and therefore its consequences affect the diagnosis of several diseases including ischemia, myocardial infarction, and symptoms of unevenness of myocardial oxygen supply in the heart [72]. An example of the ECG signal with BW and without BW noise is shown in Fig. 2.11. It can be easily visualized that the BW noise may affect the information of clinical significance as well as the detection of positions of R-peaks in the ECG recordings.

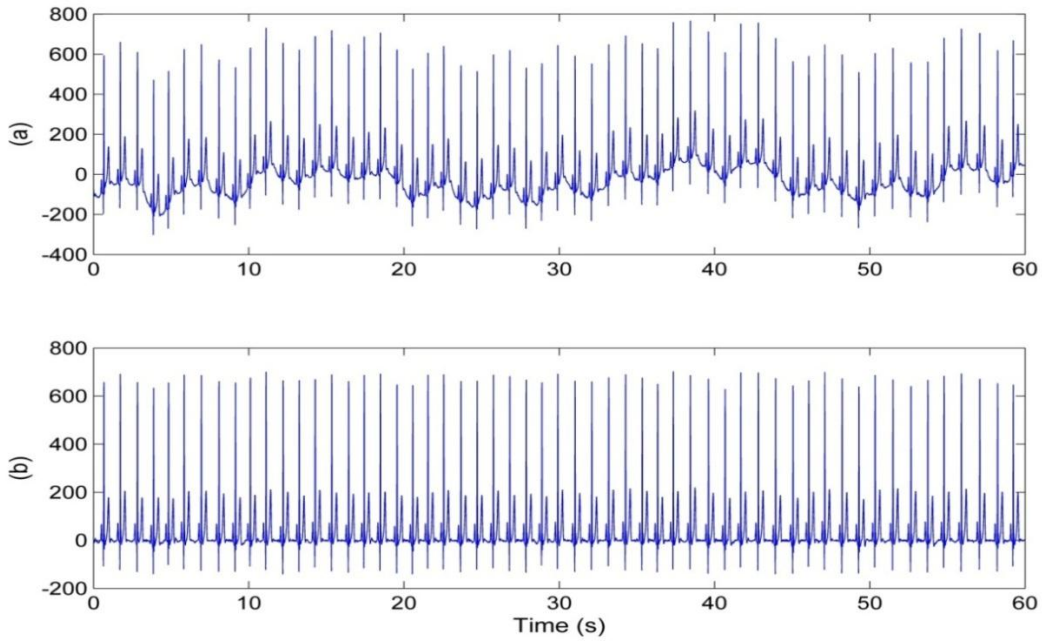

Fig. 2.11 ECG Signal. (a) ECG with BW noise, (b) Baseline corrected ECG signal.

Powerline Interference

Powerline interference in the ECG signal is another important source of noise which affects the ECG recordings. In the ECG monitoring process, cables transporting the information from the examination point to the monitoring device are at high risk of the electromagnetic interference caused by the supply line of 50 Hz or 60 Hz power frequency [74]. An example is shown in the Fig. 2.12 containing the ECG signal with powerline interference and its frequency spectrum. In Fig. 2.12, the powerline interference in the ECG signal can be observed as a peak at 60 Hz in its (ECG) frequency spectrum. Sometimes the entire ECG signal is corrupted with this kind of noise. As the frequency of power signal in the supply line lies in the same band as of ECG signal, the removal of powerline interference from the ECG recording is, however, difficult. Nevertheless, a notch filter (50 Hz or 60 Hz) can be employed to suppress the effect of powerline interference in the ECG signal [75].

Other sources of noise include EMG noise, the motion of the patient during the process, loose placement of electrodes, improper grounding of the instruments, and noise generated by electronic circuitry [66]. The EMG noise is a high-frequency noise mainly generated by the muscles activities. Before analyzing the ECG signal, these types of noise should be removed to prevent biasing in the estimating terms.

2.2.2. Baseline Wander Removal From ECG

It is discussed earlier that BW in the ECG signal is a dominant source of low-frequency noise that affects the EDR extraction, R-peak detection, ST-segment, and other morphological characteristics of the ECG signals. Thus, the BW noise needs to be removed from the ECG

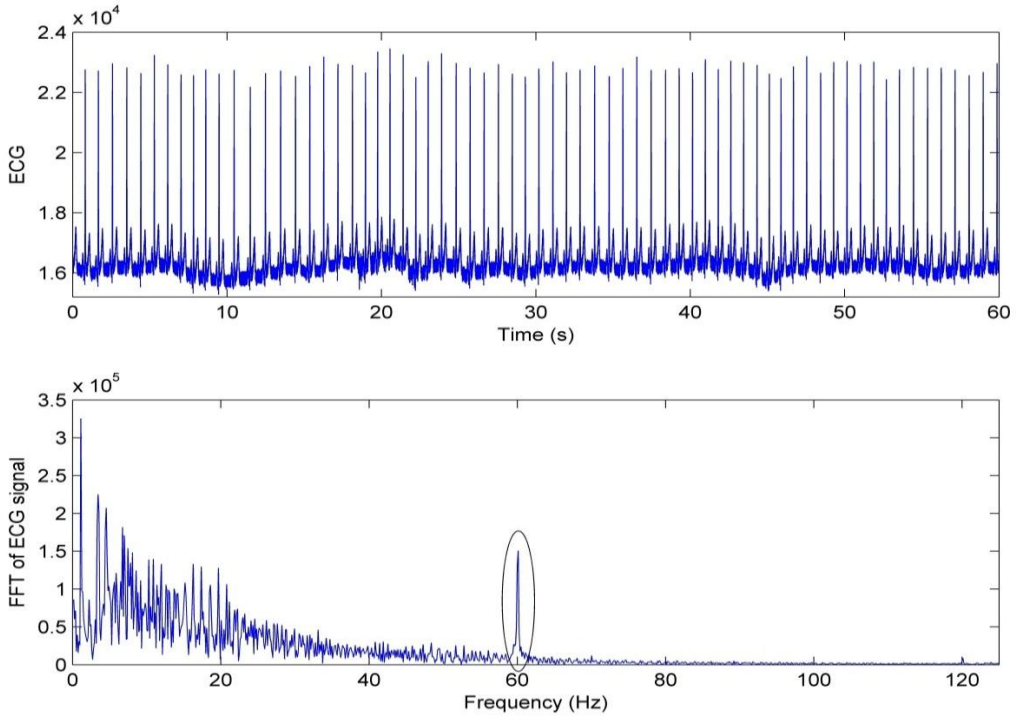

Fig. 2.12 An example of ECG signals (upper panel), and its fast Fourier transform (FFT) representation (down panel). A peak at 60 Hz (shown by an eclipse) in the FFT of ECG signal signifies the powerline interference.

signal without affecting its morphology for better clinical interpretation of the heart activities.

Several methodologies have been developed by the researchers for the removal of BW from the ECG signals [66], [68-72] [77-92]. Filtering of the ECG signal using a high pass filter (cut-off frequency 0.7 Hz) is a classical method to remove BW from the ECG [90]. This filtering also removes the overlapping low-frequency ECG components with the noise, and that affects the beat morphology (mainly ST-segments) [91]. Therefore, BW removal from ECG based on the high-pass filter can distort the waveform which can lead wrong interpretation of the ECG characteristics. Another method based on the cubic spline is also used for the removal of artifacts from the ECG signal [92]. However, this approach primarily assumes that the PR interval of ECG beat is well-defined and its location is recognizable for normal beats [91]. But, this assumption may not be valid in the case of presence of other types of noises in the ECG signal such as muscles artifacts, electrode movements, etc. [96].

Various other methods for the removal of BW from the ECG signal have also been reported in the literatures including the adaptive filtering [70-71], [93], moving average filters [94], advanced averaging filters [79-80], decimated filter banks [77], singular value decomposition [86], independent component analysis [87], nonlinear filter banks approach [78], adaptive Kalman filtering [95], morphological approach [88], and empirical mode decomposition [66],

[89], [93], [96]. The adaptive filtering technique for BW removal requires a reference signal [78]. However, the moving average filters are easy to implement to filter out the BW noise from ECG, but it can alter the output waveform at the points of sudden change such as R peaks [94]. The use of the FIR filter approach [97] for BW removal is limited due to the processing of a large number of filter coefficients [78]. The process of removal of artifacts (BW and other noises) from the ECG signal using the adaptive Kalman filtering technique requires some prior knowledge of the patient. Using the morphological approach, it is needed to have information about the heart rate of the patient before extracting the BW noise from ECG [88].

Recently, the EMD technique has also emerged as a tool for time-frequency analysis and is being used for many applications to process non-stationary signals [98]. The EMD technique decomposes a signal into different frequency components known as intrinsic mode functions (IMFs). However, the low-frequency IMFs can be used to estimate the BW noise in ECG signal, but this noise may be distributed over several other IMFs [94]. Also, in the EMD technique, it is required to select all IMFs that contain the part of BW noise for efficient removal of this kind of noise from the ECG signal. Distribution of the BW noise over different IMFs can vary according to the patients, and there is the unavailability of such a technique which can select the required number of IMFs that constitute the BW noise. The selection of required number of IMFs for the BW estimation is performed on trial basis [94]. Therefore, automated use of the EMD technique for the removal of BW from the ECG signal is difficult. Also, the computational cost of the EMD technique is very high when applying it to a long segment of the data.

Removal of the BW noise from ECG is also performed using the wavelet approach [99]. In the wavelet method, the detailed coefficients at the lower frequencies are analyzed to extract the low-frequency noise. In the wavelet decomposition, the BW noise is distributed over different levels of detailed coefficients [100]. It is required to select an adequate number of levels of the wavelet decomposition which can be processed for efficient estimation of the BW noise. Therefore, the wavelet technique also suffers from the same limitation as of the EMD technique. Also, selection of the mother wavelet is an important consideration in the wavelet approach. As the existing techniques possess certain types of limitations, the development of an automated algorithm for effective removal of BW from the ECG is desirable. In this thesis, development of an automated algorithm based on the iterative application of the Hilbert transform for the removal of BW from the ECG signal is presented. Details of the proposed technique and its performance results obtained from the experiments are presented in Chapter 3.

2.3 ECG-Derived Respiration

Deriving the respiratory signal from the ECG signal is useful for the diagnosis of several types of respiration and cardiovascular problems. The ECG-based respiration is also beneficial for simultaneous nursing of the respiration and cardiac activities. Earlier (in the first chapter), it is highlighted that the respiratory process affects the ECG characteristics. Therefore, this section includes a general description of how the respiratory event influences the ECG characteristics. A detailed overview of the EDR methods existing in the literature is also embedded at the end of this section.

2.3.1. Respiratory-Induced Variations in ECG

The use of the direct and indirect methods for the respiratory measurement is limited due to various downsides of these methods in long-term use as discussed in the last chapter. Therefore, a considerable effort is directed to achieve a reliable estimation of the respiration using the non-invasive techniques. For this purpose, various methods have been developed for acquiring the respiratory signal using some non-invasive instruments including the ECG. The idea of deriving the respiration from the ECG signal is mainly based on two well-known phenomena described as [27]:

- Modulation of heart rate
- Changes in beat morphology of ECG

The process of modulation of the heart rate during inspiration and expiration can be understood by the event of RSA which is a distinguished phenomenon in HRV. In this modulation phenomenon, the heart rate increases during inspiration followed by a decline during expiration [101]. This modulation of heart rate due to the respiration is referred as the RSA as discussed in section 2.1. The event of RSA is associated with the respiration process due to the parasympathetic intervention, and it describes modulation of the heart rate during the respiration process. Moreover, it has been assessed that the most of the RSA (around 95 %) in the resting condition are initiated by the respiratory induced variations in the vagal tone [102]. Based on the modulation of heart rate, the respiratory signal can be estimated by first determining the positions of R-peaks in the ECG signal, and then computing the difference between successive R-peak positions. Upon plotting the values of the difference between successive R peak positions against the time axis (after interpolating these RR intervals by a suitable interpolation) gives the RR interval time series or tachogram. When analyzing this tachogram, it shows oscillations resembling the actual (or reference) respiratory cycles as shown in Fig. 2.13.

On the other hand, during the respiration process, some morphological changes in the ECG signal arise due to two main mechanisms: i) the volume of lung changes during inspiration

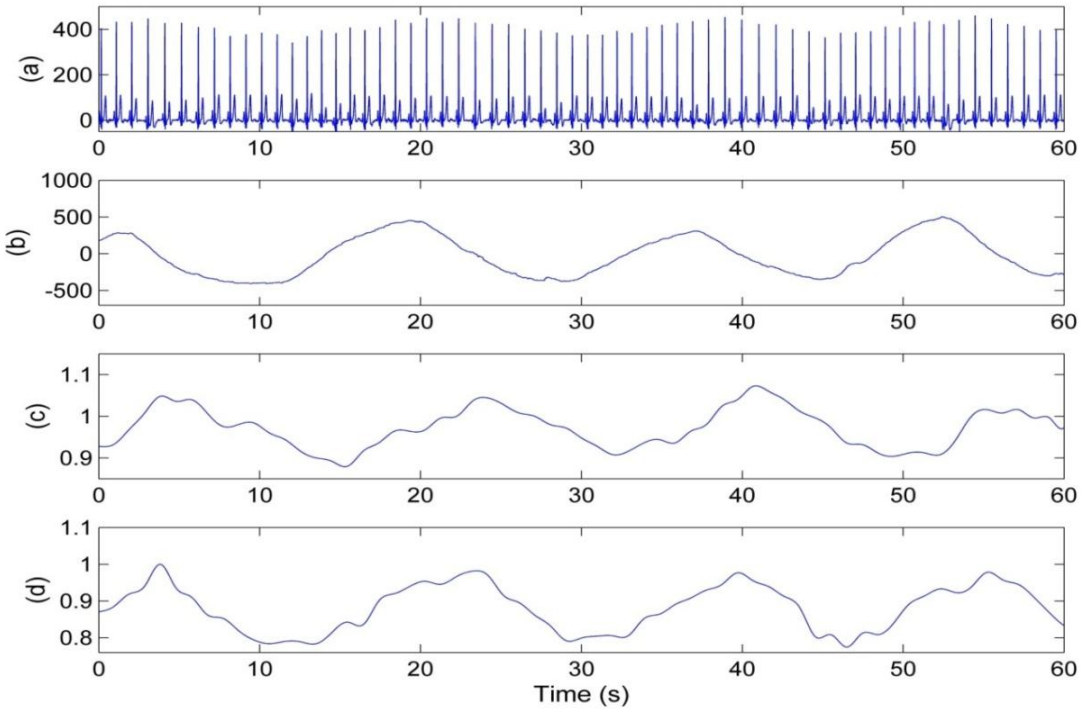

Fig. 2.13 Simultaneously recorded ECG and respiratory signals, and ECG-derived respiratory signals. (a) ECG, (b) recorded (reference) respiration, (c) RR time series (tachogram), and (d) EDR based on R peak amplitudes.

and expiration which causes change in electric impedance of the thorax, and ii) relative motion between the ECG electrodes and the heart vector [103-104]. These mechanisms cause variations in the beat morphology of the heart characterized by the ECG cycle (PQRST). Fig. 2.13 also demonstrates the respiratory signal obtained by monitoring the morphological changes in ECG signal. Here, the morphological variations in ECG caused by the respiration are obtained in terms of the change in amplitude of the R-peak in ECG signal. It can be easily visualized from Fig. 2.13 (a) and (b) that during the inspiration and expiration process, the amplitude of R peaks increases and decreases, respectively. Upon tracing this change in the amplitude of R-peaks, it closely matches with the reference (recorded) respiration (see Fig. 2.13 (b) and (d)).

Hence, these respiratory-induced variations in the ECG signal can be extracted non-invasively for the purpose of deriving the respiration. The waveform derived from ECG resembling the respiratory signal is called ECG-derived respiration (EDR) signal.

2.3.2. ECG-Derived Respiration Techniques

A variety of the EDR algorithms has been developed by the researchers to get a reliable estimation of the respiration [7], [12], [16-29], [159-163]. Most of the EDR methods available in the literature are mainly based on the analysis of RSA [16], [18-19], [28-29], tracking the

respiratory induced variations in beat morphology [7], [12], [16-18], [20-23], [26-29], and filtering of the ECG signal [24-25].

As discussed earlier, the RSA is described as the concomitant variations (modulation) in the heart beat intervals of ECG synchronized with the respiratory efforts [16]. Hence, the extraction of the successive RR intervals can provide a waveform resembling the respiration. It is a well-known fact that the degree of RSA decreases with age of the subject. As a result, the RSA-based method is not suitable to get the EDR signal for the elderly subjects [16].

Some studies used the filtering-based approach to derive the respiration from the ECG signal [24, 25]. The ECG signal is filtered using a band-pass filter in the per-defined respiratory frequency band, and the output waveform is termed as the EDR signal [24]. The filtering based approaches provide the low error at a lower respiratory rate (recorded) but yield high error when the subject is breathing at the higher rate [24]. If the subject is breathing at the lower rate and the detection of any fiducial point (such as R peak) is difficult due to the noise, then the filtering based EDR techniques can provide informative measures of the respiration.

The EMD and wavelet technique are being used into a number of applications, and these techniques have also emerged as tools for time-frequency analysis of the non-stationary signals. The EMD technique is a data-driven technique which determines the oscillatory modes present in the signal, whereas the wavelet approach uses a mother wavelet function to investigate a non-stationary signal. As the ECG is a non-stationary signal, it can be analyzed using both the EMD and wavelet approaches. An application of the EMD and discrete wavelet transform (DWT) approaches for deriving the respiratory signal from ECG is presented in [25]. The DWT technique is computationally viable, but it is less efficient to retain the actual shape of the respiratory signal because the shape of the EDR signal strongly depends on used mother wavelet. A comparison between the EMD and DWT techniques is also presented in [25], and it is found that the EMD technique performs better than the DWT based approach. Also, upon considering the factor of computational complexity, the EMD approach is less suitable for the long segments of data due to the higher computational cost.

In the context of beat morphology, a simple technique based on tracking the amplitudes of R-peaks for deriving the respiratory signal was widely used in the studies described in [7], [20-21]. O'Brien et al. compared three EDR techniques in which two methods are based on single-lead ECG, and the third method is based on two-lead ECG. The performances of these three methods were compared using the correlation coefficient between the EDR and the recorded respiration [7]. The mean value of the correlation coefficient was obtained

higher for the methods based on single-lead ECG as compared to two-lead ECG methods [7]. It was also concluded in [7] that single-lead ECG-based EDR techniques outperform than the two-lead ECG-based method (mean electric axis). Other some complex EDR methods based on beat-morphology extract the changes in QRS area [4], or rotation in the electric axis caused by the respiration [23].

Recently, the PCA technique is employed to evaluate respiratory induced beat-to-beat fluctuation in the ECG signal [26-27]. To derive the respiratory signal from ECG, Langley et al. applied the PCA technique over ECG features such as QRS complex, whole beat, P-wave, and T-wave [26]. The approach in [26] was compared with the methods based on RSA and RPA in terms of the correlation and coherence coefficients. Results demonstrated that the PCA technique outperforms the RSA method, but statistically significant results were not observed when comparing with the RPA technique. Later, Widjaja et al. proposed an improved algorithm for deriving the respiratory signal using the Kernel PCA [27]. However, it was claimed that the KPCA technique provided better results than the PCA and RPA methods, but it is less suitable for the long segments of data due to the higher computational complexity [27].

To compare the RSA & RPA methods, Cysarz *et al*. estimated the respiratory rates for the derived and recorded respiratory signals using a threshold based heuristic approach to identify the valid breath cycles [16]. Two EDR approaches based on the RSA and RPA were used to derive the respiratory signal from the ECG signal, and after that, the derived signals are filtered using a band-pass filter in the frequency band of 0.1-0.45 Hz (6-27 breaths per minute). The authors in work [16] drawn a conclusion that both the RSA and RPA methods can be employed for the younger subjects, but for the elderly subjects, the RPA based method is more suitable as compared to the RSA. In [18], [28-29], the authors also found that the RSA-based EDR method for the estimation of the respiratory signal showed the deficiency in the performance when the experiments were performed in the elderly subjects.

As mentioned earlier that most of the morphological changes in the ECG are originated through the respiration or variations in the position of the heart [47]. It was also reported in [47] that those algorithms which consider the morphological variations of the ECG signal for apnea (associated with the breathing abnormality) detection perform superior to that one based on the spectral analysis of HRV. In the literature, the phenomenon comprising the morphological changes in ECG caused by the respiration is mainly exploited using the RPA method. But, tracking the whole QRS complexes morphology in the ECG signal can benefit in terms of accurate estimation of the respiratory signal in the output. In addition to that, the filtering based EDR methods filters the ECG signal in the respiratory band. Hence, the

filtering methods do not require having prior knowledge of any fiducial point in the ECG signal which is an advantage of the filtering approaches. Therefore, the development of an efficient EDR approach based on filtering of ECG can be useful under the circumstance of severe noise imposed over the R-peaks of ECG signal.

In this thesis, our focus is devoted to the development of efficient EDR techniques based on the concepts of tracking the beat-to-beat morphological variations in the QRS complexes of ECG and filtering of the ECG signal in the predefined frequency band using the Homomorphic filtering. A detailed description of the developed EDR techniques is provided in Chapter 4 of the thesis.

2.4 SLEEP APNEA

This section includes a definitive overview of the sleep apnea disorder and its prevalence in the general population. An overview of the apnea-induced changes in the ECG waveform is also discussed. A detailed description of the methodologies existing in the literature for apnea detection using single-lead ECG is embedded at the end of this section.

2.4.1. Definition and Diagnosis

Sleep apnea is widespread breathing-related disorder characterized by the repetitive events of complete or partial cessation of airflow due to the physical obstruction of the upper airway during sleep [9-10]. An apnea episode is defined as the complete pause in the airflow through the upper airway for at least 10 seconds during sleep. Moreover, based on the breathing efforts present during the apnea episodes, the events of apnea are further classified as central, obstructive, and mixed [10]. A hypopnea event is characterized by a reduction in oronasal airflow by 25 % or 50 % along with a blood oxygen desaturation of 4% [30].

Moving to the epidemiology of sleep apnea, it is a most common breathing disorder during sleep which affects adult men and women worldwide. In an another study [10], it was summarized based on available population studies that the obstructive sleep apnea influences approximately 3 to 7 % adult men and 2 to 5 % adult women in the general population. Systematic surveys, however, that describe the range of disordered breathing during sleep, and the accompanying health deficiency in the general population are not yet presented [10]. Also, due to the limited number of sleep laboratories, most of the population remains undiagnosed [37]. Sleep apnea and hypopnea events can occur even hundreds of times during the whole night sleep, and its repetitive occurrences for a long time can cause some serious cardiovascular and neurological disorders such as hyper-somnolence,

insomnia, hypertension, congestive heart failure, acute coronary syndrome, excessive daytime sleep, memory loss, and poor daytime cognitive performance [31], [37], [76].

In clinical practice, the severity of apnea/hypopnea disorder is evaluated using the apnea-hypopnea index (AHI). The value of AHI is calculated by counting the number of episodes of apnea-hypopnea events during an hour where a subject with a value of AHI greater than 5 (AHI>5) is diagnosed with an obstructive sleep apnea [32]. Based on severity of the sleep apnea diseases in the patient, three stages of apnea-hypopneas are defined based on different ranges of the AHI values as follows: mild apnea/hypopnea (5<AHI≤15), moderate apnea/hypopnea (15<AHI≤30), and severe apnea/hypopnea (AHI>30) [9]. Numerous other measures of the severity of sleep apnea problem including the degree of nocturnal hypoxemia (e.g., average oxyhemoglobin desaturation) and level of sleep disintegration (i.e., arousal frequency) are also considered in the clinical and research grounds [10].

As discussed in the previous chapter, the PSG is a popular tool to diagnose the OSA suspects. In the PSG, for calculating the AHI value, 16 different physiological signals including ECG, electroencephalogram, oxygen saturation (SaO_2), airflow, and respiratory signal are acquired for the whole night sleep. The PSG technique also requires proper nursing with special types of equipment and supervision by an expert to study the pattern of different physiological signals for full night sleep of the patient, and that makes this method very expensive, time-consuming, and uncomfortable for the patients. In the apnea diagnosis, several attempts have been made to standardize the diagnosis process. But, it is challenging to compare various studies of the different populations to understand consequences related to the sleep apnea disorder due to discrepancies in the sample collection, investigation and interpretation of PSG through various laboratories [10].

Even though considered as a ‘‘gold-standard,’’ the PSG method is not without drawbacks. Therefore, an alternative technique is required that can be comfortably applied to the patient for the detection of apnea episodes with the lesser number of equipment. For the detection of sleep apnea, several methods have been developed by the researchers using the lesser number of physiological signals. In the context of automated apnea detection approaches, the ECG signal is commonly preferred physiological signal as it constitutes a significant amount of information about the apnea. Unlike to the direct methods (e.g., Spirometer, Pneumotachograph) for the respiration measurement used in the apnea diagnosis, the ECG signals are less disturbed by the natural breathing of the patient. Moreover, the trend of ECG-based devices for diagnosis of several kinds of diseases encourages the development of home-based healthcare equipment for routine monitoring of the healthiness conditions.

These unique features of ECG signal emphasize to use it for the detection of sleep apnea problem in the patient.

2.4.2. Sleep Apnea Induced Variations in ECG

It has been discussed earlier that the respiratory process affects the characteristics of the ECG signals. Also, the episodes of sleep apnea are also associated with the abnormality in breathing pattern of the patient. It implies that whenever the apnea episode occurs its effect is also reflected in the recorded ECG signal. These changes in ECG due to the apnea episodes can be characterized in two ways: concomitant cycle variations in RR intervals and morphological changes in the ECG beats [47].

Based on the early results, it is a well-known fact that occurrence of the apnea episodes is followed by concomitant cycle variations in RR intervals (or variations in heart rate) of the ECG signal [37] (see Fig. 2.14). This process of cyclic changes in the heart rate results in bradycardia during the apnea episode followed by tachycardia on its cessation. The pattern of bradycardia and tachycardia is thoroughly associated with the occurrence of apnea events. As a result, a number of time and frequency domain features from this pattern

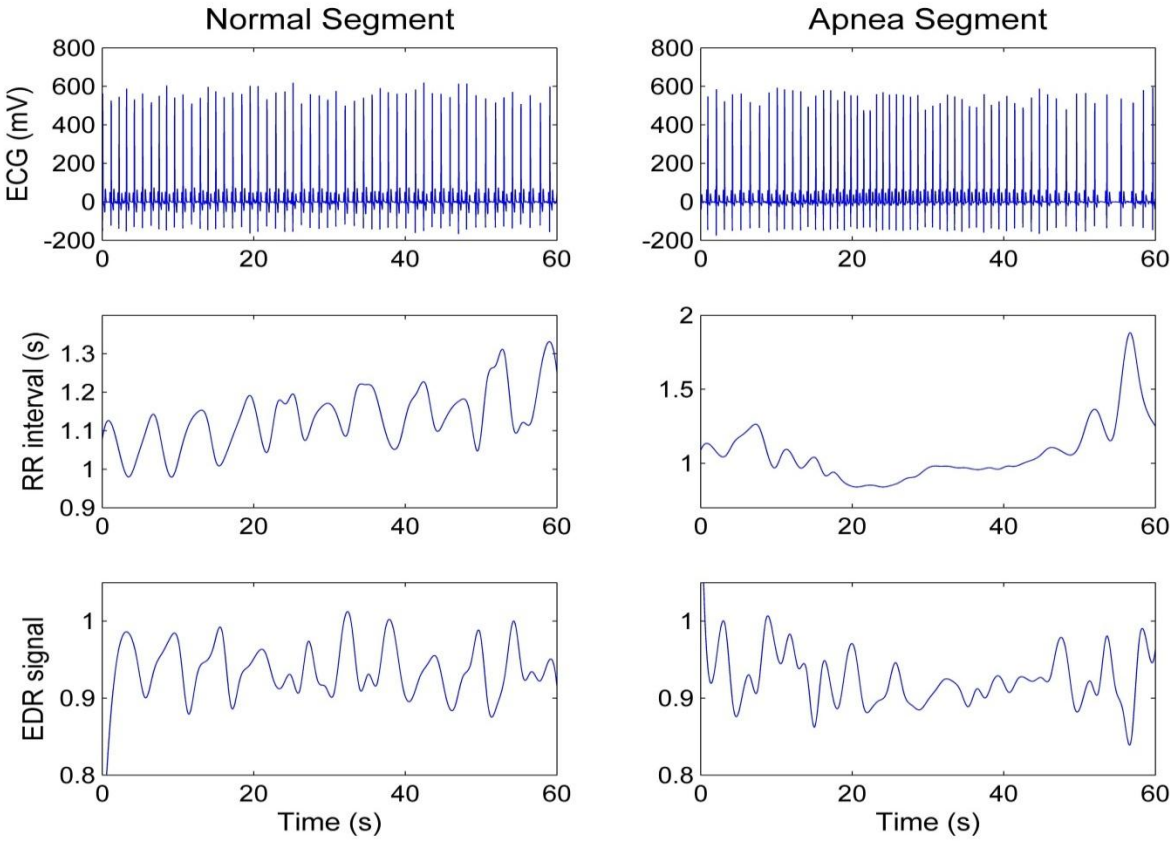

Fig. 2.14 ECG segments of apnea and normal subjects with corresponding RR interval time series (tachogram) and the EDR signals obtained using RPA method

(bradycardia/tachycardia) have been effectively employed to discriminate the apnea subjects from the normal one. From the literature, it is evident that the sympathetic activation increases during the occurrence of apnea episodes which affects HRV of the patient [105]. During apnea episodes, to what extent this sympathetic activation originated by the nerve activity increases and its effect on the heart rate, is still debatable [42]. Furthermore, the spectral components of HRV are also used to investigate the degree of the sympathetic and parasympathetic activities present during the sleep apnea episode in the patient [106-107].

In addition to that, some studies have described the association between the morphological variations in ECG beat and the occurrence of apnea episode [47], [54]. It is reported in [47] that those algorithms which include the features containing information of the morphological variations in the ECG signal caused by the apnea perform superior to that one based on the spectral features of HRV. Additionally, change in the morphology of the QRS complexes of ECG signal during the apnea episodes is also reported in [54]. Consequently, several methods for the detection of apnea problem in the patient using single-lead ECG have been developed in the literature that comprises the time and frequency domain features extracted from the HRV and EDR signals.

2.4.3. Overview of Sleep Apnea Detection Techniques

As mentioned previously, the ECG is a preferable physiological signal for the detection of apnea events in the patient. Therefore, many techniques have been proposed in the literature which extracts various time and frequency domain features from the ECG signal for the classification of apnea and normal subjects [30-53]. Using the ECG signal, most of the apnea detection methods available in the literature used the features derived from the HRV and EDR signals.

Recalling, HRV is an important signal derived from the ECG to detect the abnormalities of respiration pattern due to the apnea episodes [7]. It has been proved from studies that the sympathetic activation increases during the apnea episode [42], and the activities of the autonomic nervous system can be understood by the spectral analysis of HRV. In HRV, high-frequency components (0.15-0.4 Hz) evaluate the parasympathetic activity that is related to the respiratory rhythm whereas the low-frequency components (0.04-0.15 Hz) are usually related to the sympathetic activities [38]. In [34-35], various measures of the characteristics of RR intervals and the EDR signal obtained using the RPA methods have been exploited to discriminate the apnea segments from the normal one. To study the irregularity of HRV, Al-Angari et al. applied sample entropy on the HRV to extract the features for the classification of apnea and normal segments and achieved the classification accuracy of about 72.9% [38]. Some researchers have also studied the non-linear behavior

of the respiratory movements in HRV to detect the episodes of sleep apnea [44-46]. Bock et al. reported that changes in the respiration caused by the apnea episodes in the patient could be presented to have chaotic behavior using the correlation dimension (D2) and the largest Lyapunov exponent [44].

Furthermore, Mendez et al. in [39] monitored the beat-to-beat power spectral densities of the R-R intervals and the QRS complex area of ECG signal to classify the apnea episodes based on a bivariate time-varying autoregressive model using the k-nearest neighbor and neural networks classifiers. Later, Bsoul et al. developed a smartphone-based application 'Apnea MedAssist' for the real-time monitoring of apnea episodes where the features were derived from the RR intervals and the EDR signals based on R peak amplitude [40]. Sannino et al. also proposed a mobile-based approach for sleep apnea detection which extracts a set of IF …THEN rules from the HRV parameters and detection of the apnea event is carried out by comparing the value of computed features with the existing IF …THEN rules [41]. Recently, Song et al. proposed an approach for sleep apnea detection based on the ECG by considering the temporal dependence of signals (R-R time series and EDR signal) using a discriminative hidden Markov model and achieved an accuracy of about 97.1% in the recording based classification [43].

Some studies proved that the event of sleep apnea is associated with the morphological variations in the ECG signal [47-48]. In this regard, an algorithm based on the changes in P-wave of ECG was proposed in [48] to classify the apnea and normal events. In addition to that, Varon et al. recently proposed an automatic algorithm for the detection of apnea episodes using single-lead ECG [31]. In [31], the features were extracted using the PCA applied over the QRS complexes of ECG signal and the orthogonal subspace projection to evaluate the information shared between the EDR and the R-R time series [31].

In the literature, variation in the QRS duration due to the OSA was reported in [54], [108]. In [54], it was concluded that the duration of QRS complexes of ECG prolonged significantly (particularly in women) as the severity of sleep apnea increases. Recently, Bacharova *et al.* studied changes in the QRS morphology caused by the sleep apnea and came up with the conclusion that severity of sleep apnea is highly associated with the maximum value of QRS and a subtle shift of electric axis to the left [108]. Previously, most of the algorithms concentrated towards the use of the amplitude of R-peaks in the ECG signal to get the respiratory related efforts, but the use of the entire QRS complex morphology to acquire the information of the apnea episodes is found to be limited in the literature.

Our study is focused for deriving those features which extract the information related to the morphological changes in the ECG beat (particularly the QRS complex) caused by the

respiration and employ them to discriminate the segments of apnea from the normal one. For this purpose, use of the Hermite basis functions for monitoring the morphological changes in the ECG signal caused by the apnea episodes is exploited in this thesis. Based on the analysis presented in [47], it was reported that the combine features of both the HRV and EDR signals provided the best performance in the apnea detection. Therefore, development of an efficient technique for the detection of sleep apnea problem in the patient using the time and frequency domain features of the EDR signal (obtained using the Hermite expansion of QRS complex) and HRV is also attempted in this thesis. Details of the proposed apnea detection algorithms followed by the performance results of the independent test are provided in chapter 5 of the thesis.

2.5 Relevance to Clinical Diagnosis

Monitoring of the respiration is desirable to examine several diseases such as sleep apnea, stress condition, and some cardiovascular as well as neurological disorders. The respiratory measure is also considered as one of the human vital signs responsible for patient's degradation. Use of the conventional sensor devices for the respiration measurements suffers from several kinds of problems as discussed earlier in chapter 1. It has mentioned here that the respiratory process yields changes in the characteristics of the ECG signal. Therefore, development of an efficient method for a reliable estimation of the respiration using the ECG signal can provide a better alternative for the respiration measurements of the patient.

The ECG is an inexpensive, less complex, and easily available tool to the general population. Unlike to the conventional sensor devices for the respiration measurement, the ECG signal is isolated from the interference of natural breathings of the patient. Also, the use of the ECG signal for deriving the respiratory signal can be beneficial for simultaneous monitoring of the respiration and cardiac activities particularly in the cases where the intensive care and long-term observations are needed.

Sleep apnea, one of the common breathing related problems, is a widespread problem affecting both the adult men and women population worldwide. As mentioned earlier that the PSG method, considered as gold standard, is a very costly, time-consuming method, and it has different interpretations at different places. Moreover, due to lack of sleep laboratories around the world, automated detection of sleep apnea using a fewer number of physiological signals is required. The ECG signal is one of the most preferred physiological signals to assess the occurrence of sleep apnea episodes in the patient. Nowadays, the trend towards the use of single-lead ECG for monitoring various diseases is increasing. Hence, an efficient algorithm for apnea detection using single-lead ECG signal can be useful especially in Holter

monitors as the approach reduces the requirement of additional hardware. Thus, in routine screening for the apnea episodes, the automated method used for the detection of apnea events using single-lead ECG can reduce the cost and complexity of the diagnosis process.

Remarkably, the development of automated techniques for the diagnosis of diseases reduce the clinician efforts in clinical practice which results in better interpretations of a large data with less probability of error. Thus, this thesis comprises the objectives that are directed to achieve reliable EDR and sleep apnea detection techniques using single-lead ECG waveform only. The use of such algorithms encourages the development of low-cost and less complex home-based wearable devices for routinely monitoring of the respiration and sleep apnea problem in the patient.

CHAPTER – 3

HILBERT VIBRATION DECOMPOSITION BASED BASELINE WANDER REMOVAL OF ECG SIGNALS

In the previous chapter, details of the BW noise and its consequences on the clinical interpretation of the ECG signal have been thoroughly discussed. This chapter is devoted to providing an effective solution for the removal of BW from the ECG signal. In this chapter, we propose a new algorithm for the removal of BW from the ECG signal based on the iterative application of the Hilbert transform which is known as the Hilbert Vibration Decomposition (HVD). The performance of the proposed approach is compared with a well-known technique based on the EMD. This chapter is structured as follows. In Section 3.1, a brief overview of the BW noise and the existing solution for the removal of BW from the ECG signal is included to maintain continuity of the work. A detailed overview of the steps required to perform the HVD technique is presented in Section 3.2. The proposed approach based on the HVD technique for the removal of BW from the ECG signal is described in Section 3.3. Data used for the experimental purpose, parameters used for performance evaluation and the simulation results are presented in Section 3.4. Next, the performance of the proposed BW removal technique is discussed in Section 3.5. Finally, Section 3.6 concludes the chapter.

3.1 INTRODUCTION

BW is a major source of low-frequency artifacts in the ECG signal. In general, the BW noise in ECG appears in the frequency range below 0.5 Hz [69-71]. It is mainly caused by the respiratory process, movement of skeleton muscles, variations in the electrode positions, and bias in the instrumentation amplifiers [66-68]. Removal of BW from the ECG signal is necessary for better interpretation of ECG by the clinician and detection of certain types of patterns in the ECG signal for subsequent automatic processing. Also, the BW noise needs to be removed from the ECG signal before investigating the ECG for deriving the respiration and detection of the sleep apnea problem in the patient. The presence of BW may cause morphological variations in the ECG waves such as P, QRS, and T. These morphological variations in ECG may increase the possibility of error in the detection of R peaks positions and the ST segments in the ECG signal.

As discussed in Chapter 2, many techniques to remove BW noise from the ECG signal have been developed in the literature including the high-pass filtering of ECGs, adaptive-filtering

[70-71], [93], adaptive Kalman filter [95], decimated filter banks [77], non-linear filter bank approach [78], morphological approach [88], independent component analysis [87], and moving average filters [94]. These methods, however, possess some limitations in their practical implementation for effective removal of BW from the ECG signal as highlighted in Chapter 2. The EMD technique has also been applied to the ECG signal to estimate the BW noise in it [98]. Using the EMD, the ECG signal can be decomposed into a series of IMFs [78]. These higher-order IMFs obtained by the EMD technique are filtered through a low-pass filter to estimate the BW noise. A similar technique for BW removal based on the EMD technique is also proposed in [89] where the low-pass filter is designed by averaging two basic morphological operators: opening and closing. In the EMD-based approach, the number of IMFs to be low-pass filtered to estimate the BW noise is selected by trial basis [89]. Also, the computational cost of the EMD technique is very high when applying it to a long segment of the data. Due to the limitations of existing techniques, the development of an efficient algorithm is needed which can be easily implemented to estimate the BW noise in ECG at reduced computational cost.

Recently, the HVD technique has attracted the attention of researchers to process the non-stationary signals. Using the HVD, a non-stationary wideband signal can be decomposed into a sum of components with slowly varying amplitudes and frequencies [6]. In the HVD, the first component represents the highest instantaneous amplitude component, and the residue signal contains information of the lower amplitude components [6]. In this chapter, an approach for BW removal based on the HVD technique is proposed. The main motivation for using the HVD technique stems from the fact that the BW component in the ECG signal generally has a significant fraction of the total energy of the ECG signal. Thus, the BW noise in ECG can be estimated using the highest energy component of the HVD technique.

3.2 REVIEW OF HILBERT VIBRATION DECOMPOSITION

Development of the HVD method is based on the iterative application of the Hilbert transform [109], and thus it doesn't contain any spline fitting or complex empirical algorithm. The first component of HVD denotes the largest amplitude component, and the residual signal contains information of the lower amplitude components of a given multicomponent signal [109]. This section includes representation of the multi-component composition of a signal with slowly varying instantaneous amplitude and frequency. The basic idea for estimation of the instantaneous frequency and envelope of the largest energy component from the composition is also discussed in the successive paragraphs. Details of the process and mathematical expressions of the HVD method are based on the original work presented in [109].

A non-stationary wideband signal $g(t)$ can be represented in terms of several mono-components of slowly varying instantaneous amplitude and frequency. Hence, the signal $g(t)$ can be expressed as [109-110]

$$g(t) = \sum_k a_k(t) \cos\left(\int \omega_k(t) dt \right), \tag{3.1}$$

where $a_k(t)$ and $\omega_k(t)$ are the instantaneous amplitude and the instantaneous frequency of k^{th} component, respectively. Here, the parameter k denotes different components having different instantaneous frequency and amplitude. Based on the value of k, the original signal can be defined as a mono-component signal if $k = 1$, or multi-component signal if $k \geq 2$. The instantaneous frequency and amplitude of the components are computed from the analytic signal representation of the original signal $g(t)$.

The analytic signal $A(t)$ for the given signal $g(t)$ can be defined as [110]

$$A(t) = g(t) + i\tilde{g}(t) = A_m(t) e^{i\theta(t)}, \tag{3.2}$$

where $\tilde{g}(t)$ is obtained from the Hilbert transform of the original signal $g(t)$. Here, $A_m(t)$ and $\theta(t)$ denote the instantaneous amplitude and phase of the complex signal which are defined as [110]

$$A_m(t) = \sqrt{g(t)^2 + \tilde{g}(t)^2}.$$

$$\theta(t) = \arctan\left(\frac{\tilde{g}(t)}{g(t)} \right).$$

The instantaneous frequency (IF) $\omega(t)$ can be defined as the first order derivative of the instantaneous phase $\theta(t)$. Thus,

$$\omega(t) = \frac{d\theta(t)}{dt}.$$

Separation of the largest energy components

Some mathematical concerns need to be inspected for a better understanding of the HVD technique. The objective of the HVD technique is to decompose a multi-component signal $g(t)$ into slowly varying amplitude and frequency components. To perform the HVD, the IF and the envelope of the largest energy component need to be estimated. Consider the simplest example of a signal $g(t)$ which is composed of two quasi-harmonics, each of slowly varying amplitude and frequency. Thus, the input signal $g(t)$ can be described as [109]

$$g(t) = a_1(t)e^{i\int_0^t \omega_1(t)dt} + a_2(t)e^{i\int_0^t \omega_2(t)dt}, \tag{3.3}$$

where $a_1(t)$ and $a_2(t)$ are the envelopes (instantaneous amplitudes), $\omega_1(t)$ and $\omega_2(t)$ are the instantaneous frequencies (IFs) of two components. Both the envelope and the instantaneous frequency are the slowly varying functions in the time domain [109]. The IF $\omega(t)$ and envelope $a(t)$ of the signal $g(t)$, composed of two quasi-harmonics, can be defined as [109]

$$a(t) = \left[a_1^2 + a_2^2 + 2a_1a_2 \cos\left(\int(\omega_2 - \omega_1)dt\right)\right]^{1/2},$$

$$\omega(t) = \omega_1 + \frac{(\omega_2 - \omega_1)\left[a_2^2 + 2a_1a_2 \cos\left(\int(\omega_2 - \omega_1)dt\right)\right]}{a^2(t)}. \tag{3.4}$$

The envelope $a(t)$ constitutes two different parts, namely a slow varying part consisting the sum of amplitudes of two components and a fast varying part. Also, the IF $\omega(t)$ in (3.4) consists of the slowly varying part with the asymmetrical deviation about the IF ω_1. However, in principal, the IF $\omega(t)$ also comprises of two parts, i.e., a slowly varying function ω_1 and a rapid varying asymmetrical part. This rapid varying asymmetrical portion of the IF exhibits an important property [109]. Upon integrating the rapid varying oscillatory part of the IF in the full interval $[0\ T]$, considering that $a_1 > a_2$,

$$\int_0^T \frac{(\omega_2 - \omega_1)\left[a_2^2 + 2a_1a_2 \cos(\int(\omega_2 - \omega_1)dt)\right]}{a^2(t)}dt = 0, \tag{3.5}$$

where,

$$T = \frac{2\pi}{\omega_2 - \omega_1}.$$

From the above result, the average value of the rapid varying oscillatory part of IF $\omega(t)$ is equal to zero. Therefore, the average value of IF $\omega(t)$ in (3.4) is represented by only the IF of the first part ω_1 which is the frequency of largest component [109]. Thus, we can write as [109]

$$\langle \omega(t) \rangle = \int_0^T \omega(t)dt = \omega_1(t). \tag{3.6}$$

This important property of the IF provides the simplest path to find the frequency of the largest energy component. The frequency of the largest energy component can be obtained

by smoothing or averaging or low pass filtering of the IF $\omega(t)$. These operations on the IF help to get the frequency of the largest energy component by suppressing the rapid varying asymmetrical part of $\omega(t)$.

Envelope Detection

Similar to radio signal demodulation, the HVD method uses the envelope estimation method known by several other names, synchronous detection, coherent demodulation, in-phase/quadrature demodulation, and signal mixing [109]. For the envelope estimation of known frequency, the composite signal is multiplied by two reference signals differ by the exact phase of 90^0 [109]. After this multiplication operation, the output signal consists of two projections, namely the in-phase and the quadrature phase. The square root of the sum of squares of these projections represents the envelope of the composition [109].

Let a single component $g_{l=r}(t) = a_{l=r}(t)\cos(\int \omega_{l=r}(t)dt)$ with the exact same frequency of the reference signal $\cos(\int \omega_r(t)dt)$ is multiplied with the l components. Then the in-phase projection is represented as [109]

$$g_{l=r}(t) = \sum_l \left[a_l(t)\cos\left(\int \omega_l(t)dt + \varphi_l(t)\right)\right]\cos\left(\int \omega_r(t)dt\right)$$

$$= \frac{1}{2}a_l(t)\left[\cos(\varphi_l(t)) + \cos\left(\int (\omega_l(t) + \omega_r(t))dt + \varphi_l(t)\right)\right], \qquad (3.7)$$

where $a_l(t)$, $\varphi_l(t)$,and $\omega_l(t)$ denote the instantaneous amplitude, the phase and the IF of the l^{th} component, respectively, and $\omega_r(t)$ is the IF of r-reference largest signal.

The quadrature phase projection $\tilde{g}_{l=r}(t)$ of the composite signal is described as [109]

$$\tilde{g}_{l=r}(t) = \frac{1}{2}a_l(t)\left[\sin(\varphi_l(t)) - \sin\left(\int (\omega_l(t) + \omega_r(t))dt + \varphi_l(t)\right)\right]. \qquad (3.8)$$

From (3.7) and (3.8), both the in-phase and quadrature projections of the composite signal consist of two parts in the expression, namely the slowly varying part and the rapid varying asymmetrical oscillation part. Again, the rapid varying oscillatory part in both the in-phase and quadrature projections can be removed by the low-pass filtering operation. After the filtering operation, the slowly varying amplitude part can be obtained by [109]

$$a_{l=r}(t) = 2\sqrt{\langle g_{l=r}(t)\rangle^2 + \langle \tilde{g}_{l=r}(t)\rangle^2}.$$

In the first iteration of the HVD, the component corresponds to the largest energy is obtained and defined as

$$g_1(t) = a_1(t)\cos\left(\int \omega_1(t)dt\right). \quad (3.9)$$

Using the idea of signal shifting, the largest energy component is subtracted from the composite signal to get the residual part after the first iteration. This residual signal is then used as the composite signal to perform the second iteration. These above steps are repeated for each iteration to decompose a non-stationary signal into slowly varying amplitude and frequency components. Other details of the process can be seen in [109].

3.3 PROPOSED METHODOLOGY

As discussed in the previous section, the HVD extracts the mono-components of a signal by using its analytic form where the first component corresponds to the highest instantaneous amplitude [109]. The component with the highest instantaneous amplitude is referred as the dominant component of a given signal. The HVD technique estimates the largest energy component frequency as an average function of the IF of the composition [109]. In summary, the HVD technique is an iterative method where each iteration includes the following three steps: (i) estimation of the instantaneous frequency (IF) of the largest component, (ii) extraction of the corresponding envelope of the largest component, and (iii) subtraction of the largest component from the composite signal.

Let $x(t)$ be the ECG signal which can be represented as a sum of different mono-components with slowly varying instantaneous amplitudes and frequencies. Therefore, by using the HVD technique, the ECG signal $x(t)$ can be expressed as

$$x(t) = \sum_k a_k(t)\cos\left(\int \omega_k(t)dt\right), \quad (3.10)$$

where $a_k(t)$ and $\omega_k(t)$ are the instantaneous amplitude and the IF of k^{th} component, respectively. These two parameters are determined from the analytic signal representation of the original signal which is discussed in the previous section.

By using the HVD technique, the first component separated from the original ECG signal contains the varying highest amplitude, and the residual signal is the combination of other lower amplitude components. Thus, if the signal is decomposed by using the HVD technique then it is true that the energy of component $x_k(t)$ is higher than the energy of component $x_l(t)$ for $l \geq k$.

Since the proposed technique for BW removal stems from the fact that the BW signal in the ECG signal generally has a significant amount of the total energy of the ECG signal. As the HVD technique decomposes a given signal into the highest energy to the lower energy

components, it can be employed to extract the BW noise from the ECG signal. Therefore, it is proposed that the first component $x_1(t)$ obtained from the ECG decomposition using the HVD technique represents BW in it. Hence, using the HVD, the largest energy component $x_1(t)$ of the ECG signal $x(t)$ can be expressed using (3.9) as

$$x_1(t) = a_1(t)\cos\left(\int \omega_1(t)dt\right).$$

The baseline corrected ECG signal $x'(t)$ is obtained by subtracting the estimated BW $x_1(t)$ from the original ECG signal $x(t)$. So we have

$$x'(t) = x(t) - x_1(t). \tag{3.11}$$

Hence, the BW noise in ECG can be estimated by performing the HVD of the ECG signal for single iteration.

3.4 Experiment and Simulation Results

This section includes description of the data used for the experiment and the performance measures used to evaluate the performance of the proposed BW removal technique. The performance results of the proposed BW removal technique for different artificial BW noise added in the original ECG recordings are also presented.

3.4.1. Data

The data from the *MIT-BIH arrhythmia* database [111] are used to evaluate the performance of the proposed BW removal technique. The data consists of 48 half-hour ambulatory ECG recordings. These recordings are recorded from 47 patients and analysed by the *BIH Arrhythmia* Laboratory. The ECG recordings were sampled at 360 Hz with 11-bit resolution over ±5 mV range. To assess the performance of the proposed BW removal technique, three out of 48 recordings, namely 100, 105, and 119, are selected and used in this study.

3.4.2. Artificial Baseline Wander

To assess the actual performance of the proposed method, an artificial BW signal is added in the ECG recordings used in this study. An artificial BW signal is obtained by low-pass filtering of a randomly generated signal [89]. The samples of random signal are uniformly distributed in the range [0, A], where A is the maximum amplitude of the artificial BW. In this work, five different artificial BW signals of different amplitudes (100, 300, 500, 700, and 900) are added in the ECG recordings. The artificial BW noise is used to evaluate the actual performance of the proposed method in the cases of different severity level of BW noise in the ECG signal.

3.4.3. Performance Measures

Quantitative analysis of the performance of the proposed BW removal technique is assessed using two criterions known as the correlation coefficient, and the output signal-to-noise ratio. The correlation coefficient is used to measure the similarity between two signals, whereas the signal-to-noise ratio is used to compare the level of the required signal with the level of unwanted signal (noise).

The correlation criterion (γ) is defined as [89]

$$\gamma = \frac{\langle x, x' \rangle}{\|x\| \|x'\|}, \tag{3.12}$$

where x and x' are the original ECG and the baseline corrected ECG recordings, respectively. Using (3.12), we can make quantitative analysis of how two signals are similar to each other. If the value of γ is 1 then two signals are identical. If the value of γ is -1 then two signals are inverse of each other.

The output signal-to-noise ratio (SNR) is defined as [88]:

$$SNR = 10 \log \frac{\sum_{i=0}^{M-1} x^2(i)}{\sum_{i=0}^{M-1} \left[x(i) - x'(i) \right]^2}, \tag{3.13}$$

where x and x' denote the original clean ECG and the baseline corrected ECG signal, respectively, and M represents length of signal.

3.4.4. Results

To assess the performance of proposed technique, three recordings (100, 105, and 119) of the *MIT-BIH arrhythmia* database are selected as described previously. In each ECG recording, five artificial BWs of different amplitudes (100, 300, 500, 700, and 900) are added to evaluate the performance of the proposed technique in the case of severe baseline distortion. The proposed method is compared with the baseline normalization method based on the EMD with mathematical morphology (EMD – MM) technique as described in [89].

A comparison of the proposed method with the EMD-MM based technique is presented in Table 3.1 in term of the correlation criterion and the output signal-to-noise ratio. The correlation criterion is a good measure of the performance of the techniques for BW removal from the ECG signal. It can be seen from Table 3.1 that in most of the cases the performance of the proposed method is significantly improved than the baseline

Table 3.1 Comparison of the performance results of the proposed method with the EMD – MM based BW removal technique

Recorded ECG signal number in the Data	Amplitude of the artificial Baseline wander (BW)	Correlation (γ)		SNR (dB)	
		Proposed method (HVD)	EMD – MM	Proposed method (HVD)	EMD – MM
100	100	0.966	0.864	12.5	11.9
	300	0.943	0.867	10.6	10.2
	500	0.905	0.871	8.3	7.8
	700	0.879	0.876	6.3	6.1
	900	0.874	0.860	5.01	4.9
105	100	0.984	0.826	16.5	12.8
	300	0.976	0.826	16.1	12.0
	500	0.959	0.841	16.0	12.1
	700	0.935	0.859	15.95	12.4
	900	0.906	0.827	15.9	12.4
119	100	0.965	0.787	13.01	11.1
	300	0.961	0.844	12.5	10.7
	500	0.954	0.789	12.1	10.5
	700	0.943	0.778	12.2	10.3
	900	0.930	0.825	12.1	10.2

normalization method based on the EMD-MM in [89]. In our proposed technique, we considered the input ECG as the clean ECG signal. But, we all know the fact that these signals are recorded using some equipment and the signals can't be recorded in ideal conditions such that no BW noise present in the recorded signal. Therefore, during the BW removal, both the artificial BW and existing BW in the ECG recordings are removed using our proposed approach. In ECG signal no 100, there is large variation in SNR after adding BW of amplitude 100 & 900, but for ECG signal no 105 and 119 for addition same amplitude of BW variation in SNR is not that prominent. This is mainly because the BW contained in the ECG signals 105 and 119 is larger than the artificial BW. The proposed baseline filtering approach removes both the existing and artificial BWs and results in an output signal quite different from the input one. Therefore, there is large variation in SNR for ECG signal no 100

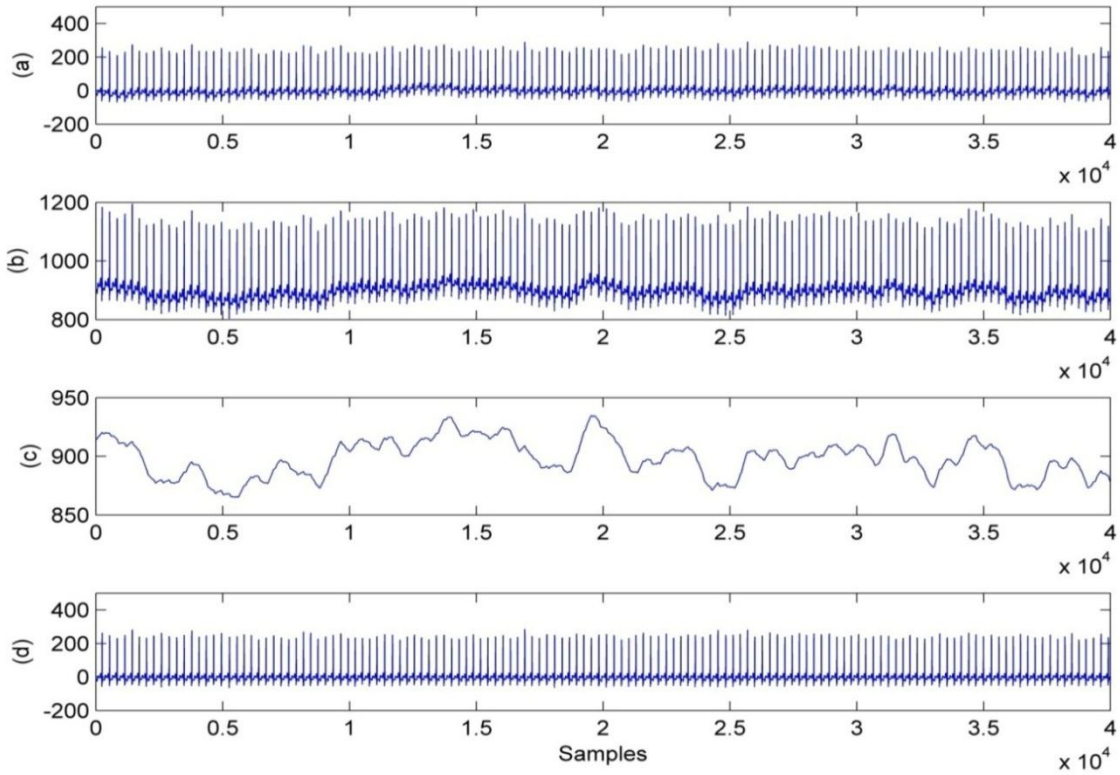

Fig. 3.1 BW noise removal from ECG using HVD technique. (a) Original ECG signal; (b) ECG with artificial BW of amplitude 900; (c) Estimated BW signal; (d) Baseline corrected ECG signal $x'(t)$

after adding artificial BW of amplitude 100 & 900 as compared to that of ECG signal no 105 and 119 for same artificial BW.

An example of baseline corrected ECG signal is shown in Fig. 3.1 where it can be seen that the proposed approach can remove high amplitude baseline distortion from the ECG. In this example, the baseline corrected ECG signal in not identical to the test ECG recording because the proposed method extracts both the artificial and existing BWs in the ECG recording. Fig. 3.2 presents another example of baseline corrected ECG segment using the proposed approach. Here, the ECG segment is selected from a different dataset, known as the *Fantasia* data [115], to examine the applicability of the proposed approach for BW removal over the different data. It is visualized from Fig. 3.2 that the ECG segment itself contains a significant amount of BW noise in it, and therefore no other artificial BW is added in the original ECG signal. It can be observed from Fig. 3.2 that the proposed approach can remove the real-time BW noise added during recording of the ECG signals.

3.5 DISCUSSION

In this chapter, an effective BW noise removal technique based on the HVD method is proposed. The overall performance of the proposed technique for BW removal is significantly

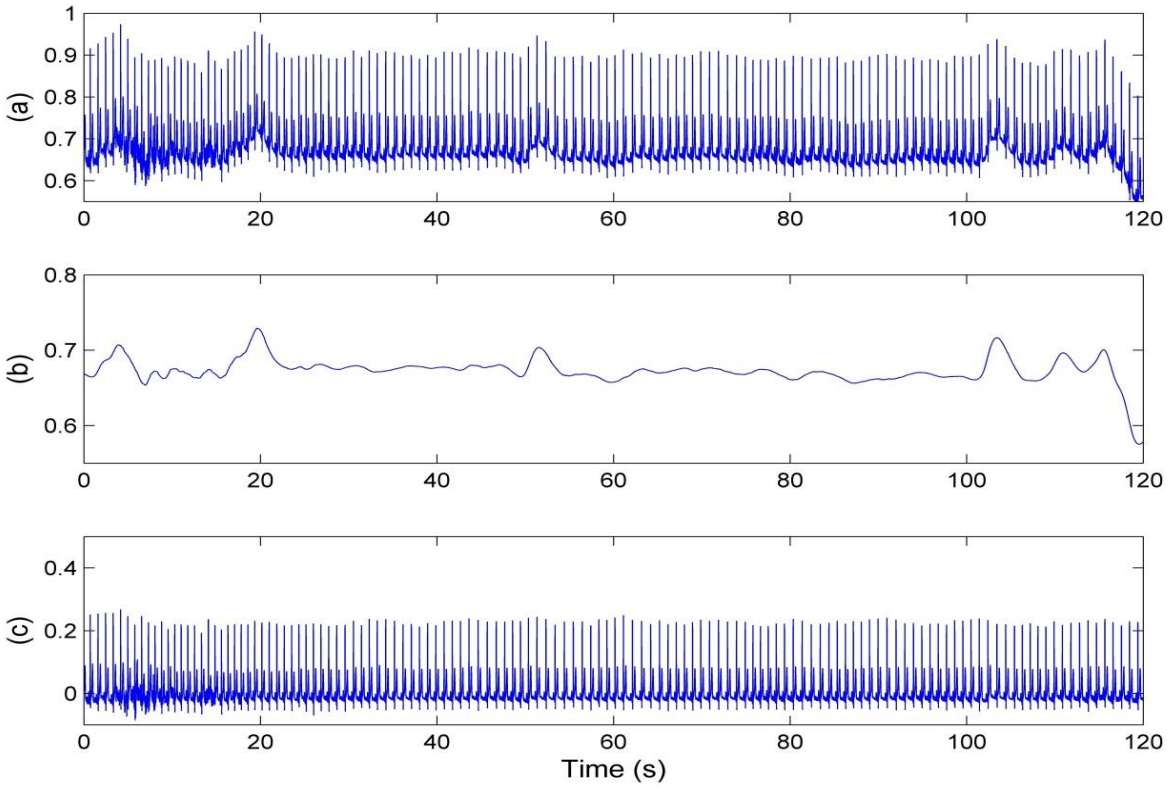

Fig. 3.2 BW removal of an ECG segment selected from subject *F1y03m* of *Fantasia* data. (a) Original ECG segment; (b) estimated BW using HVD method; (c) baseline corrected ECG signal.

improved than the EMD-MM based technique, as described in [89], for different artificial BW signals with similar amplitudes. In the proposed work, the largest energy component of the ECG signal obtained by the HVD corresponds to the BW noise in it. Therefore, it is needed to compute only the largest energy component of the ECG signal using the HVD technique to separate BW from the ECG, and that component can be obtained in the first iteration of the HVD. This shows that the proposed method is computationally efficient as compared to the EMD based approach which is not suitable for long segments of the data due to the higher computational cost.

In the EMD based approach, number of IMFs need to be considered to estimate BW noise of the ECG signal, are selected by trial basis [89], and hence it is considered as a major limitation of the EMD based approaches. In our proposed approach, the highest energy component, obtained in the first iteration of the ECG decomposition using the HVD, estimates the BW noise. Therefore, unlike to the EMD-based technique, the proposed approach is seen to be free from analyzing different components of the HVD which shows the easy applicability of the HVD-based approach for the removal of BW in ECG.

The proposed technique for the filtering of BW noise from the ECG signal operates well when the baseline is always larger than the signal peak value. The large signal DC offset

(mean value) is the required condition for the efficient removal of BW noise from the ECG signal using the HVD technique. If the BW noise is small as compared to the signal peak value, the required condition can be simply achieved by adding to the initial ECG signal a constant value larger than the signal peak value. Therefore, the proposed technique can be effectively applied for the BW removal from ECG in the case where the baseline is small as compared to the signal peak value.

3.6 CONCLUSION

A new technique for the removal of BW from the ECG signal based on the HVD technique is presented. In the proposed technique, the ECG signal is decomposed into a sum of components with slowly varying amplitudes and frequencies using the HVD. It is proposed that the largest energy component (highest instantaneous amplitude component) obtained from the ECG decomposition using the HVD represents the BW signal in it (ECG). Simulation results demonstrate that the proposed technique performs better than the EMD-MM based approach in most of the cases (artificial BWs with different amplitude). Theoretically, it is also observed that the proposed method based on the HVD for BW removal is computationally efficient and performs better under the condition of severe baseline distortion without affecting the actual morphology of the ECG signal.

CHAPTER – 4

ECG-DERIVED RESPIRATION TECHNIQUES BASED ON HOMOMORPHIC FILTERING AND HERMITE BASIS FUNCTIONS

In the previous chapter, the usefulness of the HVD technique for the removal of BW noise from ECG is investigated which is a desirable step before deriving the respiratory signal from the ECG signal. In this chapter, our aim is to develop an efficient technique for a reliable estimation of the respiratory signal from single-lead ECG. For this purpose, two new EDR techniques based on the homomorphic filtering and the Hermite basis functions are presented here. In the first EDR approach, the homomorphic filtering is employed to extract the respiratory component from the ECG signal. In the second EDR method, the respiratory-induced beat-to-beat variation in the QRS complexes of ECG signal is monitored using the lower order Hermite basis functions. The experiments are performed over simultaneously recorded ECG and respiratory signals of the *Fantasia* dataset. The performance of the proposed EDR techniques is compared with the state-of-art techniques to evaluate their effectiveness for the estimation of the respiration using the ECG signal.

This chapter is organized as follows. An introduction pointing out the significance of the EDR methods for the clinical use followed by a brief overview of the existing work is provided in Section 4.1. In Sections 4.2, the use of homomorphic filtering for deriving the respiratory signal from the ECG signal is exploited. The QRS complex approximation using the Hermite basis functions and its use for monitoring the respiratory-induced changes in the QRS complexes of ECG signal is described in Section 4.3. Subsequent subsections of Section 4.2 and Section 4.3 comprise the data used for the experiments, parameters used for the performance assessment, and the results obtained through simulations. A comparison of the results of the proposed EDR techniques with the existing methods is also embedded in the successive sub-sections. The performance results of the proposed EDR techniques and their usefulness in the monitoring of respiration are discussed in Section 4.4. Finally, Section 4.5 concludes the outcomes of this chapter.

4.1 INTRODUCTION

Monitoring of the respiration is essential for the analysis of respiration-related diseases and the cardiovascular problems. The respiratory rate is also used as an important sign of patient deterioration [7]. Respiration can be monitored by direct integrating a sensor device to the

airway or, employing some indirect method, which measures changes in the body volume due to the respiration process. As a matter of the fact that both the direct and indirect methods for the respiration monitoring possess certain limitations, therefore a substantial amount of research is directed to achieve a reliable estimation of the respiration using single-lead ECG. The respiratory-induced morphological changes in the ECG are mainly caused by two factors: i) the electric impedance of thorax is varied throughout the inspiration and expiration due to changes within the lung's volume [27], and ii) relative motion between the ECG electrodes and the heart vector [103-104]. These respiratory related variations in the ECG signal can be extracted to obtain the accurate estimation of the respiratory signal.

Many EDR algorithms have been developed in the literature to estimate the respiration from the ECG signal [7], [12], [16-29]. A majority of the EDR algorithms available in the literature are mainly based on analysis of the RSA [16], [18-19], [28-29], tracking the respiratory-induced variations in the beat morphology of ECG [7], [12], [16-18], [20-23], [26-29], and filtering of the ECG signal [24-25]. These algorithms offer many advantages as well as limitations when implementing to the random population. For example, the degree of RSA in the HRV reduces with age of the subjects which limits the use of the RSA-based EDR method for the elderly subjects. As the noise majorly affects peaks of the R-wave in the ECG signal, the RPA-based EDR method performs poorly in the noisy environments. Therefore, further research needs to be carried out to get a reliable estimation of the respiration so that the EDR signal can be utilized for monitoring several respiratory measures and the diagnosis of the respiratory-related disorders.

In the literature, the RSA-based EDR method is well developed. Therefore, to achieve improved performance than the existing EDR methods, we mainly concentrated on the development of effective EDR techniques based on the concepts of filtering of ECG and tracking the beat-to-beat morphological variations in the ECG signal. Based on the filtering concept, the use of the homomorphic filtering to process the ECG signal for obtaining the respiratory signal is exploited in this chapter. On the other hand, the RPA method monitors the amplitude of QRS complexes to obtain the EDR signal. But, the use of the entire QRS complex morphology to estimate the respiratory signal is observed to be lacking in the literature. Therefore, this work investigates the whole QRS complex morphology using the lower order Hermite basis function to estimate the respiratory signal. These two EDR methods are discussed in detail in the subsequent sections.

4.2 ECG-Derived Respiration using Homomorphic Filtering

In many signal processing applications, the homomorphic filtering approach is used to remove multiplicative noise from the signal [112-113]. Homomorphic filtering is a well-known

technique for the signal and image processing. It involves a nonlinear mapping of the given signal into a different domain where linear filtering can be applied to get desired component [112]. In this section, a new technique based on generalized homomorphic filtering for deriving the respiratory signal from single-lead ECG is presented. The main motivation for using the homomorphic filtering as EDR technique stems from the assumption that the ECG signal is generated by the convolution of the electrical signals of heart activities and the transfer function of an LTI system which is influenced by the respiratory process. Thus, the homomorphic filtering can be applied to the ECG signal to separate the respiratory influence from the cardiac activities. Details of the proposed EDR technique is described in the subsequent sub-sections.

4.2.1. Review of Homomorphic Filtering

The main idea of homomorphic filtering is to transform convolved components of a given signal into the additive form where linear filtering can be applied to separate the desired signal components. The block diagram representation of the homomorphic filtering is shown in Fig. 4.1 which shows the basic steps involved in the process of homomorphic filtering [112]. A block diagram representing the steps involved in deconvolving the input signal in its components is provided in Fig. 4.1(a). The mathematical overview of the entire process involved in the homomorphic filtering is described as follows.

Let $s(n)$ be a given signal which is originated by the convolution of two components $s_1(n)$ and $s_2(n)$, i.e., $s(n) = s_1(n) \otimes s_2(n)$. Here, the operator $\otimes$ denotes convolution operator. The characteristic function $D(.)$, shown in Fig. 4.1(b), conveys the property [112]

$$D[b_1 s_1(n) \otimes b_2 s_2(n)] = b_1 D[s_1(n)] + b_2 D[s_2(n)], \tag{4.1}$$

where b_1 and b_2 are scalars, and the system $D(.)$ is invertible. It can be seen from Fig. 4.1(b) that the signal is first transformed into the Fourier domain using the discrete Fourier transform (DFT) to transform the convolving components of given signal into multiplicative form. Next, the logarithmic operation is performed followed by the inverse discrete Fourier transform (IDFT). The logarithmic operation is used to transform the multiplicative components of the signal into additive form so that the linear operations can be applied. The output of the characteristic system $D(.)$ is called the complex cepstrum $\hat{s}(n)$ which is used as input for the linear system as shown in Fig. 4.1 (a).

The homomorphic system passes the desired signal unaltered, but removes undesired components of the signal with the help of some linear operations. Therefore, the output of the characteristic function $D(.)$ is filtered to remove the undesired signal components using

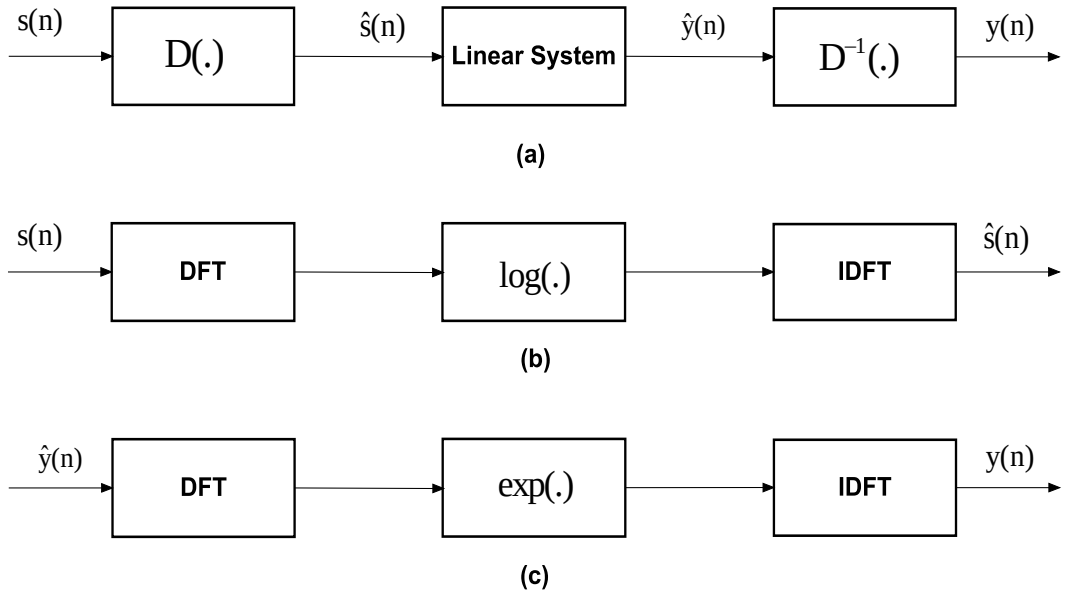

Fig. 4.1 The homomorphic system for deconvolution. (a) Canonical form representation. (b) Characteristic function $D(.)$ (c) $D^{-1}(.)$

the filtering techniques. Thus, we have

$$s(n) = s_1(n) \otimes s_2(n). \tag{4.2}$$

$$\hat{s}(n) = D\{s(n)\} = \hat{s}_1(n) + \hat{s}_2(n). \tag{4.3}$$

It can be seen from (4.3) that the signal components appear in the additive form in the log domain that can be processed using the linear system L to separate undesired signal components from the composite. Hence, the output of linear system $\hat{y}(n)$ can be represented as

$$\hat{y}(n) = L\{\hat{s}_1(n) + \hat{s}_2(n)\} = \hat{y}_1(n) + \hat{y}_2(n). \tag{4.4}$$

For a given input sequence $s(n)$, the DFT operation may possess to have a large number of zeros at the origin that can shift the phase by a large amount. Hence, to retain the information of interest, the linear phase shift needs to remove before getting the cepstrum $\hat{s}(n)$. The signal obtained at the output of linear system has to retain in its original form. For this purpose, first, the DFT operation is applied to the signal $\hat{y}(n)$ as shown in Fig. 4.1 (c). Next, the exponential operation is performed followed by the IDFT to get the desired signal in the output. Hence, the output of inverse homomorphic deconvolution operation can be described as

$$y(n) = D^{-1}\{\hat{y}_1(n) + \hat{y}_2(n)\} = y_1(n) \otimes y_2(n). \quad (4.5)$$

Using the above steps, the desired signal component can be separated from the input signal $s(n)$ using the homomorphic deconvolution operation. In the case of ECG as input to the homomorphic filtering, it is possible to separate the respiratory influence from the ECG signal.

4.2.2. Proposed Approach

Analysis and modeling of the ECG signal using homomorphic filtering was first proposed in [114]. In [114], four types of ECG signals were selected and deconvolved followed the cepstrum filtering to extract more features and components for the diagnostic purpose. In the proposed work, the ECG signal is filtered using the homomorphic filtering approach to estimate the respiratory signal in the output. The EDR using homomorphic filtering is based on the assumption that the ECG signal is convolved output of the electric signals generated by the heart activities and the transfer function of an LTI system which is influenced by the respiratory process. Hence, using the homomorphic deconvolution, the electric activities of the heart and the respiratory influence in the ECG waveform can be transformed into the additive form where the cepstrum filtering can be performed to extract the signal of interest. A block diagram is shown in Fig. 4.2 which describes steps involved in deriving the respiratory signal from ECG using the homomorphic filtering approach.

Let $x(n)$ be the given ECG signal which can be represented using k components such that $x(n) = b_1 x_1(n) \otimes b_2 x_2(n) \otimes \cdots \otimes b_k x_k(n)$, where $b_1, b_2, \cdots, b_k$ are the scalars. Using the de-convolution property of the characteristic system $D(.)$, components of $x(n)$ can be written as

$$D\left[b_1 x_1(n) \otimes b_2 x_2(n) \otimes ..... \otimes b_k x_k(n)\right] = b_1 D[x_1(n)] + b_2 D[x_2(n)] + ... + b_k D[x_k(n)]. \quad (4.6)$$

Here n varies from 1 to M, and M denotes the total number of samples in the ECG signal. It can be observed from (4.6) that the signal components are separable in the cepstrum which are not separable in the original signal $x(n)$. Hence, in the present work, a band pass filter with the pre-defined frequency band is applied on the cepstrum of ECG signal to extract the respiration related influence from the composition. To retain the signal $\hat{y}(n)$ in its original domain, the inverse characteristic function $D^{-1}(.)$ is applied to the filtered signal.

In the homomorphic filtering approach, many possible equivalent representations of the characteristic function $D(.)$ exist, but the use of the DFT provides the most applicable and

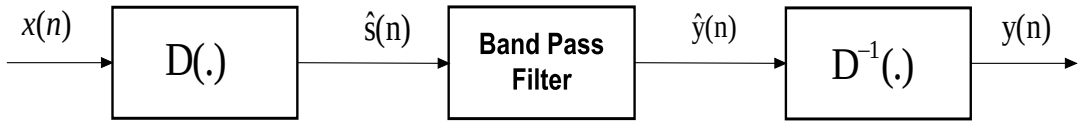

Fig. 4.2. Homomorphic filtering based EDR scheme

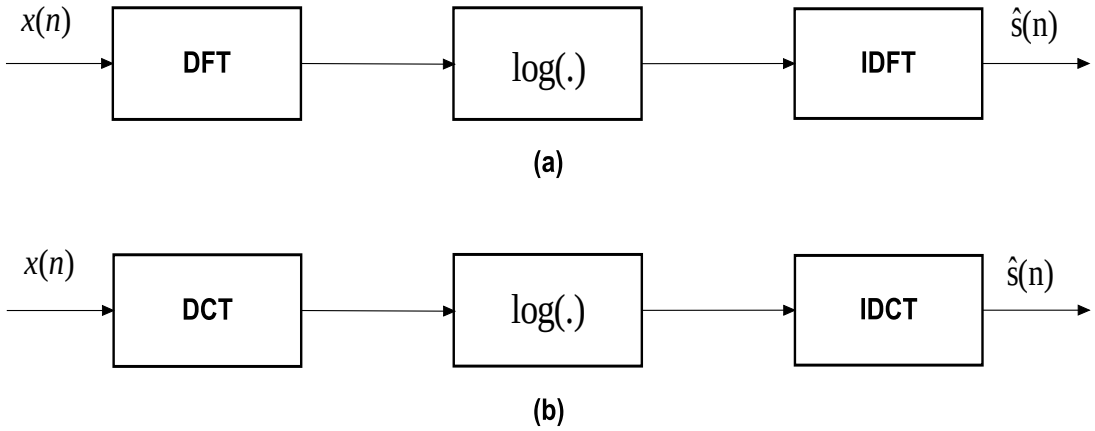

Fig. 4.3 Characteristic function $D(.)$. (a) $D(.)$ based on DFT. (b) $D(.)$ based on DCT

straightforward way to define the characteristic function $D(.)$ (see Fig. 4.1(b)). Instead of using DFT, other transforms can also be used in the characteristic function $D(.)$ to form a generalized representation of the homomorphic filtering. In this work, two operations, namely the discrete Cosine transform (DCT) and the DFT are used in homomorphic filtering to form two characteristic functions to investigate their individual applicability for the EDR extraction. Fig. 4.3 depicts two characteristic functions based on the DFT and DCT used in this work. In the proposed EDR approach, the EDR signals obtained using two characteristic functions based on the DFT and DCT are denoted as R_{DFT} and R_{DCT}, respectively, for further use. For the simulations, the EDR signals are decimated to get a sampling rate of 15 Hz.

4.2.3. Experiment and Simulation Results

a) Data

The data from the *Fantasia* database are used in this work which is available at PhysioNet [115]. The database includes simultaneously recorded ECG and respiratory signals at a sampling rate of 250 Hz. The database contains the recordings of twenty young subjects (21- 34 years old) and twenty elderly subjects (68 – 85 years old). During data acquiring process, all subjects were in resting state and watched the movie *Fantasia* (Disney, 1940) to help maintain wakefulness.

To evaluate the performance of R_{DFT} and R_{DCT}, a 5 minutes segment of the ECG recording of each subject is selected manually in such a way that the selected segment is not affected

by movement artifacts and abrupt changes in the respiration. The recorded respiratory signals are used to assess the performance of EDR signals, and therefore it is also referred as the reference respiratory signal throughout the thesis.

b) Pre-processing of ECG

Before obtaining the EDR signal, the ECG signal needs to be first preprocessed to remove the supply interference and BW noise in it. The ECG signal is first filtered through a notch filter (60 Hz) to remove supply interference. Next, the BW noise in the ECG is removed employing a FIR high-pass filter (20^{th} order) using Kaiser window with a cut-off frequency of 0.05 Hz. The shape of the Kaiser window is determined by a control parameter beta (β). In this work, the value of control parameter is taken as four (β = 4). Now, the preprocessed ECG signal is used for deriving the respiratory signal.

c) Computation of respiratory rate

To estimate the respiratory rate of EDR signals, the counting based approach as described in [16] is employed. The EDR signal is first filtered using a FIR band-pass filter in the frequency band of 0.1 – 0.5 Hz (6-30 breaths per minute). Next, the time series is standardized in order to suppress the impact of large breaths. The standardization of time series is performed by first determining the local maxima points in the time series and then the time series is divided by the value that exceeded the third quartile (75^{th} percentile) of all local maxima [16]. A threshold value is defined to determine the valid respiratory cycles in the time series. Those values of the local maxima in the time series that exceeded the threshold value are considered as the valid respiratory cycles [16]. The average respiratory frequency is estimated by computing reciprocal of the average length of valid respiratory cycles. The value of the threshold is selected as 0.3. Here, the respiratory rate is measured for the windows of duration 60 seconds (s) with 50 s overlap. Therefore, a new respiratory rate is determined every 10 s. To estimate the respiratory rate of the reference (recorded) respiratory signal, the similar process, as discussed above, is used in this work.

d) Performance Measures

The correlation and magnitude squared coherence coefficients are used to assess the similarity between the derived and the reference respiratory signals. On the other hand, to test the agreement between the reference and derived respiratory rates, the respiratory rate error is evaluated. The parameters used to assess the performance of the EDR signals are described as follows.

Correlation Coefficient: The maximum cross-correlation is computed on the minute-by-minute basis such that the value of correlation is not influenced due to the phase difference between the reference respiration (decimated at a sampling rate of 15 Hz) and the EDR

signal [26]. For the reference respiration $R_{ref}[k]$ and derived respiration $R_{EDR}[k]$, the correlation coefficient C can be computed by [7]

$$C = \frac{1/(M-1)\sum_{k=1}^{M-n}(R_{ref}[k]-\overline{R_{ref}[k]})(R_{EDR}[k+n]-\overline{R_{EDR}[k+n]})}{\sqrt{1/(M-1)^2\sum_{k=1}^{M}(R_{ref}[k]-\overline{R_{ref}[k]})^2\sum_{k=1}^{M}(R_{EDR}[k]-\overline{R_{EDR}[k]})^2}}, \quad (4.7)$$

where M is the total number of samples in the signal, n is the shifting parameter, $\overline{R_{ref}[k]}$ and $\overline{R_{EDR}[k]}$ are the means of signals $R_{ref}[k]$ and $R_{EDR}[k]$, respectively.

Magnitude Squared Coherence Coefficient: The magnitude squared coherence coefficient between the reference respiration ($R_{ref}[k]$) and the derived respiration ($R_{EDR}[k]$) denoted by $C_{RE}(f)$ is defined as [27]:

$$C_{RE}(f) = \frac{|P_{RE}(f)|^2}{P_{RR}(f)P_{EE}(f)}, \quad (4.8)$$

where $P_{RR}(f)$ and $P_{EE}(f)$ are the power spectral densities of the signals $R_{ref}[k]$ and $R_{EDR}[k]$, respectively, and $P_{RE}(f)$ is the cross spectral density of the signals $R_{ref}[k]$ and $R_{EDR}[k]$. For calculating the magnitude squared coherence, the range of frequencies around the fundamental respiratory frequency having at least half of the maximum power are considered [27]. Thus, the magnitude squared coherence is determined as the mean coherence in the range of frequencies around the fundamental respiratory frequency [27]. The spectra are obtained by Welch's method using 2^{10} point fast Fourier transform (FFT) with a periodic Hamming window of the length of eight equal sections in both the reference respiratory signal and the EDR signal.

Respiratory rate error: To measure the agreement between the reference (recorded) and the derived respiratory rates, three parameters specifically, the mean absolute error (MAE), average percentage error or relative error (PE), and the concordance correlation (ρ_c) are computed. The parameters MAE and PE are defined as [18]

$$MAE = \frac{1}{J}\sum_{i=1}^{J}\left|bpm^i{}_{EDR} - bpm^i{}_{ref}\right|, \quad (4.9)$$

$$PE = \frac{1}{J}\sum_{i=1}^{J}\frac{\left|bpm^i{}_{EDR} - bpm^i{}_{ref}\right|}{bpm^i{}_{ref}}\times 100\ \%, \quad (4.10)$$

where, bpm_{EDR} and bpm_{ref} are notations for the derived respiratory rate and the reference respiratory rate, respectively, and J denotes the valid windows over the whole dataset used in the experiment.

The concordance correlation between two respiratory rates bpm^{i}_{ref} and bpm^{i}_{EDR} ($i = 1, 2, \cdots, J$) can be defined as [18]

$$\rho_c = \frac{2 s_{rE}}{{s_{ref}}^2 + {s_{EDR}}^2 + (\overline{bpm}_{EDR} - \overline{bpm}_{ref})^2}, \tag{4.11}$$

where,

$$s_{rE} = \frac{1}{J}\sum_{i=1}^{J}(bpm^{i}_{ref} - \overline{bpm}_{ref})(bpm^{i}_{EDR} - \overline{bpm}_{EDR}),$$

$${s_{ref}}^2 = \frac{1}{J}\sum_{i=1}^{J}(bpm^{i}_{ref} - \overline{bpm}_{ref})^2,$$

$${s_{EDR}}^2 = \frac{1}{J}\sum_{i=1}^{J}(bpm^{i}_{EDR} - \overline{bpm}_{EDR})^2,$$

where, $\overline{bpm}_{ref}$ and $\overline{bpm}_{EDR}$ are the mean values of the reference respiratory rate and the derived respiratory rate, respectively. A detailed description of the concordance correlation coefficient can be seen in [120].

Statistical Analysis: To assess whether the results of the proposed EDR technique are significantly better than the other techniques, the Friedman's statistical test is performed. It is a nonparametric statistical test similar to the parametric two-way ANOVA [27]. For multiple comparisons, Tukey's honesty significant difference criterion is used where $p < 0.05$ is considered as statistically significant [27].

e) *Results*

As discussed earlier, the respiratory signal can be obtained by band-pass filtering of the cepstrum of ECG signal. It is a well-known fact that the most of the variation in the respiratory frequency in the resting state lies within the frequency range of 0.2 Hz to 0.4 Hz [24]. Therefore, a 50th order Butterworth band-pass filter with a pass-band frequency range of 0.2 to 0.4 Hz is used to extract the respiratory related influence from the cepstrum of ECG signal. The performance of the proposed EDR technique based on homomorphic filtering (R_{DFT} and R_{DCT}) is compared with two well-known EDR algorithms based on PCA [26] and RPA [16]. In the RPA method, the series of R-peak amplitudes in ECG is computed and then

the time series is transformed into an equidistance time series at the desired sampling frequency using a cubic spline interpolation. In the PCA-based EDR technique, the QRS complexes of ECG beats are used as the features to compute the covariance matrix [26]. In the PCA technique, the eigenvector of the first principal component is used to obtain the EDR signal [26]. In the experiment, for each ECG segment, four different EDR signals are acquired using four different EDR methods: RPA, PCA, homomorphic filtering with DFT and homomorphic filtering with DCT. Therefore, a total of 160 EDR signals are extracted from the selected ECG segments of 40 subjects. The respiratory signal derived using the PCA, and RPA-based methods are denoted as R_{PCA} and R_{Ramp} throughout the study.

EDR signal using homomorphic filtering

Upon comparing the performance of R_{DFT} and R_{DCT} over forty subjects, the Friedman's test shows that no significant difference is observed in the values of the correlation and magnitude squared coherence coefficients for p <0.05. The correlation coefficients for the R_{DFT} and R_{DCT} are obtained as 0.73 and 0.69, respectively and the magnitude squared coherence coefficients for the R_{DFT} and R_{DCT} are obtained as 0.89 and 0.85, respectively. The values for the correlation and coherence coefficients presented in this work are the median values calculated over forty subjects. It can be observed from the simulation results that the EDR technique based on homomorphic filtering using DFT (R_{DFT}) performs better than that based on the homomorphic filtering using DCT (R_{DCT}).

Proposed EDR technique vs. existing EDR techniques

Fig. 4.4 compares the performance of the proposed EDR technique with the existing EDR methods in term of the correlation and coherence coefficients. Friedman's test shows the significant differences in both the correlation and magnitude squared coherence coefficients of the four EDR techniques for the value of p <0.05. The correlation and coherence values for R_{DFT} are found to be statistically significantly better than the R_{Ramp} and R_{PCA}. Although, the correlation and coherence values for R_{DCT} are observed to be statistically significantly better than R_{Ramp}, but the statistical significant difference is not observed when compared the values of R_{DCT} and R_{PCA}. The correlation and magnitude squared coherence coefficients for the PCA-based EDR technique are obtained as 0.67 and 0.85, respectively, and the correlation and magnitude squared coherence coefficients for the RPA based EDR method are obtained as 0.61 and 0.80, respectively. From the above results, it is found that the proposed EDR technique based on homomorphic filtering with DFT (R_{DFT}) performs better than the PCA, and RPA based algorithms in terms of the correlation and magnitude squared coherence coefficients. It can also be noticed from Fig. 4.4 that the correlation coefficients are more bounded in the homomorphic filtering based approach (R_{DFT}) as compared to the PCA and RPA methods. The results are calculated with the part of recordings which do not

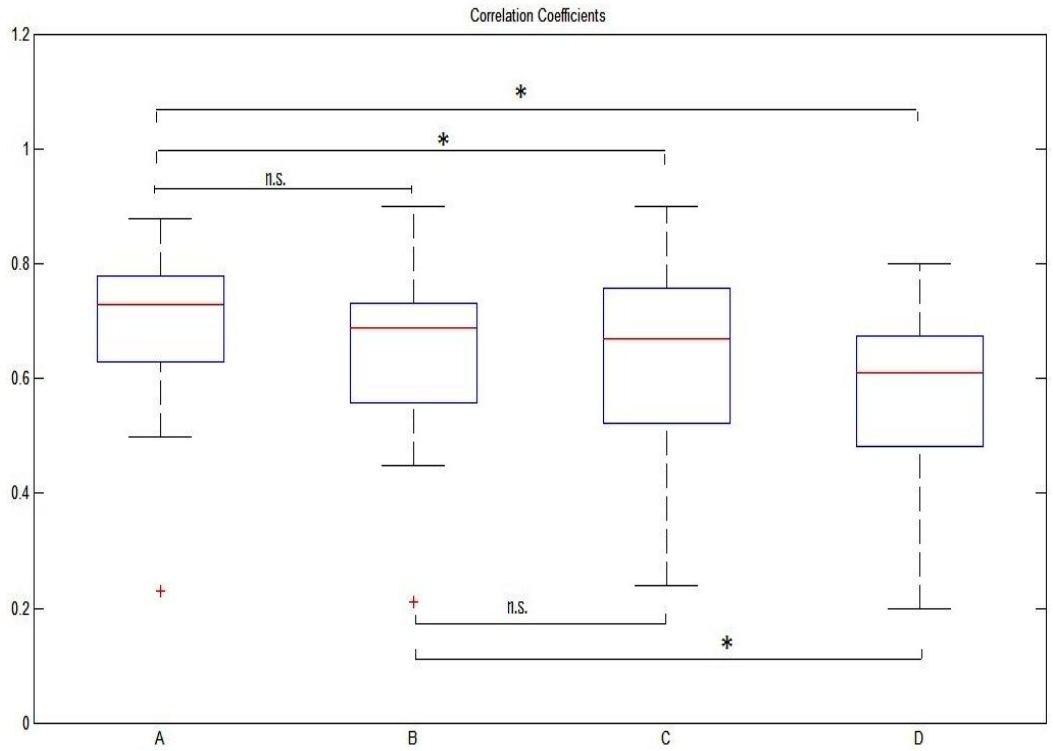

(a)

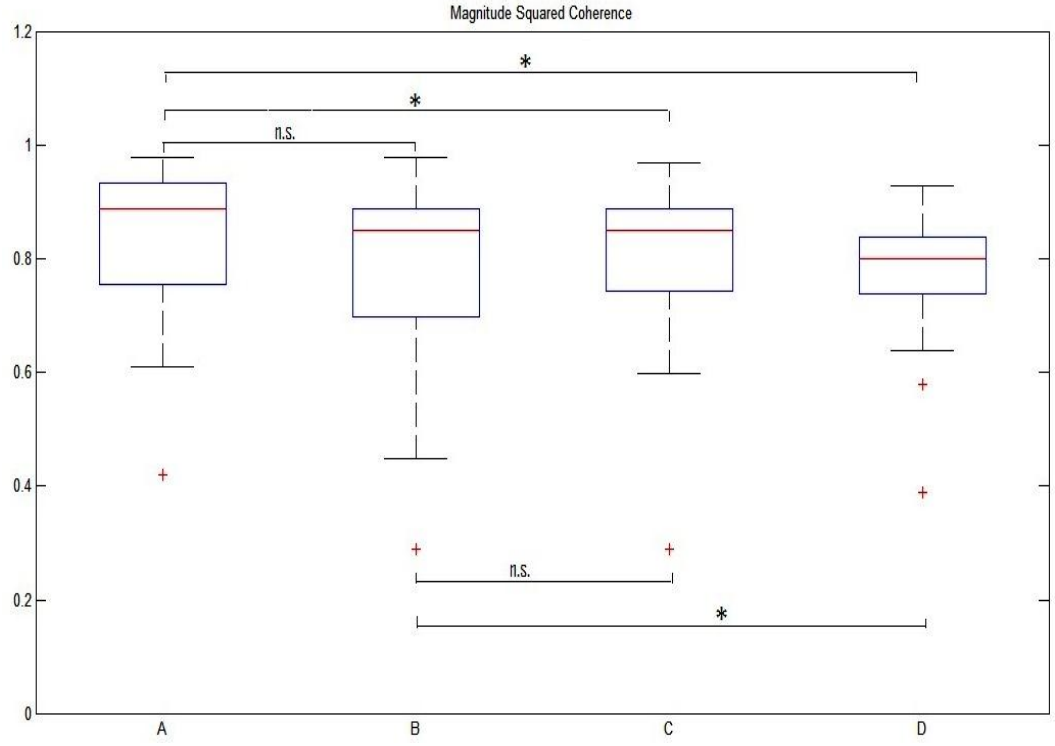

(b)

Fig. 4.4. Comparison of different EDR signals using box plot representation. (a) Correlation coefficients, (b) Magnitude squared coherence coefficients. [Boxes are represented for different algorithms: (A) R_{DFT}, (B) R_{DCT}, (C) R_{PCA}, (D) R_{Ramp}; (box plot showing median, interquartile range, significant differences ($p<0.05$) are indicated by the asterisk (*), n.s.: not significant)]

contain movement artifacts and abrupt changes in the ECG and respiratory signals to get optimum performance. In the case of if the ECG signal is affected by abrupt changes, it is hard to detect the R peaks of the ECG with less probability of error. In that case, the PCA and RPA techniques may provide poor results as compared to the filtering based approach.

A comparison of the respiratory rate error computed between the reference respiration and derived respiration signals for different techniques is also shown in Table 4.1. Using the EDR technique based on homomorphic filtering with DFT, the absolute error (MAE) and relative error (PE) between two respiratory rates derived from the reference and derived respiratory signals is obtained as 0.86 bpm (breaths per minute) and 5.7%, respectively. The respiratory rate error between the R_{PCA} and R_{ref} is determined as 0.85 (5.3%) which is approximately equal to that obtained between the R_{DFT} and R_{ref}. The respiratory rate error for R_{DFT} is found to be lower as compared with the R_{DCT}, and R_{Ramp}. The concordance correlation coefficient value for the R_{DFT} is obtained as 0.76 which is greater than the values obtained for R_{Ramp} (0.755), and R_{DCT} (0.54). Based on the results shown in Table 4.1, it can be observed that the performance of the proposed method using DFT is comparable with the PCA-based technique. Also, the performance of the proposed EDR technique using DFT (R_{DFT}) is found to be better than the R_{DCT}, and R_{Ramp}.

Table 4.1 Comparison of respiratory rate accuracy of different EDR techniques

Algorithms	MAE (bpm)	PE (%)	ρ_c
R_{DFT}	0.86	5.7	0.76
R_{DCT}	1.18	8.4	0.54
R_{PCA}	0.85	5.3	0.80
R_{Ramp}	0.89	5.8	0.76

Fig. 4.5 represents an example of simultaneously recorded ECG and respiratory signals along with the respiratory signals derived using different EDR techniques. It can be visualized from Fig. 4.5 that all the respiratory cycles can be obtained using the proposed EDR technique based on homomorphic filtering with DFT (R_{DFT}). On the other hand, the EDR signals obtained using the PCA and RPA approaches poorly resemble the reference respiratory signal.

Results comparison with different filters

Selection of band-pass filter for the cepstrum filtering is an important issue to address. Therefore, for performance assessment, three band pass filters namely, the Butterworth,

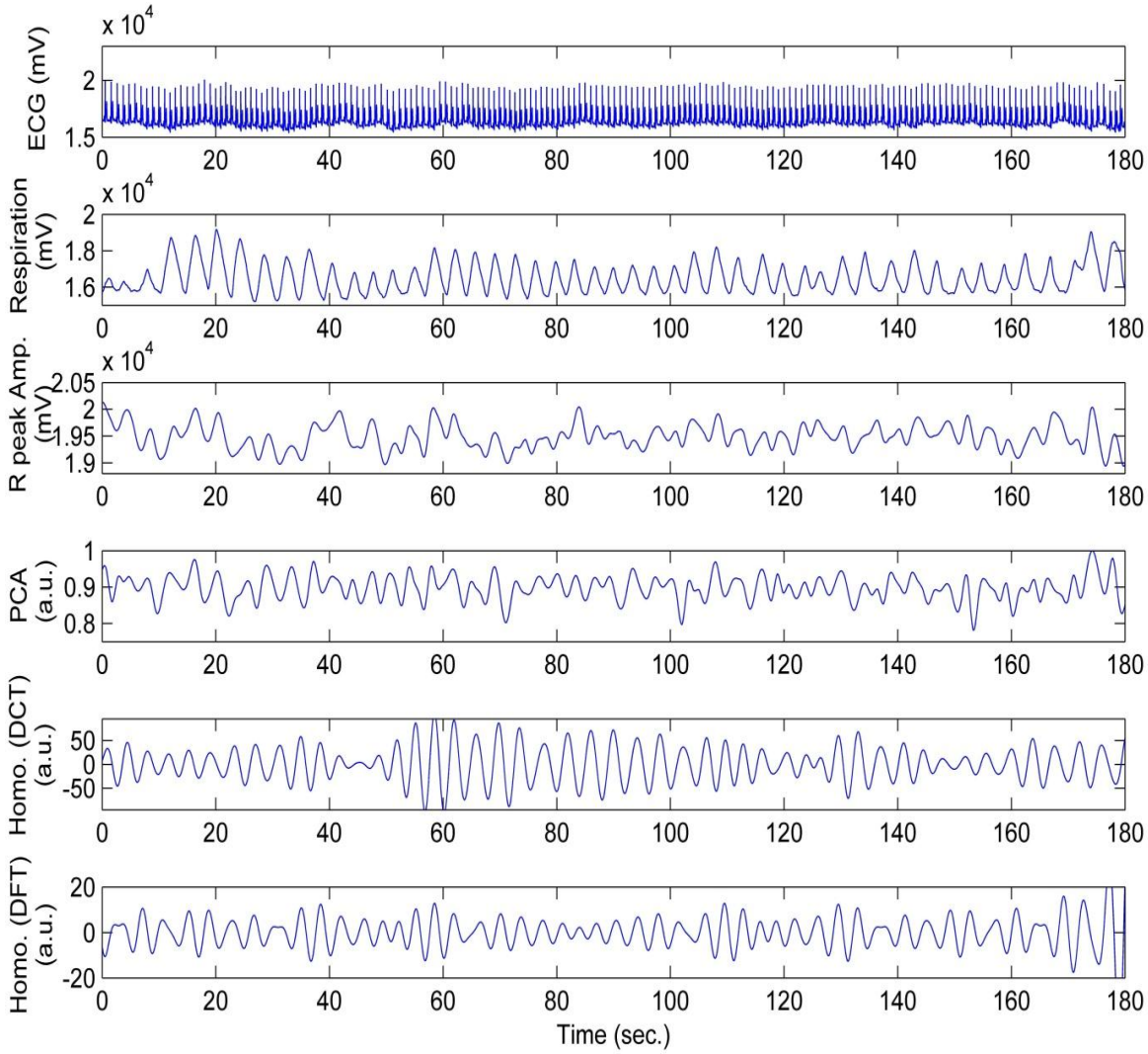

Fig. 4.5. EDR signals obtained using different approaches of the subject *f1y06m* for the duration of 116 to 296 seconds. (a) ECG signal. (b) Reference respiratory signal (R_{ref}). (c) EDR using RPA method, (d) EDR using linear principal component analysis, (e) EDR using homomorphic filtering with DCT, and (f) EDR using homomorphic filtering with DFT

Chebyshev–I and FIR filter with Kaiser Window (β = 0.5)) are used to extract the respiratory component from the ECG signal using the proposed EDR technique with DFT.

However, simulations are performed using the filters, as mentioned above, with different filter orders, but in most of the cases, the filter order of 50 provided satisfactory results. Hence, all experiments are performed by selecting filter order as 50. The performance of different filters is assessed by the correlation coefficient computed between the reference and derived respiratory signals.

The performance of EDR signals obtained employing different filters in the proposed technique varies with different ECG signals. Using the EDR technique based on

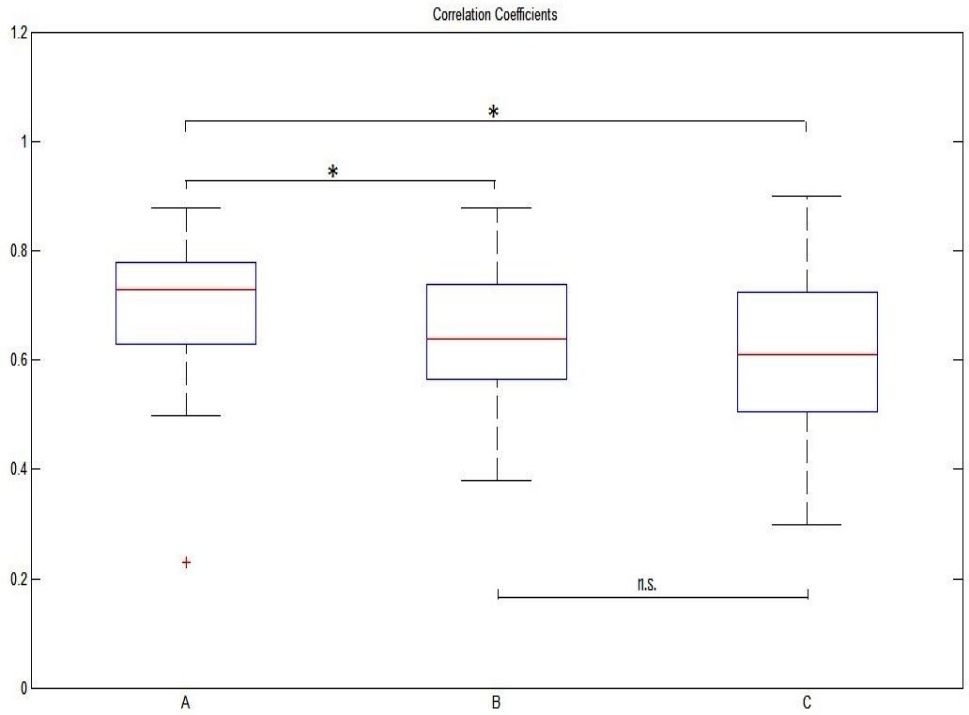

Fig. 4.6. Box plot representation of the correlation coefficients obtained using different types of band-pass filters (A) Butterworth Filter, (B) FIR with Kaiser Window, (C) Chebyshev–I. (box plot showing median, interquartile range, significant differences ($p<0.01$) are indicated by the asterisk (*), n.s.: not significant)

homomorphic filtering with DFT, a box plot representation of the values of the correlation coefficient computed using different filters is shown in Fig. 4.6. The median value of the correlation coefficients for the Butterworth filter is obtained as 0.73. On the other hand, the correlation values for the FIR filter with Kaiser Window and the Chebyshev-I filter are determined as 0.64 and 0.61, respectively. Upon visualizing Fig. 4.6, it can be noticed that the Butterworth filter outperforms as compared to the window based FIR filter and Chebyshev-I filter. The correlation values for R_{DFT} using the Butterworth filter are found to be statistically significantly better than that obtained for the FIR filter with Kaiser window and the Chebyshev-I filter in the homomorphic filtering technique for the value of $p< 0.01$. The correlation values for the FIR filter and the Chebyshev-I filter are not found to be statistical significant different to each other. It is a well-known fact that the Butterworth filter gives a maximally-flat response and it exhibits nearly flat pass band with no ripple. As a result, distortion in the respiratory signal derived using the Butterworth filter is less as compared to other two filters. Therefore, the results obtained using the Butterworth filter are more bounded across the median value as compared to other two filters. Upon investigating the simulation results, it is observed that the EDR signals based on the proposed technique using the Chebyshev-I filter and the FIR filter with the Kaiser Window poorly resemble the reference respiratory signal.

f) Limitation

The main limitation of the homomorphic filtering based EDR technique (also with existing filtering techniques) is associated with the frequency range used for the cepstrum filtering. If the respiratory frequency lies outside the predefined band (0.2 Hz to 0.4 Hz), then the respiratory signal derived using the filtering approach poorly matches with the reference respiration. A possible solution to overcome this problem is based on the accurate adjustment of the lower and upper cut-off frequencies of the band-pass filter. If we select a wider range of frequency, e.g., 0.1 Hz to 0.8 Hz, then other components of the ECG signal may fall in the selected frequency range. As a consequence, the distorted signal (EDR) may be obtained in the output. A suitable selection of band pass filter and filter order also improve the quality of the EDR signal. The order of the filter also affects the EDR signal in terms of the shape of the respiratory cycles. In this work, we have examined the simulation results with varying filter order, and in most of the selected segments from the *Fantasia* data, the Butterworth band-pass filter of order 50 provided satisfactory results.

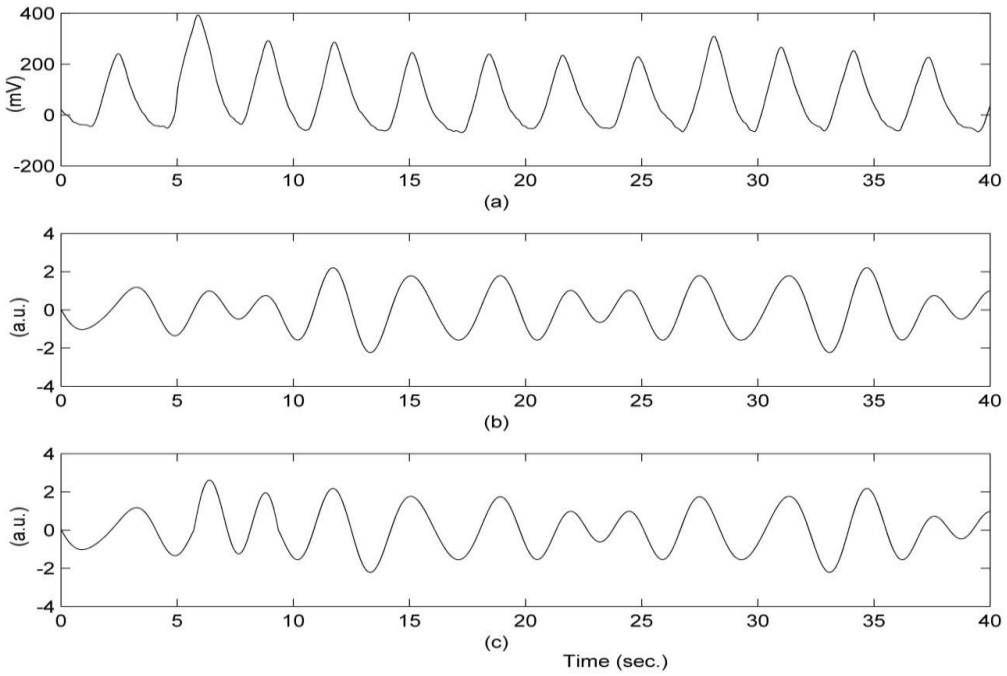

Fig. 4.7 EDR signals using homomorphic filtering of the subject *f2y04m* for the duration of 214 to 254 seconds. (a) Reference respiratory signal. (b) R_{DFT} derived from original ECG recording. (c) R_{DFT} derived from pre-processed ECG.

In this work, we also investigate the improvement or degradation in the respiratory signal derived from the pre-processed ECG signal. Empirically, using the proposed EDR technique, it is observed that the respiratory signal derived from the pre-processed ECG doesn't degrade or improve significantly as compared to the EDR signal obtained from the original ECG. It can be seen in Fig. 4.7 that the respiratory signals extracted using proposed

technique (R_{DFT}) from original ECG and pre-processed ECG are observed to be approximately similar.

4.3 ECG-Derived Respiration using Hermite Basis Functions

In Section 4.2, we have assessed the use of the homomorphic filtering for deriving the respiratory signal using single-lead ECG. In the filtering based EDR techniques, the ECG signal is filtered in the predefined frequency band to get the respiratory signal in the output. As discussed previously, if the respiratory frequency lies outside the predefined frequency band, the output EDR poorly resembles the reference respiration which is the main limitation of the filtering based EDR approaches. To overcome this limitation, we require to developing a more reliable EDR technique that should be independent of the frequency characteristics of the respiration. For this purpose, we focus towards tracking the changes in the morphology of ECG beats for estimating the respiratory signal.

In the context of beat morphology, it is assumed that most of the morphological changes in the ECG signal are originated through the respiration or variations in the body position [47]. It was also reported in [47] that those algorithms which consider the morphological variations of ECG for the purpose of apnea (associated with the respiration) classification perform superior to the approaches based on the spectral analysis. Therefore, in this section, our aim is to derive the respiratory signal through tracking the morphological changes in the ECG beat (particularly the QRS complex) caused by the respiratory process.

The Hermite basis functions have been broadly applied to process the ECG signals for several types of applications such as clustering of QRS complexes of an ECG [117], detection of acute myocardial infarction [118], and beat recognition [119]. In the above studies, the QRS complexes of ECG signal are approximated using the Hermite basis functions for different applications. The use of the Hermite functions to approximate the QRS complexes of any ECG is motivated by the shape similarity between the lower order Hermite basis functions and the QRS complex. As the shape of the lower order Hermite basis functions closely matches with the QRS complex of ECG signal, these functions can be employed to monitor variation in the QRS complex caused by the respiratory process. Therefore, in this section, our aim is to investigate beat-to-beat variation in the QRS complex of ECG signal due to the respiration using the Hermite basis functions for deriving the respiratory signal. We hypothesize that the respiration, which is a quasi-periodic signal, affects the energy in the QRS complexes and the distribution of energy along each component in the orthogonal signal expansion based on the Hermite basis functions of ECG signal also. This hypothesis is based on the fact that most of the variations in the morphology of ECG are induced by the respiratory process and skeleton muscle movements

[47]. The proposed hypothesis is validated through simulation results, and therefore the beat-to-beat variation in the energy of QRS complex during inspiration and expiration can be monitored for a reliable estimation of the respiratory signal from single-lead ECG.

4.3.1 Hermite Decomposition

The QRS complex of an ECG signal can be decomposed in terms the Hermite basis functions due to the shape similarity between the QRS complex and the lower order Hermite functions [117]. The coefficients of the Hermite expansion of QRS complex can be used to characterize the morphological changes in the QRS complex of ECG signal. The Hermite decomposition of a given signal $x(t)$ can be represented using the linear combination of the Hermite basis functions as [117]

$$x(t) = \sum_{n=0}^{N-1} c_n(\sigma)\phi_{n,\sigma}(t) + e_\sigma(t), \tag{4.12}$$

where $c_n(\sigma)$ denote the coefficients of Hermite expansion, $\phi_{n,\sigma}(t)$ are the Hermite basis functions (see Fig. 4.8) defined as [117]

$$\phi_{n,\sigma}(t) = \frac{1}{\sqrt{\sigma 2^n n! \sqrt{\pi}}} e^{-t^2/2\sigma^2} H_n(t/\sigma), \tag{4.13}$$

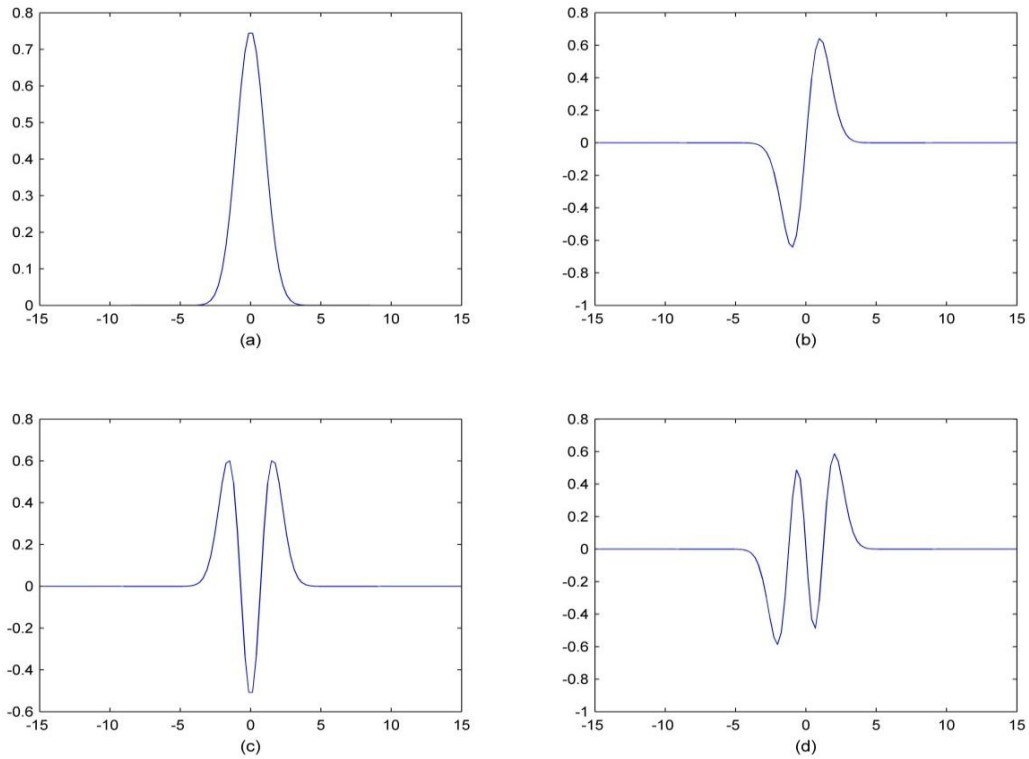

Fig. 4.8 The first four Hermite basis functions for $\sigma = 1$ plotted as a function of time (same scale in all figures). (a) $n = 0$, (b) $n = 1$, (c) $n = 2$, and (d) $n = 3$.

where $H_n(t/\sigma)$ is the n^{th} order Hermite polynomial, N represents the total number of Hermite basis functions used in (4.12), σ is width parameter which approximates the half-power duration of the Hermite functions, and the error is denoted by $e_\sigma(t)$. The error $e_\sigma(t) \to 0$ as $N \to \infty$.

The Hermite polynomials obey recursive relation [117]

$$H_n(x) = 2xH_{n-1}(x) - 2(n-1)H_{n-2}(x). \tag{4.14}$$

where, $H_0(x) = 1$ and $H_1(x) = 2x$

For any fixed value of the width parameter σ, the Hermite basis functions $\phi_{n,\sigma}(t)$ satisfy the orthonormal property

$$\int_{t=-\infty}^{\infty} \phi_{n,\sigma}(t)\phi_{m,\sigma}(t)dt = \delta_{mn}(t), \tag{4.15}$$

where $\delta_{mn}(t)$ is the Dirac delta function. The orthonormal property permits easy calculation of the Hermite coefficients $c_n(\sigma)$ in (4.12). Using the orthonormal property of Hermite basis functions, for a fixed value of the width σ, the coefficients $c_n(\sigma)$ can be calculated using the expression

$$c_n(\sigma) = \int_{t=-\infty}^{\infty} \phi_{n,\sigma}(t)x(t)dt \tag{4.16}$$

The difference between the $x(t)$ and its Hermite expansion in (4.12) is evaluated using the summed square error (SSE) defined as [117]

$$\int_{t=-\infty}^{\infty} \left|e_\sigma(t)\right|^2 dt = \int_{t=-\infty}^{\infty} \left| x(t) - \sum_{n=0}^{N-1} c_n(\sigma)\phi_{n,\sigma}(t) \right|^2 dt. \tag{4.17}$$

The width parameter σ in the Hermite expansion can be varied for minimizing the error defined in Eq. (4.17). The suitable value of σ can be obtained iteratively by minimizing the error between the input signal $x(t)$ and its Hermite expansion. The equations (4.16) and (4.17) represent two different operations between two infinite duration continuous-time signals, but in real life cases it is discretized, and the summation is carried out for a finite number of terms.

4.3.2 Proposed Methodology

This section describes the proposed methodology for deriving the respiratory signal by decomposing the QRS complexes of single-lead ECG using the lower order Hermite basis function. It is generally agreed upon that most of the morphological changes in the ECG caused by the respiration and muscle movements [47]. Hence, we hypothesize that the respiration, which is a quasi-periodic signal, affects the energy in the QRS complexes and the distribution of energy along each component in the orthogonal signal expansion based on the Hermite basis functions of ECG signal also. Therefore, the Hermite decomposition of the QRS complex can play an important role to extract the respiratory-induced variations in the QRS complex of ECG signal. The respiratory related variations in the statistics of the Hermite coefficients can be exploited to derive the respiration signal.

To decompose the QRS complexes of an ECG using the Hermite basis functions, we require extracting the QRS complexes from the ECG. For this purpose, the locations of R-peaks in the ECG signal should be known. In this work, the locations of R-peaks in the ECG are determined by the Pan-Tompkins' algorithm as described in [116]. A window is employed around the R-peak position (centered on R-peak) to obtain the QRS complexes in the ECG. The length of the window is chosen as 200ms to make sure that whole QRS complex is covered even in cases of the artifacts. Next, the extracted QRS complexes are appended with zero signals on both sides of the duration of 100 milliseconds (ms) to make the selected beats close to zero outside the QRS duration [117]. Then after, these QRS complexes are approximated in terms of a linear combination of the lower order Hermite basis functions as given in (4.12).

Let L denote the total number of QRS complexes extracted from a segment of ECG. The Hermite decomposition of the k^{th} QRS complex $xq_k(t)$ can be rewritten with the help of (4.12) as

$$xq_k(t) = \sum_{n=0}^{N-1} c_{n,k}(\sigma)\phi_{n,\sigma}(t) + e_{\sigma,k}(t), \qquad k = 1, 2, \cdots, L. \tag{4.18}$$

The resulting coefficients $c_{n,k}(\sigma)$ obtained from the decomposition in (4.18) characterize the QRS complex of ECG signal. If the energy of the QRS complex of ECG beat varies with the respiration, then this change will also affect the energy of Hermite coefficients. Therefore, the beat-to-beat energy of the Hermite coefficients can be computed for monitoring the respiratory-induced influence in the QRS complexes of ECG signal. The energy in the coefficient obtained from the Hermite decomposition of k^{th} QRS complex $xq_k(t)$ denoted by E_k is obtained as

$$E_k = \sum_{n=0}^{N-1} \left| c_{n,k}(\sigma) \right|^2, \qquad k = 1,2,\cdots,L. \tag{4.19}$$

For an epoch of ECG having L QRS complexes, a vector $\boldsymbol{E}$ can be formed containing the beat-to-beat energy of Hermite coefficients corresponding to L QRS complexes. Thus, the vector $\boldsymbol{E}$ can be expressed as

$$\boldsymbol{E} = \{E_1, E_2, \cdots, E_L\}. \tag{4.20}$$

The vector $\boldsymbol{E}$ represents beat-to-beat variation in the energy of Hermite coefficients for an epoch of ECG having L QRS complexes. The vector $\boldsymbol{E}$, when plotted against time for different epochs, will show variations which resemble the recorded respiratory cycles (see example in Fig. 4.9). This vector $\boldsymbol{E}$ itself is the derived respiratory signal using the proposed approach and is denoted by R_{HDE} for further use.

Furthermore, due to the respiration process, morphological changes (change in amplitude, width of the QRS complex, etc.) occur in the ECG signal which in turn will change the expansion coefficients in the Hermite expansion. Therefore, the energy distribution in the individual component of Hermite expansion of the QRS complexes changes with the

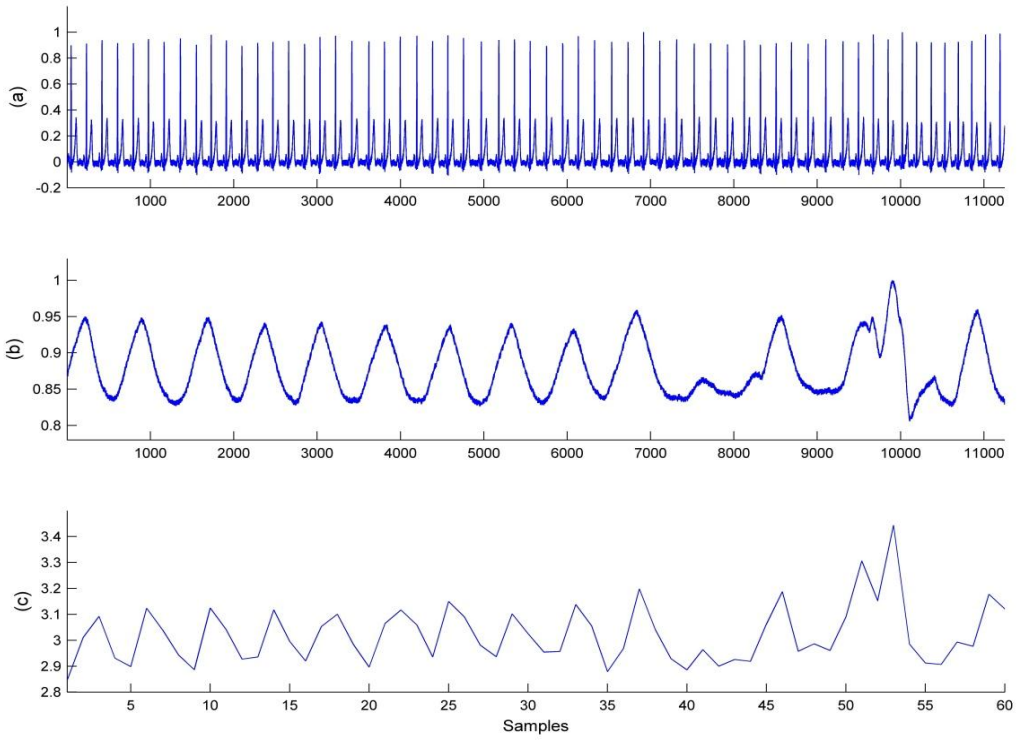

Fig. 4.9 Simultaneous recorded ECG and respiratory signals with the energy values of Hermite coefficients obtained for each QRS complex of ECG segment. (a) ECG, (b) Respiration, and (c) Energy values ($\boldsymbol{E}$) computed using (4.19).

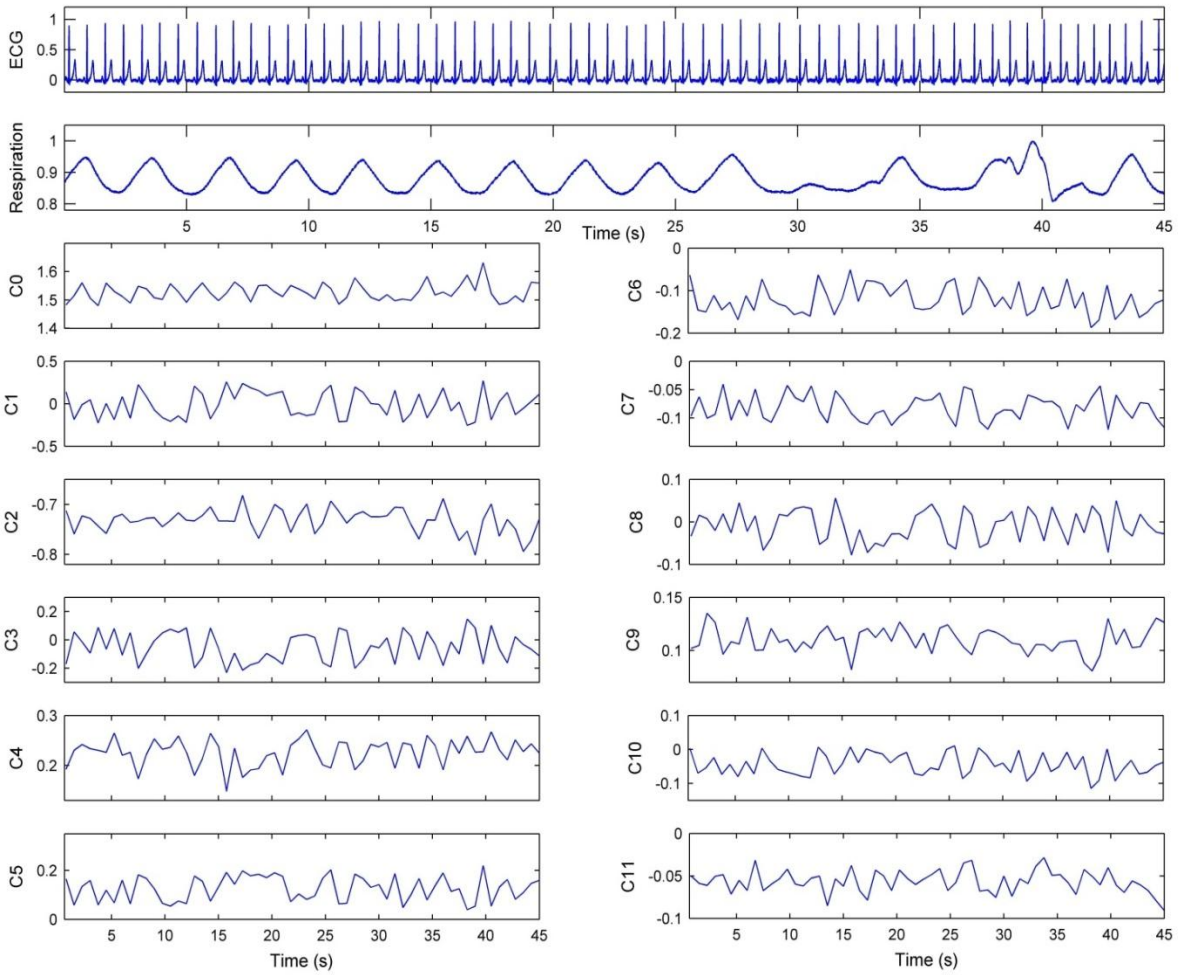

Fig. 4.10 Beat-to-beat variation in the coefficient of Hermite expansion of the QRS complex. [C0 to C11 denote the Hermite coefficients].

respiration which affects the variance of Hermite coefficients. This change in the coefficients of Hermite expansion for the signal under consideration is shown in Fig. 4.10. Hence, the beat-to-beat measure of the standard deviation of Hermite coefficients can also be used to track the respiratory influence in the QRS complexes of an ECG signal.

The standard deviation of the coefficients obtained from the Hermite decomposition of k^{th} QRS complex $xq_k(t)$ denoted by λ_k is computed from

$$\lambda_k = \sqrt{\frac{\sum_{n=0}^{N-1}(c_{n,k}(\sigma)-\mu_k)^2}{N-1}}, \tag{4.21}$$

where μ_k denotes the mean value of the coefficients $c_{n,k}(\sigma)$, and $k = 1,2,\cdots,L$.

For an epoch of ECG having L QRS complexes, a row vector $\boldsymbol{\lambda}$ can be formed to obtain

$$\boldsymbol{\lambda} = \{\lambda_1, \lambda_2, \cdots, \lambda_L\}. \tag{4.22}$$

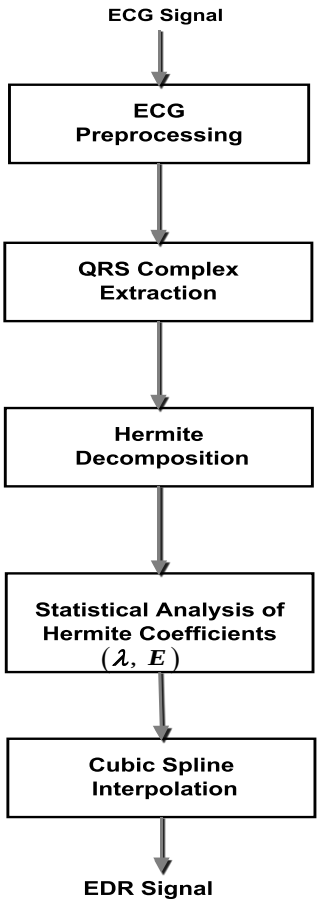

Fig. 4.11 Block diagram representation of the proposed EDR scheme based on the Hermite basis functions

The vector λ, when plotted against time, shows the beat-to-beat variance of the Hermite coefficients closely matching the recorded respiratory signal. The EDR signal obtained using the vector λ is denoted by R_{HDSD} for further use. It may be mentioned here that the vectors E and λ derived here for entire QRS complexes can be viewed as the discrete time signals which can be modeled as the input of an LTI filter producing the required respiratory signal. We propose to model this filter as the first order/higher order interpolation filters [155]. In this work, the vectors E and λ are resampled at a sampling rate of 4 Hz using a cubic spline interpolation. The resultant signals are further used for the experimental purpose. A block diagram is also presented in Fig. 4.11 to have a clear overview of the proposed scheme based on the Hermite basis function for deriving the respiratory signal from single-lead ECG.

4.3.3 Experiment and Simulation Results

This section comprises of details of the dataset used in the analysis, data preprocessing steps to get the clean ECG signal and removal of the ECG segments with abnormal amplitude peaks from the recordings. Various parameters used for performance

measurement are also mentioned. The performance of the EDR signals obtained using our proposed method is then presented.

a) Data

The performance of the proposed EDR technique is evaluated using the *Fantasia* database [115]. Detailed information of the data is described in Section 4.2.3 of this chapter. For the experimental purpose, the ***entire*** *Fantasia* dataset is used here to examine the performance of the proposed EDR technique based on the Hermite basis functions.

b) Data preprocessing

In general, the recordings available in the dataset contain the BW noise and some abnormal amplitude peaks which need to be eliminated before the analysis. The proposed algorithm is based on the identification of the respiratory-induced morphological variation of the QRS complexes of ECG signal. Therefore, any abnormal peaks in the QRS complexes or miss-detected R-peaks may result in the large variation in the values of the coefficients, and that can distort the output respiratory waveform.

To remove the BW noise from ECG signal, two median filters of widths 200 milliseconds (ms) and 600 ms, respectively, are applied in cascade form to process the ECG [73]. The P and QRS waves are removed using the first median filter of width 200 ms, and the output is again filtered using the second median filter of width 600 ms to remove the T waves. The output of second median filter represents the low-frequency BW, and it is subtracted from the original ECG signal to obtain the BW removed from the ECG.

To remove the ECG segments with the abnormal amplitude peaks, a heuristic criterion is proposed here which analyzes each ECG epoch of 60s duration. The main steps of the criterion are as follows.

1. Each epoch of ECG is segmented using a window of 1s duration to get 60 *frames*.
2. The L_∞ norm of the amplitudes is determined for each *frame*, and a *vector* is formed containing 60 norm values obtained from 60 *frames*.
3. Now we compare the maximum value of elements in the *vector* with the median value of the *vector*. If the maximum value of the *vector* is greater than two times of the median value of the *vector*, then that particular epoch is discarded.

However, the proposed criterion is not a complete solution to obstruct all ECG segments with the abnormal peaks in the experiment, but it can eliminate a significant fraction of the ECG segments with abnormal amplitude peaks in the *Fantasia* datasets.

c) Performance measures

The performance of the Hermite basis functions based EDR approach is assessed using the correlation coefficient, the magnitude squared coherence coefficient and agreement between

the respiratory rates of the derived and reference respiratory signals. All these performance measures have been described earlier in Section 4.2.3 (‘*Performance Measures*’). Computation of the respiratory rates of the derived and reference respiratory signals is carried out using the procedure described in Section 4.2.3 (‘*Computation of Respiratory Rates*’).

d) Comparison of EDR techniques

This section discusses the performance results of the proposed EDR technique based on the correlation coefficient, magnitude squared coherence coefficient, and error in the respiratory rates estimated from the reference respiration and the EDR signals. The performance results of the proposed EDR technique are compared with three well recognized EDR algorithms based on the PCA [26], RPA [16], and RSA [16]. Details of the PCA and RPA methods are provided earlier in Section 4.2.3 (‘Results’). In the RSA-based EDR method, first, the R-R intervals are obtained by calculating the difference between the positions of successive R-peaks. Thereafter the time series is transformed into an equidistance time series at a sampling frequency of 4 Hz using a cubic spline interpolation. Here, for the simulations, the EDR signals are resampled at a frequency of 4 Hz using a cubic spline interpolation. The reference respiratory signal is also resampled at 4 Hz after applying an anti-aliasing filter.

The Hermite decomposition of the QRS complexes of ECG is performed using 12 lower order Hermite basis function (i.e., $N = 12$). The optimal value of the parameter σ is obtained for each epoch of ECG through a step-by-step increment in σ by minimizing the error in (4.17). We compute the error in (4.17) for different values of σ varying from 0.1 to 15 with increments of 0.1, and the value of σ for which the Hermite expansion error is minimum is used to compute the Hermite coefficients for deriving the respiratory signal.

Fig. 4.12 depicts the correlation measured between the reference and derived respiratory signals obtained using different EDR methods. The median values of the correlation coefficients computed for different EDR methods are determined as: R_{HDSD}: C = 0.693, R_{HDE}: C = 0.688, R_{PCA}: C = 0.664, R_{Ramp}: C = 0.661 and R_{RSA}: C = 0.479. Using Friedman’s statistical test, the significant difference is noticed in the values of correlation coefficients obtained for five different EDR signals for the value of $p<0.001$. Upon comparing the EDR signals obtained using the proposed approach, the significant difference between the correlation values computed for R_{HDSD} and R_{HDE} is not observed for the value of $p<0.05$. The correlation values obtained for both the R_{HDSD} and R_{HDE} are observed to be significantly greater than the correlation computed for the R_{PCA}, R_{Ramp}, and R_{RSA} for $p<0.01$, $p<0.01$, and $p<0.0001$, respectively. Hence, it can be observed from the correlation values that both the

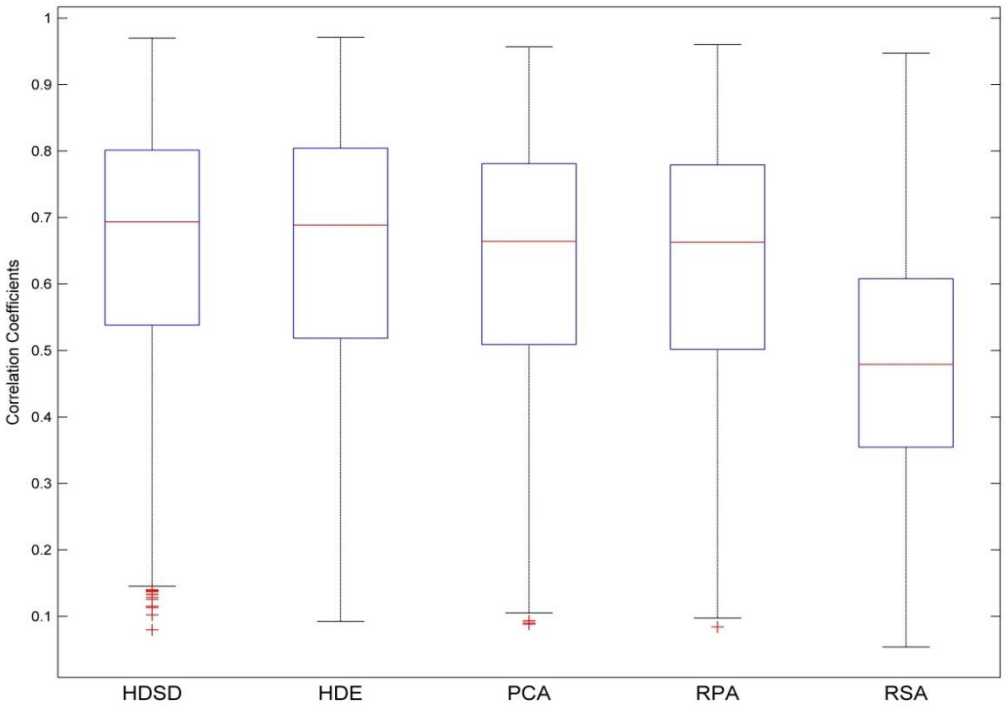

Fig. 4.12 Boxplot illustration of the correlation coefficients determined for different EDR methods [HDSD = The EDR obtained through the beat-to-beat measure of the standard deviation value of Hermite coefficients (R_{HDSD}), and HDE = The EDR obtained through the beat-to-beat measure of the energy in Hermite coefficients (R_{HDE})].

EDR signals, R_{HDSD} and R_{HDE}, better resemble the reference respiratory signal as compared with the respiratory signals derived using the existing methods.

To measure how the derived and reference respiratory signals are similar in frequency, the coherence coefficient is computed. Fig. 4.13 depicts the coherence coefficients computed between the reference respiration and EDR signals. The median values of the coherence coefficients for the R_{HDSD}, R_{HDE}, R_{PCA}, R_{Ramp} and R_{RSA} are obtained as 0.846,0.837, 0.827, 0.823, and 0.74, respectively. Using Friedman's statistical test, the coherence values for different EDR methods found to be statistical significant different for the value of $p<0.01$. Upon comparing the EDR signals obtained using the proposed approach, the significant difference between the coherence values computed for R_{HDSD} and R_{HDE} is not observed for the value of $p<0.05$. The coherence values obtained for the R_{HDSD} and R_{HDE} are observed to be significantly greater than the R_{PCA}, R_{Ramp}, and R_{RSA} for the values of $p<0.01$, $p<0.01$, and $p<0.0001$, respectively. Hence, based on the correlation and coherence coefficients, it can be concluded that the EDR signals, R_{HDSD} and R_{HDE}, obtained using our proposed approach better resembles the reference respiratory signal as compared with the existing methods.

To compare the estimated respiratory rates of the derived respiration and reference respiration signals for all subjects, the mean absolute error, and average percentage error

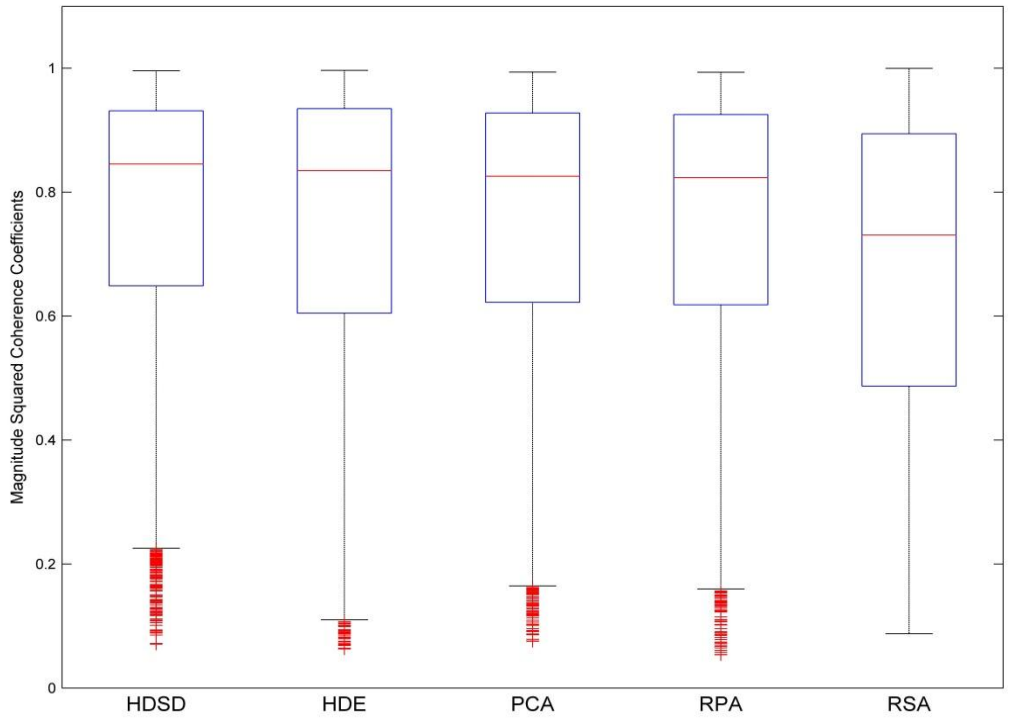

Fig. 4.13 Boxplot representation of the magnitude squared coherence coefficient values obtained for different EDR methods.

are shown in Table 4.2. The concordance correlation is computed to quantify the agreement between the respiratory rates of the reference and derived respiration signals and is also shown in Table 4.2. It can be seen from the comparison presented in Table 4.2 that the lowest absolute error (MAE) and relative errors (PE) are obtained by the proposed method (R_{HDSD}) as 1.20 bpm and 9.0 %, respectively. However, the performance of R_{HDE} is observed to be marginally lesser as compared to the R_{HDSD}, but it outperformed the EDR signals obtained using the existing methods by achieving the lower values of MAE and PE as 1.22 bpm, and 9.1 %, respectively. Also, the EDR signal using the proposed method (R_{HDSD}) provides a better agreement in the respiratory rates with a higher value of the concordance correlation coefficient (ρ_c = 0.76).

The error in respiratory rates estimated from the reference respiration and derived respiration signals for the young and elderly subjects is presented in Table 4.3. It is a well-known fact that the RSA-based EDR approach is a better choice than the RPA method for the estimation of the respiratory rate in the young subjects, but it is not suitable for the elderly population [16]. This variation in the performance of the RSA method for the young and elderly subjects can also be observed from the experimental results illustrated in Table 4.3. Based on the results presented in Table 4.3, the EDR signals obtained using our proposed technique provided a better agreement in the respiratory rates for the elderly subjects as

Table 4.2 Mean absolute error, average percentage error, and concordance correlation measured over entire *Fantasia* dataset

Algorithms	MAE (bpm)	PE (%)	ρ_c
R_{HDSD}	1.20	9.0	0.76
R_{HDE}	1.22	9.1	0.75
R_{PCA}	1.36	10.1	0.71
R_{Ramp}	1.30	9.5	0.73
R_{RSA}	1.51	10.4	0.67

Table 4.3 Comparison of errors in the estimated respiratory rates for the young and elderly subjects of *Fantasia* dataset

Algorithms	Young Subjects			Elderly Subjects		
	MAE (bpm)	PE (%)	ρ_c	MAE (bpm)	PE (%)	ρ_c
R_{HDSD}	1.37	10.8	0.71	1.01	7.1	0.81
R_{HDE}	1.38	10.9	0.70	1.02	7.1	0.81
R_{PCA}	1.55	12.2	0.65	1.14	7.9	0.78
R_{Ramp}	1.47	11.5	0.68	1.10	7.5	0.79
R_{RSA}	1.26	9.2	0.79	1.81	11.9	0.50

compared to the existing methods. On the other hand, in the case of young subjects, only the RSA method performed better than our proposed EDR algorithm.

Fig. 4.14 shows the histogram plot of absolute error in the respiratory rates computed between the reference respiration (R_{ref}) and the EDR signals (R_{HDSD} and R_{HDE}) using the entire *Fantasia* dataset. It can be seen from Fig. 4.14 that, for both the EDR signals (R_{HDSD} and R_{HDE}), around 79% of the errors in the respiratory rates are under 2 bpm that shows the effective performance of the proposed EDR technique. Based on the above results, it can be stated that the performance of both the EDR signals (R_{HDSD} and R_{HDE}) obtained using the proposed algorithm is found approximately analogous. Fig. 4.15 shows an example of simultaneous recorded ECG and respiratory waveforms along with the derived respiratory signals obtained using different EDR methods. It can be visualized from Fig. 4.15 that the EDR signals acquired using our proposed method (R_{HDSD} and R_{HDE}) better matches the reference respiration.

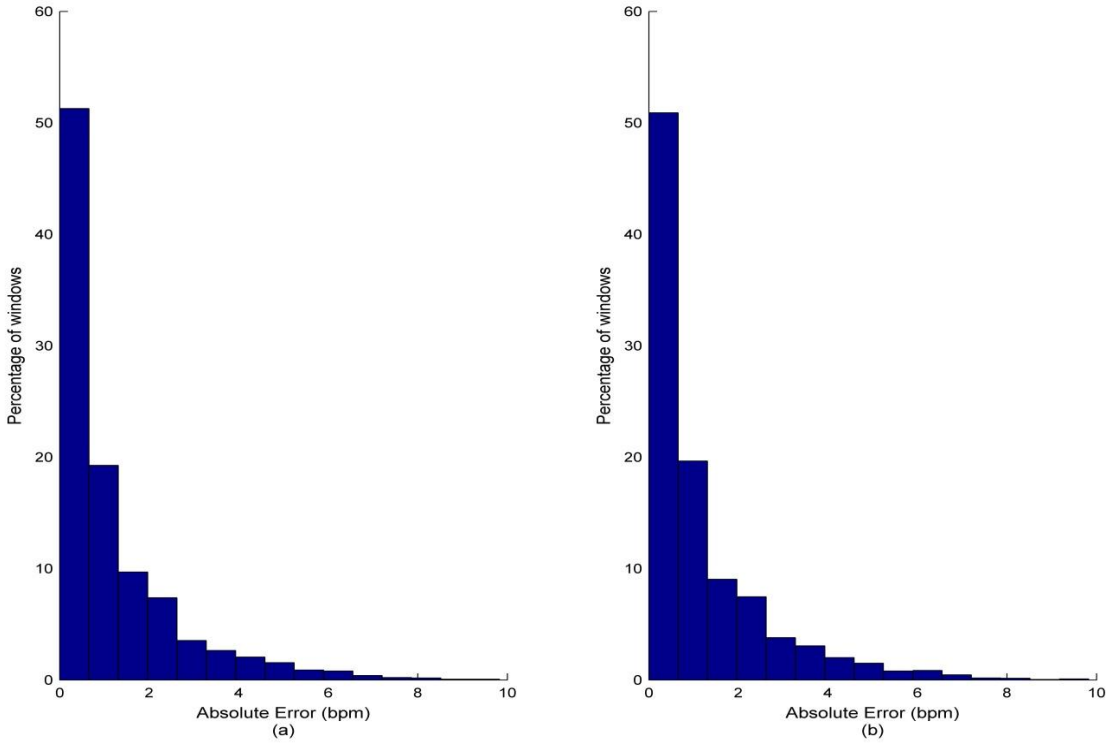

Fig. 4.14 Histogram of the absolute error in the respiratory rates computed between the reference respiration and EDR signals. (a) R_{HDSD}, (b) R_{HDE}.

e) EDR vs. Hermite basis functions

In this work, we have also investigated the dependency of the resemblance of EDR signal with the reference respiration on the number of Hermite basis functions (N) used to perform decomposition in (4.18). For this purpose, the EDR signals are obtained using the Hermite expansion of the QRS complexes of ECG signal using five different values of N ($N = 3$, 6, 9, 12, and 15). A comparison between these EDR signals is carried out by evaluating the correlation coefficient and the respiratory rate error. The performance results of EDR signals derived using the different value of N are presented in Table 4.4. It can be observed from the results shown in Table 4.4 that as the value of N increases in the Hermite expansion, the derived respiratory signal better resembles the reference respiration. It is also noticeable that the performance results of EDR estimated using 15 Hermite basis functions ($N = 15$) is marginally improved than the case of $N = 12$. Therefore, by considering the factor of computational cost, the estimation of the respiratory signal from single-lead ECG using 12 lower order Hermite basis functions is to be a better choice.

In the current work, the ECG segments with the abnormal amplitude peaks need to be removed from the experiment. In the real-time analysis, any minimal artifacts or noise can disturb the QRS complex morphology of ECG beat, and that may result in poor resemblance of the derived respiration with the reference respiration as shown in Fig. 4.16. In this work,

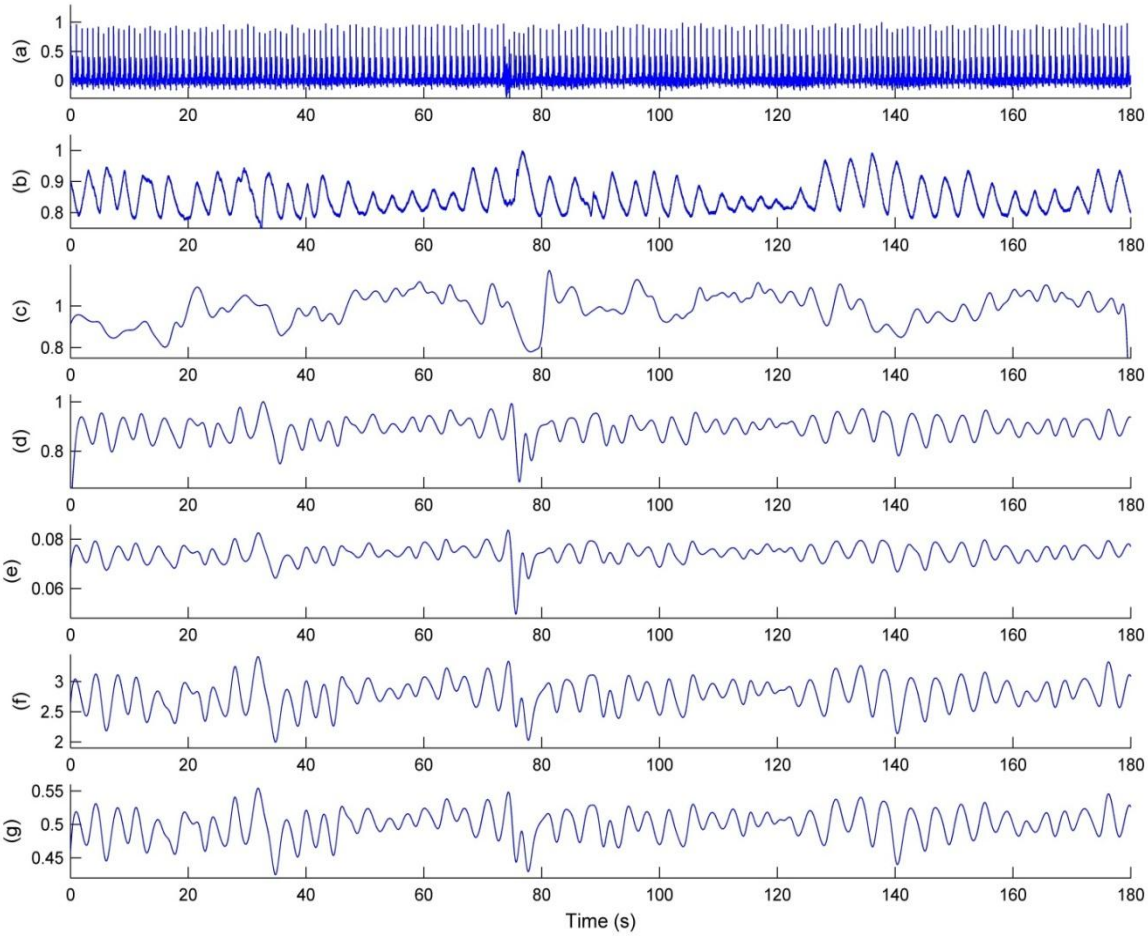

Fig. 4.15 EDR signals using different EDR methods of subject *f1y06m* shown from 1 to 180 seconds. (a) ECG; (b) Reference respiration, (c) R_{RSA}, (d) R_{Ramp}, (e) R_{PCA}, (f) R_{HDE}, and (g) R_{HDSD}. [Here, the ECG and respiratory signals are normalized with the maximum values]

Table 4.4 Comparison between EDR signals derived using different numbers of Hermite basis functions (N) over *Fantasia* dataset

	N	C	MAE (bpm)	PE (%)	ρ_c
R_{HDSD}	3	0.522	1.95	14.3	0.481
	6	0.657	1.32	9.9	0.715
	9	0.669	1.25	9.4	0.744
	12	0.693	1.20	9.0	0.755
	15	0.690	1.20	9.0	0.758
R_{HDE}	3	0.613	1.38	10.2	0.711
	6	0.654	1.34	9.9	0.714
	9	0.664	1.27	9.5	0.741
	12	0.688	1.22	9.1	0.752
	15	0.685	1.21	9.1	0.754

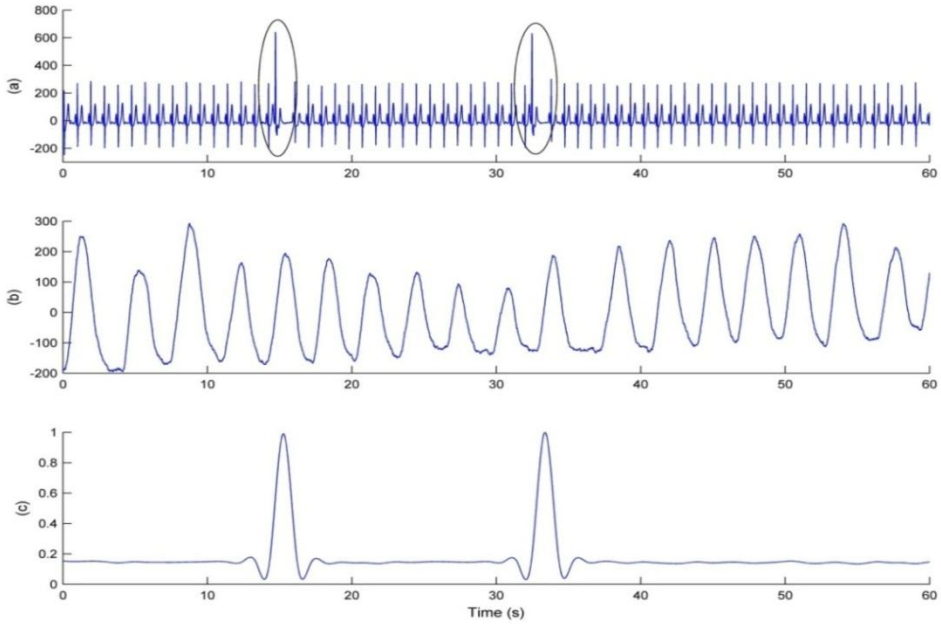

Fig. 4.16 An example of ECG-derived respiration using the proposed EDR technique. (a) original ECG; (b) reference respiration (R_{ref}); and (c) R_{HDSD}. The circles in the waveform (a) show the QRS complexes with artifacts (abnormal peaks). Effect of these abnormalities in the QRS complexes is reflected in the shape of the EDR signal (R_{HDSD}) as shown in waveform (c).

a criterion, described in Section 4.2, is proposed to eliminate the ECG segments with abnormal amplitude peaks from the analysis to prevent biasing in the estimation of the terms.

4.4 DISCUSSION

In this chapter, two new EDR algorithms based on the homomorphic filtering and the Hermite basis functions using single-lead ECG are presented. The performance of the proposed EDR methods is assessed over the *Fantasia* dataset based on the correlation coefficient, the coherence coefficient and the measures of error in the respiratory rates computed between the reference and derived respiratory signals. In the homomorphic filtering based EDR approach, the cepstrum of the ECG signal is filtered using a Butterworth band-pass filter in the frequency range of 0.2 to 0.4 Hz. Next, the filtered cepstrum is transformed into the original signal domain by reverse mapping as described in section 4.2. The proposed EDR technique based on homomorphic filtering provided improved results than the RPA based method. Besides, the usefulness of the Hermite basis function to track the respiratory-induced variation in the morphology of QRS complex of the ECG signal is also investigated for the purpose of a reliable estimation of the respiration. The use of the Hermite basis functions for EDR extraction is motivated by the shape similarity between the lower order Hermite basis functions and the QRS complex of ECG signal. In the proposed

EDR algorithm, the QRS complexes of an ECG are approximated using the truncated Hermite basis functions, and the resultant coefficients are used to monitor the respiratory-induced influence in the ECG. From the experimental results, the performance of the proposed EDR algorithm based on the Hermite basis functions is found to be outperforming the existing algorithms in the literature.

Both the proposed EDR algorithms are analyzed on different ECG segments of the *Fantasia* dataset. The performance of the Homomorphic filtering based EDR approach is evaluated using 5 minutes of the ECG segment selected from each subjects recording, whereas the Hermite basis functions based EDR algorithm is tested on the entire *Fantasia* dataset. Therefore, the experimental results presented in section 4.1 and section 4.2 should not be used to compare the performance of these two proposed EDR algorithms. To compare the performance of the proposed EDR algorithms, the experiment needs to be performed over the same ECG segments. For this purpose, the Hermite decomposition based EDR method is examined over the same ECG segments which are used to analyze the performance of the homomorphic filtering based EDR approach (section 4.2.3). Using the selected ECG segments, the performance of the Hermite decomposition (HD) based EDR method is obtained to be better than the homomorphic filtering approach. The median values of the correlation coefficients for the HD based method are obtained as R_{HDSD}: C = 0.77, and R_{HDE}: C = 0.75. On the other hand, the median values of the coherence coefficients computed for R_{HDSD} and R_{HDE} is obtained as 0.93 and 0.92, respectively. In addition to that, the median values of the correlation and coherence coefficients for the RSA-based method are determined as 0.56 and 0.77, respectively. The respiratory rate errors computed over the same data using different EDR algorithms are presented in Table 4.5. Based on the above results, it can be concluded that the EDR algorithm based on the Hermite basis functions outperformed the existing approach by achieving a higher value of the correlation and coherence coefficients, and a small error in the respiratory rate.

Unlike the RSA and morphology based EDR methods, the filtering approaches do not require prior knowledge of any fiducial point (such as R peak locations) in the ECG signal. Therefore, the filtering based EDR approaches can be useful under the circumstance of severe noise imposed over the R-peaks of ECG signal. On the other hand, in the filtering based EDR approach, the ECG signal is filtered in the pre-defined respiratory frequency band. If the respiratory frequency lies outside the pre-defined respiratory band, the reconstructed respiratory signal will be unmatched to the actual (reference) respiratory waveform. In addition to that, any variations in the respiratory pattern are not reflected in the derived respiratory signal obtained using the filtering approach as these methods produce a smooth waveform in the output. However, the proposed EDR method based on the

Table 4.5 Comparison of respiratory rate error obtained for different EDR methods over the same data

Algorithms	MAE (bpm)	PE (%)	ρ_c
R_{HDSD}	0.82	5.1	0.81
R_{HDE}	0.82	5.2	0.81
R_{DFT}	0.86	5.7	0.76
R_{DCT}	1.18	8.4	0.54
R_{PCA}	0.85	5.3	0.80
R_{Ramp}	0.89	5.8	0.76
R_{RSA}	1.20	7.6	0.73

homomorphic filtering also possesses such types of limitations, but it provided improved results than the existing RPA and RSA methods in the controlled case. It may be mentioned here that, instead of using DFT, other transforms can also be used in the characteristic function $D(.)$ to form a generalized representation of the homomorphic filtering. We empirically selected different transforms such as DFT, DCT, and Discrete Sine Transform (DST) for the characteristic function. From the experiments, both the DFT and DCT are observed to be performing better than the DST. Also, the EDR signals obtained using the DFT and DCT are found to closely resemble the recorded respiration as compared to the EDR obtained using the DST based characteristic function. Hence, both the DFT and DCT based characteristic functions are used to estimate the respiratory signal from single-lead ECG.

As discussed earlier, the magnitude of RSA in HRV degrades with the increase in age of the patient. In other words, the performance of the RSA-based EDR technique is effective while investigating the younger population, but it provides poor performance for the elderly populations. Hence, this limitation of the RSA-based EDR method put a serious question mark on its usability over the random populations.

On the other hand, the morphology-based EDR techniques are less sensitive or insensitive to the respiratory rate (frequency) and age of the subject. Also, the EDR technique based on tracking the respiratory-induced morphological variations in the ECG signal can provide the respiratory signal closely matching with the actual respiratory pattern. Recently, the EDR algorithm based on the PCA is proposed in [26], and it was found that the PCA algorithm outperforms the RPA method [26]. Although, use of the PCA was based on the assumption of linearity between the respiratory signal and the ECG signal, but this assumption may not always be true for the real-time signals. In our proposed EDR method based on the Hermite basis functions, the respiration is derived by monitoring the respiratory-induced

morphological variations in the ECG signal without any assumption. The proposed EDR method based on Hermite expansion is investigated over the large dataset to assess its effectiveness for continuous respiratory monitoring for a long time, and it outperformed the existing EDR methods by achieving the higher value of the correlation and coherence coefficients, and a lower value of the respiratory rate error.

4.5 CONCLUSION

In this chapter, two new EDR techniques based on the homomorphic filtering and the Hermite basis functions using single-lead ECG are presented. The use of the Homomorphic filtering as EDR technique is based on the assumption that the ECG signal is generated from the convolution of the electrical signals generated during the heart activities and the transfer function of an LTI system which is influenced by the respiratory process. On the other hand, the use of the Hermite basis functions for EDR signal is motivated by the fact of the shape similarity between the lower order Hermite basis functions and the QRS complex of an ECG. Therefore, in our second EDR method, the QRS complexes of ECG signal are approximated using the truncated Hermite basis functions and the coefficients of the approximation are then used to estimate the respiratory signal.

The simulations are performed using the *Fantasia* dataset, and performances of the proposed EDR algorithms are assessed using the correlation coefficient, the coherence coefficient, and agreement in the respiratory rates. From the simulation results, the proposed EDR technique based on homomorphic filtering using DFT (R_{DFT}) performed better than the RPA method. Moreover, the performance results of EDR technique based on the Hermite basis functions is found to be better than the RPA, PCA, RSA, and homomorphic filtering approaches. Results suggest that the proposed EDR techniques (particularly the Hermite functions based approach) can be utilized for continuous monitoring of the respiration in the real-time scenario. This work using single-lead ECG to derive the respiration encourages the development of home-based wearable sensors for regular monitoring of the respiratory-related measures.

CHAPTER – 5

SLEEP APNEA DETECTION TECHNIQUES USING SINGLE-LEAD ECG

In the previous chapter, we have analysed the usefulness of the homomorphic filtering and the Hermite basis functions to derive the respiratory signal from single-lead ECG. The research work is further extended to detect a breathing related disorder known as the sleep apnea using single-lead ECG. The episode of sleep apnea is associated with abnormalities in the breathing pattern of the patient. It is a well-known fact that the respiratory process induces some changes in the characteristics of ECG signal in different ways. Consequently, any abnormality in the respiratory pattern is also reflected in the ECG characteristics. These abnormalities in the ECG can be monitored for the detection of sleep apnea problem. This chapter is devoted to the detection of sleep apnea problem in the patient using single-lead ECG. For this purpose, two new algorithms for the detection of sleep apnea using single-lead ECG are presented here. The first technique for sleep apnea detection is based on the QRS approximation using the lower order Hermite basis functions. On the other hand, the second approach uses the features derived from the HRV and EDR signals to discriminate the subjects with apnea from the normal one. Here, the EDR signal is obtained using the Hermite expansion of the QRS complexes of ECG signal as described in chapter 4.

A detailed introduction about the sleep apnea disorder and its consequence in the ECG characteristics has been discussed in chapter 2. Therefore, only a brief introduction to the sleep apnea disorder and a summary of the existing algorithm for sleep apnea detection using the ECG signal are included in Section 5.1 to maintain continuity of the work. Two new proposed techniques for the detection of sleep apnea problem, as mentioned above, are described in Section 5.2, and Section 5.3. The performance results of the proposed apnea detection techniques are presented in the subsequent sections. The classification accuracy also depends on the selection of the classifier. Therefore, a short review of some well-known classifiers is also embedded in Section 5.2. The performance of the proposed apnea detection techniques is discussed in Section 5.4. Finally, Section 5.5 concludes the main findings of the chapter.

5.1 INTRODUCTION

Sleep apnea is commonly known as the breathing problem during night sleep. It is associated with the complete or partial pause in the airflow due to the physical blocking of

the upper airway for the short duration of time [9-10]. In general, an event of apnea is diagnosed if the patient suffers complete break of airflow through the upper airway for at least 10 seconds during sleep. It is a widespread problem in both men and women in adult age. Based on the available population studies, the sleep apnea affects around 3 to 7% adult men and 2 to 5 % adult women worldwide [10]. Repetitive occurrences of sleep apnea episodes result in the most common problem of excessive daytime sleepiness, poorer daytime performance [37]. The interrupted sleep due to the sleep apnea can escalate the possibility of depression, memory loss, and cardiovascular problems [11], [37], [121-122]. Hence, the problem of sleep apnea needs to be diagnosed at an early stage to prevent severe health consequences.

As discussed previously, diagnosis of apnea is carried out with a popular tool known as PSG. Use of the PSG technique for the diagnosis of sleep apnea disorder is very expensive, time-consuming, and complex process. Also, due to lack of the sleep laboratories, a majority of the apnea population remains undiagnosed [37]. Therefore, an alternative method is required to diagnose the apnea problem in the patients with the lesser number of physiological signals. This can subsequently help in making the home-based diagnosis process simple, less complex and inexpensive for the patients.

In the literature, a number of algorithms have been developed to extract some key features from the ECG signal to classify the apnea recordings from the normal one [30-53]. A majority of the apnea detection techniques in the literature are based on the time and frequency domain features extracted from HRV and the EDR signal obtained using the RPA method. Many researchers have also studied the non-linear behavior of the respiratory movements in the HRV to detect the episodes of sleep apnea using ECG [44-46]. Some studies show that the event of sleep apnea is associated with the morphological variations in the ECG signal [47-48]. In this context, Boudaoud *et al.* presented an algorithm for apnea detection based on the evaluation of changes in the P-wave of ECG signal [48]. Furthermore, Varon *et al.* applied the features derived from the PCA applied over the QRS complexes of ECG, RR intervals, and the EDR signal to classify the segments of apnea from the normal one [31].

Some studies reported variation in the QRS duration due to the episodes of OSA [54], [108]. In [54], it was concluded that duration of the QRS complexes of ECG signal prolonged significantly (particularly in women) as the severity of sleep apnea increases. Recently, Bacharova et al. studied changes in the QRS complex morphology caused by sleep apnea and came up with the conclusion that severity of sleep apnea is highly associated with the maximum value of QRS complex and a subtle shift of electric axis to the left [108]. In the context of ECG morphology, this chapter is mainly focused on deriving those features which extract information related to the morphological changes in ECG signal due to the respiration

and employ them to classify the apnea and normal subjects.

A comparative analysis of different apnea detection algorithm using ECG is presented in [47], and it was reported that the combine features of both the HRV and EDR signals provided the best classification accuracy. Previously, most of the apnea detection approaches used the RPA method to get the EDR signal for feature extraction. Based on the results shown in Chapter 4, the performance of the EDR technique based on the Hermite expansion is observed to be superior to the RPA method. This finding suggests that the EDR signal obtained using the Hermite expansion can be useful for the development of an effective technique for sleep apnea detection. The time and frequency domain features of the HRV and the EDR signal, obtained using the Hermite expansion, can provide information of the concomitant variations in RR intervals and changes in the QRS complex morphology caused by the occurrence of apnea episodes, respectively. Therefore, a technique based on the time and frequency domain features of the HRV and EDR signals to classify the apnea patient from the normal one is also developed in this chapter. Details about the proposed methodologies for the detection of sleep apnea are provided in the subsequent sections of this chapter.

5.2 Sleep Apnea Detection based on Hermite Basis Functions

This section describes a technique based on the Hermite basis functions for sleep apnea detection. The methodology is mainly based on the QRS approximation using the lower order Hermite basis functions, and the resultant coefficients of the approximation are used as the features for the classification.

Recalling, the use of the Hermite basis functions for sleep apnea detection stems from the fact that the shape of the Hermite basis functions closely matches to the shape of the QRS complexes of ECG signal. Therefore, variation and statistics of the coefficients obtained from the Hermite decomposition of the QRS complexes can be used to identify the morphological changes occurred in the QRS complexes of ECG signal due to the apnea. As a result, the coefficients of Hermite decomposition can be utilized to discriminate the apnea segments from the normal one. A brief overview of the Hermite approximation of the QRS complexes and different types of classifiers used in this work are presented in Section 5.2.1. Details of the proposed apnea detection methodology are described in Section 5.2.2. Selection of the best features from the feature vector is also discussed in Section 5.2.2. Finally, the experiment and simulation results are presented in Section 5.2.3.

5.2.1 Review of Hermite Decomposition and Classifiers

In this Section, a brief introduction of the Hermite decomposition for a given signal is presented. The classification accuracy also depends on the selection of the classifier.

Therefore, a short review of some well-known classifiers is also embedded in this sub-section.

a) Hermite Decomposition

The Hermite decomposition of the signal $x(t)$ can be represented in terms of N orthogonal functions $\phi_{n,\sigma}(t)$ as [117]

$$x(t) = \sum_{n=0}^{N-1} c_n(\sigma)\phi_{n,\sigma}(t) + e_\sigma(t), \tag{5.1}$$

where, $c_n(\sigma)$ are the coefficients of Hermite decomposition, the approximation error $e_\sigma(t) \to 0$ as $N \to \infty$, and $\phi_{n,\sigma}(t)$ are the Hermite basis functions.

The energy of the approximation error signal in (5.1) can be computed by

$$\int_{t=-\infty}^{\infty} \left|e_\sigma(t)\right|^2 dt = \int_{t=-\infty}^{\infty} \left| x(t) - \sum_{n=0}^{N-1} c_n(\sigma)\phi_{n,\sigma}(t) \right|^2 dt. \tag{5.2}$$

Clearly, the energy of the approximation error signal depends on the selected value of the scale parameter σ. The optimal value of σ can be achieved by the iterative increment in σ to obtain the lowest possible error between the signal $x(t)$ and its Hermite approximation. The process and other details of the Hermite decomposition can be referred in Section 4.3.1 of Chapter 4.

b) Classifiers

For the classification problems, different types of classifiers have been proposed by the researchers and are being used in many types of applications. In this section, four well-known classifiers are briefly introduced which are frequently employed for the apnea detection problem.

1) Support vector machine (SVM): The SVM algorithm is a well-known supervised learning model used for the classification and regression analysis [37]. The SVM technique first maps the training data into a higher dimensional space using a kernel function and then forms a linear optimal separating hyperplane (OSH) between the two groups in the mapped space. The data vectors nearest to the OSH are called support vectors [37].

2) Least square support vector machine (LS-SVM): The LS-SVM algorithm was proposed by Suykens et al. [123], and it is the least squares version of the SVM. The main difference between the SVM and LS-SVM is that the SVM algorithm solves quadratic programming problems for training while the LS-SVM algorithm solves a set of linear equations [123].

3) K-Nearest Neighbor (KNN): The KNN is also a supervised learning algorithm and it uses the nearest distance approach in deciding the group of the new vector in the training set [124-125]. In the training phase of the KNN classifier, the feature space is split into several regions, and the training data are mapped into the similar groups of feature space [125]. The unlabeled testing data are then classified to a particular group of feature space based on the minimum distance between the input data vector and that particular group.

4) Multilayer Perceptron Neural Network (MLPNN): The MLPPNs are the commonly used supervised learning models for the classification which are incorporated by the feed-forward structure. The MLPNN *architecture* includes three layers: an input layer, an output layer, and one or more hidden layers [126]. However, in the MLPNN architecture, more than one hidden layer can be employed, but some previous studies in [127-128] have shown that any complex decision boundary can be modeled using a single hidden layer architecture. Therefore, use of single hidden layer based MLPNN model is sufficient for our problem. The neurons in the hidden layer are interconnected using an activation function which can be of different types such as a threshold, or sigmoidal [126].

5.2.2 Proposed Methodology

In this section, a methodology for sleep apnea detection using the Hermite decomposition of the QRS complex is described. The occurrence of an apnea event leads to some morphological changes in the QRS complexes of ECG signal. Therefore, variation and statistics of the coefficients of Hermite decomposition of the QRS complexes can be used to evaluate the presence of apnea episodes in the ECG signal. The proposed methodology consists of three steps: feature extraction, feature selection, and classification. These three steps are discussed sequentially in this section as follows.

For the Hermite decomposition of the QRS complexes of any ECG, we need first to extract the QRS complexes from ECG signal. The QRS complexes of an ECG can be extracted by knowing the positions of R-peaks in it. In the present work, the Pan-Tompkins' algorithm is used to detect the positions of R-peaks in the ECG signal [116]. A search back post processing algorithm proposed in [49] is applied to identify and correct the false detected R-peaks. A window of size 200 ms centered around the R-peak (fiducial point) is used to extract the QRS complexes from ECG signal. Next, each QRS complex is zero padded on both sides of the duration of 100 milliseconds. This zero padding is used to make sure that the selected beats are close to zero outside the QRS complex [117].

Let L be the total number of QRS complexes obtained from an epoch of the ECG signal. The Hermite decomposition of the k^{th} QRS complex $xq_k(t)$ can be represented with the help of Eq. (5.1) as

$$xq_k(t) = \sum_{n=0}^{N-1} c_{n,k}(\sigma)\phi_{n,\sigma}(t) + e_{\sigma,k}(t), \tag{5.3}$$

where $k = 1, 2, \cdots, L$. The mean coefficient vector ψ of the QRS complexes of an epoch of the ECG can be obtained by averaging the coefficient vectors $c_{n,k}(\sigma)$ as

$$\psi = \frac{1}{L}\sum_{k=1}^{L} c_{n,k}(\sigma). \tag{5.4}$$

The values in the mean coefficient vector ψ are used to form the feature vector for the apnea classification. Additionally, the average value of energy (E_e) of the errors $e_{\sigma,k}(t)$ for $k = 1, 2, \cdots, L$ is also computed and used as a feature in the feature vector.

For the performance improvement, two features in the time domain based on the R-R time series are also included in the feature vector. For an epoch of ECG, the mean of R-R intervals (mRR) and the standard deviation of R-R intervals (sRR) are computed and used in the feature vector. In this work, the Hermite decomposition of QRS complexes was performed using fifteen lower order Hermite basis functions ($N = 15$). Therefore, a set of 18 features (16 features ($c_0, c_1, c_2, \cdots, c_{14}$ and E_e) from the Hermite decomposition and two features (mRR and sRR) from R-R intervals) are extracted from each ECG segment. Next, the features in the feature vector are transformed using the logarithmic transformation. This transformation is applied to make the distribution of the features close to the normal.

Feature Selection: For the classification, only those features are included which are significant and enhance the classification accuracy. Therefore, an algorithm is required to select the best features and eliminate insignificant features to lower the chances of the wrong detection. The hill-climbing feature selection algorithm proposed in [134] was used to select those features which provide a major contribution in the separation of two classes. The hill-climbing algorithm is an iterative algorithm which searches for the features that fairly enhance classification accuracy [134]. Next, the selected features are used for the detection of apnea segments.

Classification: For the classification, four different classifiers namely, the SVM, LS-SVM, MLPNN, and KNN are used to test the *performance* of the proposed sleep apnea detection technique. In the current study, the Gaussian radial basis function is used as the kernel function in both the SVM and LS-SVM models. In the KNN classifier, the Euclidian distance is used to decide the class of testing vector. For the MLPNN architecture of single hidden layer of 5 neurons, the hyperbolic tangent sigmoid transfer function is used as the activation

function, and the Levenberg – Marquardt algorithm (back-propagation algorithm) is applied to compute the weights of the model.

5.2.3 Experiment and Simulation Results

This section includes details of the dataset used in the analysis. Various parameters used for performance measurement and feature selection method are also discussed. Finally, the classification performance of the proposed method is presented.

a) Data

In this study, the *Apnea-ECG* dataset [33], [115], available at PhysioNet, is used to test the performance of the proposed technique for sleep apnea detection. The *Apnea-ECG* dataset on PhysioNet was generated for the Computers in Cardiology Challenge 2000 [47]. The dataset contains two sets (released set and withheld set) of 70 single-lead ECG recordings of varying lengths between 7h and 10h (mean: 492 ± 32 min), sampled at the rate of 100 Hz, with the resolution of 16-bits. Each ECG recording was annotated on the minute-by-minute basis which shows the presence of apnea episode during that minute. In this dataset, no difference between the events of apnea and hypopnea is indicated in the annotation.

In the dataset, based on the AHI value, the subjects were into three classes such as A, B, and C. In class A, the recordings contain 10 or more episodes of apnea per hour (AHI≥10) including at least 100 minutes of apnea during the entire recording. In class B, each recording includes 5 or more apnea episodes per hour (AHI≥5) and at least 5 to 99 minutes of apnea during the entire recording. The class B recordings are also considered as the borderline recordings [34]. Lastly, recordings with the AHI<5 are considered as the normal group (or class C).

The released set of *Apnea-ECG* data is used for training the classifiers, and the withheld set is used to validate the performance of the proposed algorithm for apnea detection. A total of 32727 annotated minutes (released set: 16854 minutes; withheld set: 15873 minutes) are extracted from the ECG recordings which were manually verified for any artifacts and abnormal amplitude peaks in the ECG segments. After that, the ECG segments are used for the experimental purpose to evaluate the performance of the proposed technique.

b) Performance Measures

In this study, the percentage sensitivity (Sn), specificity (Sp), accuracy (Ac), and area under the receiver operating characteristic (ROC) curve (AUC) are used to evaluate the performance of the proposed algorithm for sleep apnea detection. Using true positive (TP), false positive (FP), true negative (TN), and false negative (FN), the sensitivity, specificity, and accuracy are defined as follows [126]

$$Sn = \frac{TP}{TP + FN}. \tag{5.5}$$

$$Sp = \frac{TN}{TN + FP}. \tag{5.6}$$

$$Ac = \frac{TP + TN}{TP + TN + FP + FN}. \tag{5.7}$$

Here, the parameter accuracy (Ac) is computed as the percentage of correctly classified segments of the total.

c) Results

This section presents the features selected using the hill-climbing feature selection algorithm as well as the classification accuracies obtained using the different classifiers over the withheld set (35 recordings) of *Apnea-ECG* dataset. In this work, the classification of ECGs with apnea is performed in two ways: per-segment classification (minute-by-minute basis) and per-recording classification (where the entire ECG recording of a subject is discriminated between the apnea and normal recording).

Selection of width parameter σ ***:*** Fig. 5.1 shows that, for a fixed value of the width parameter σ , the error decreases as the number of Hermite basis functions used in the expansion increases. In Fig. 5.1, the average summed square error is calculated over the

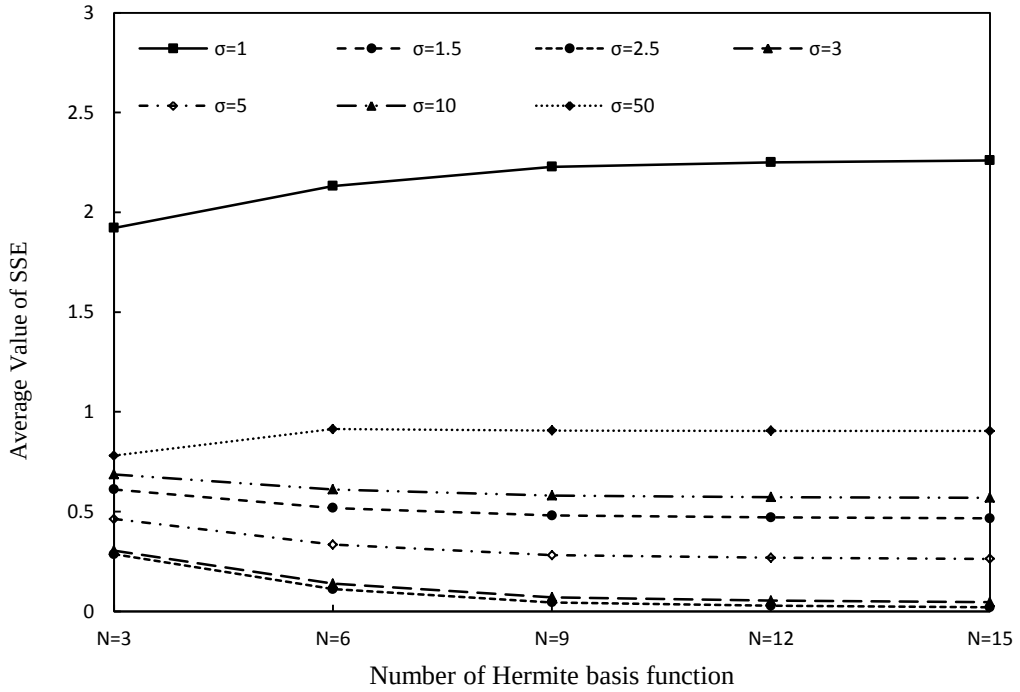

Fig. 5.1 The dependency of summed square error (SSE) on the parameters σ and the number of Hermite functions used in the Hermite expansion.

normal segments of the *Apnea-ECG* dataset using the different number of Hermite basis functions as well as different values of the parameter σ. In the Hermite expansion of normal segments for the different value of the width σ (1, 1.5, 2.5 3, 5, 10, 50), the lowest value of the error is obtained for $\sigma = 2.5$, and it remains nearly constant for the values of $N = 12$ and $N = 15$. The reconstructed QRS complex using 15 lower order Hermite basis functions closely resembles the original one when using the value of width parameter $\sigma = 2.5$. As a result, the smallest error in the Hermite expansion is obtained for $\sigma = 2.5$. Fig. 5.2 depicts an example showing the original QRS complex and the reconstructed one using the different values of σ (1, 2.5, 5, and 10). In Fig. 5.2, it can be visualized that the best reconstruction of the QRS complex using 15 lower order Hermite basis functions is obtained for the value of $\sigma = 2.5$. Therefore, in this study, the QRS decomposition in (5.3) is performed using 15 lower order Hermite basis functions ($N = 15$) and a fixed value of width parameter $\sigma = 2.5$.

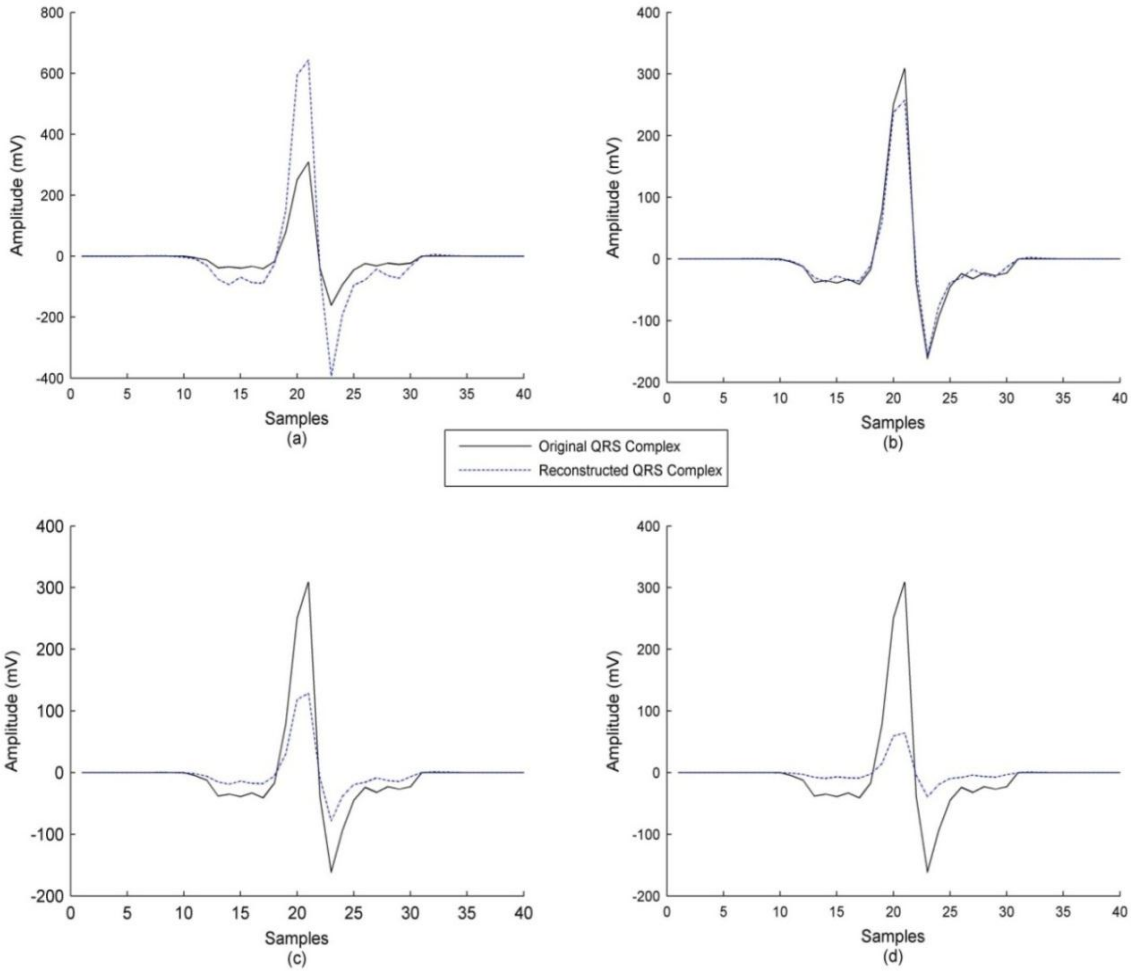

Fig. 5.2 Representation of the original QRS complex and the reconstructed one using 15 lower order Hermite basis functions for different values of sigma (σ). (a) σ =1, (b) σ =2.5, (c) σ =5, and (d) σ =10.

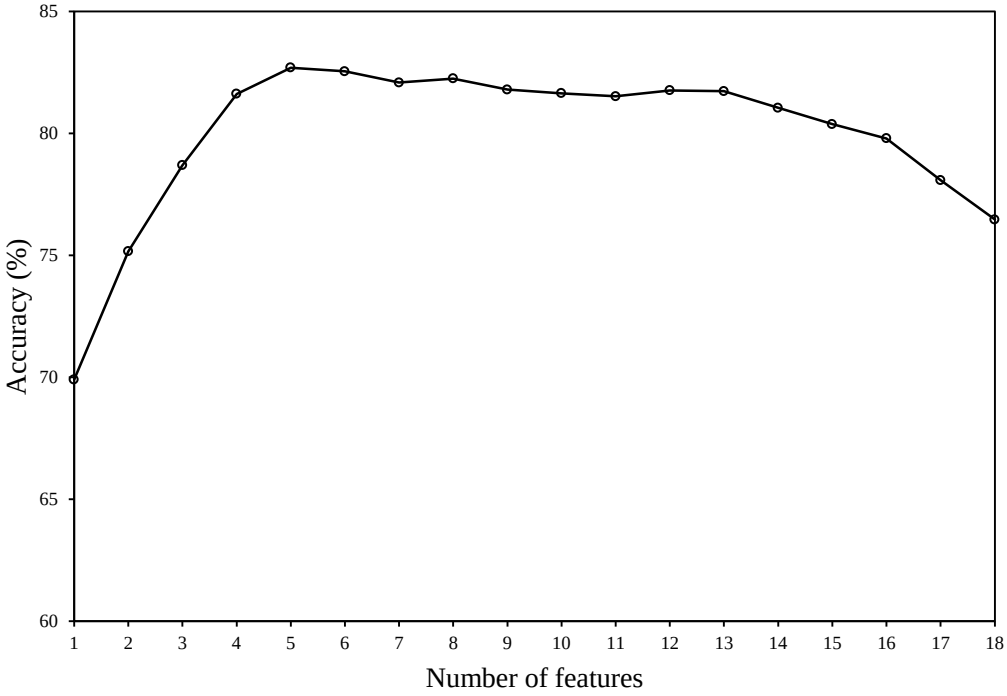

Fig. 5.3 Classification accuracy and number of features selected using the feature selection algorithm (hill-climbing).

In total, 16854 ECG minutes were acquired from the released set of *Apnea-ECG* dataset and used for training the classifiers. All four classifiers are trained with the same training data. The performance of the classifier is tested over the withheld set (test set) that is independent of the training data. The performance of the proposed algorithm is evaluated using different classifiers based on the sensitivity, specificity, accuracy, and area under the characteristic curve.

***Feature selection*:** As discussed in the methodology section, the hill-climbing feature selection technique is employed to pick those features which increase the classification accuracy positively. The SVM with the Gaussian radial basis function (RBF) kernel is applied in the feature selection process due to its extensive use in the classification problems. Fig. 5.3 depicts the classification accuracy as a function of the number of selected features using the feature selection algorithm (hill-climbing). The maximum classification accuracy is obtained about 82.6% by selecting five features, and after that, the accuracy starts decreasing as more features are included in the process which can be seen in Fig. 5.3. For the maximum classification accuracy, the selected features using the feature selection algorithm are as follows: C_1, C_8, C_{13}, E_e, and sRR.

Minute-by-minute apnea detection: Table 5.1 shows the performance of the proposed algorithm over the testing set for the minute-by-minute (per-segment) detection using the

Table 5.1 Per-segment classification performance using different classifiers

Classifiers	Sn (%)	Sp (%)	Ac (%)	AUC (%)
KNN	72.5	73.8	73.3	73.8
MLPNN	77.5	83.4	81.2	80.7
SVM (RBF Kernel)	76.7	88.2	82.6	82.0
LS-SVM (RBF Kernel)	79.5	88.4	83.8	83.4

different classifiers. It can be seen from Table 5.1 that the LS-SVM using the RBF kernel outperforms as compared to other classifiers by achieving the higher values of performance parameters (Ac = 83.8%, Sn = 79.5%, Sp = 88.4%, and AUC = 83.4 %). It is also noticeable from the experimental results that the KNN classifier provides the lowest classification accuracy among all four classifiers. Using the proposed algorithm, the per-segment accuracies computed using the LS-SVM classifier is comparable with the techniques existing in the literature.

Per-recording classification: To classify the apnea and normal recordings (35 recordings of the withheld set), the AHI value is computed for each recording using all four classifiers. The AHI values computed using our proposed approach are compared with the threshold value used in clinical practice. If the AHI value for any recording is greater than 5, then it is considered that the subject is suffering from the sleep apnea disorder [43]. On the other hand, a recording is diagnosed as the normal one if the estimated AHI value is less than 5 [43]. The AHI value for any recording is computed as the average number of minutes with apnea per hour. The performance of the proposed algorithm in the per-recording classification is evaluated based on the accuracy, sensitivity, specificity, and area under the characteristic curve (AUC). Table 5.2 shows the per-recording classification performance of the proposed technique using different classifiers. Table 5.2 also contains the correlation values computed between the actual AHI and the experimentally determined AHI values using the proposed method. It can be noticed from Table 5.2 that the correlation and accuracy measures are higher for the MLPNN, SVM, and LS-SVM classifiers as compared to the KNN.

Tenfold cross-validation: To assess the performance of the proposed technique over different sets of data, tenfold cross-validation is performed. To perform this validation scheme, the entire dataset (70 recordings) is split randomly into ten sets of recordings. The

Table 5.2 Performances of the various classifiers based on per-recording classification

Classifiers	Sn (%)	Sp (%)	Ac (%)	AUC (%)	Corr.
KNN	100	63.6	88.57	77.3	0.621
MLPNN	95.8	90.9	94.28	93.4	0.759
SVM (RBF Kernel)	95.8	100	97.14	97.8	0.813
LS-SVM (RBF Kernel)	95.8	100	97.14	97.8	0.841

process runs for ten iterations, and in the each iteration, nine sets are used for training the best performing classifiers (MLPNN, SVM, and LS-SVM), and the remaining set is used for testing purpose. For training the classifiers in Tenfold cross-validation scheme, a small set of 16000 samples (equal number of each apnea and normal samples) was selected from the training set by random sampling. The selection of such a small size of training samples is restricted by the use of the SVM for the classification. In the SVM, a kernel matrix is computed for the formulation and the size of the matrix is limited by the hardware used in this study (MATLAB R2013a, Intel(R) Core(TM) i5, 2.2 GHz, 8GB RAM running WINDOWS 7). The per-segment classification accuracies computed on ten different test sets are shown in Fig. 5.4. In the tenfold cross-validation scheme, the values of accuracy obtained using the MLPNN, SVM, and LS-SVM classifiers are varied from 70.14% to 93.86% (mean ± standard deviation, 79.2% ± 7.3%), 72.6% to 93.01% (80.8% ± 6.01%), and 73.22% to 93.41% (81.2% ± 6.4%), respectively. From these results, it is observed that our proposed algorithm provides satisfactory results when tested over different sets of data.

d) Hermite Basis Functions vs. Classification Accuracy

In the result section, Fig. 5.1 depicts dependency of error (QRS approximation) on the number of Hermite basis functions used in the expansion described by (5.3). To evaluate the general dependency of the classification error on the number of Hermite basis function used in (5.3), we performed the classification task using different numbers of Hermite basis functions ($N = 3$, 6, 9, 12, 15, and 18) and obtained the accuracies. Three other features (E_e, mRR, and sRR) are also included along with N Hermite coefficients in the feature vector where the value of feature E_e depends on the number of Hermite basis functions used for the QRS decomposition. The features in the feature vector that better discriminate the two classes (apnea and normal) are selected using the hill-climbing feature selection algorithm. The classification accuracies obtained using the SVM for different values of N are

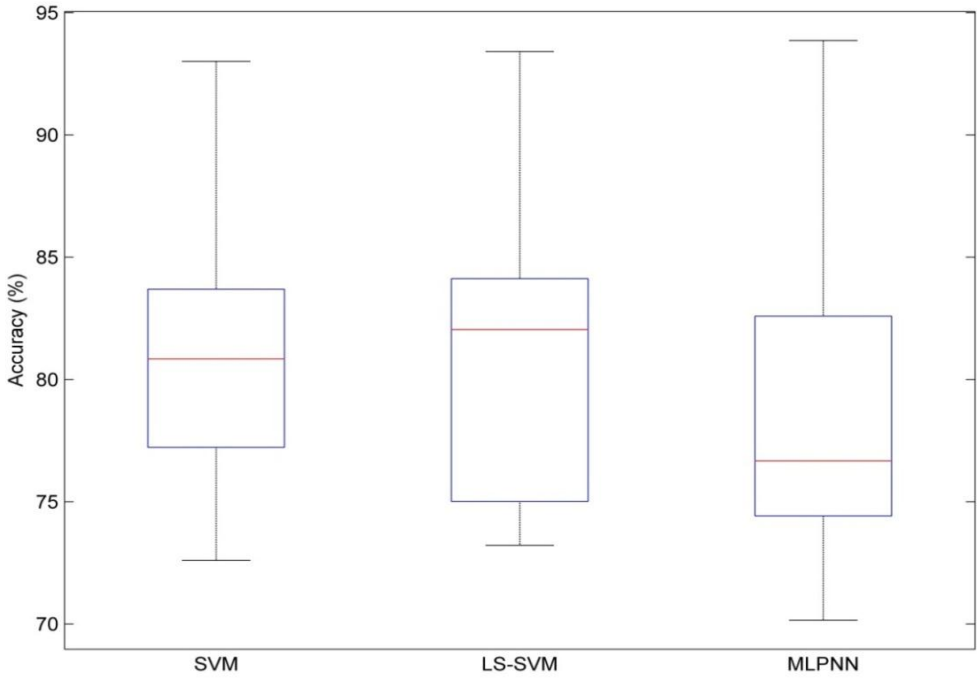

Fig. 5.4 Classification accuracy of apnea segments using the MLPNN, SVM, and LS-SVM classifiers in tenfold cross-validation [Each box plot indicates the median (50th percentile) and interquartile range (25th and 75th percentile)]

shown in Fig. 5.5. It can be observed from Fig. 5.5 that the classification accuracy increases as the number of Hermite basis functions (N) used for QRS approximation increases, but the classification accuracy for $N=18$ (Ac = 82.8%, Sn = 76.3%, Sp = 88.5%, and AUC = 82.1 %) is improved marginally as compared to $N=15$ (Ac = 82.6%, Sn = 76.7%, Sp = 88.2%, and AUC = 82.0 %). Therefore, by considering the factors of computational complexity and the classification accuracy together, the coefficients of QRS approximation using 15 lower order Hermite basis functions are selected for effective classification between the apnea and normal segments.

e) Comparison with existing approaches

The performance of the proposed approach is compared with the existing methodologies described in [7], [38-41], [135]. In [7], [38], [40], and [41], the authors obtained accuracies of about 72.9%, 82.2%, 89.9%, and 88.6%, respectively, but they used only released dataset for training and validation instead of the entire *Apnea-ECG* dataset. The algorithms presented in [39] and [135] also obtained higher classification accuracies, but their dataset used only selected recordings by removing about one-third of the recordings in the preprocessing steps before actual analysis. On the other hand, using the entire dataset, our proposed algorithm provides satisfactory performance for the per-segment classification with the classification accuracy of about 84%.

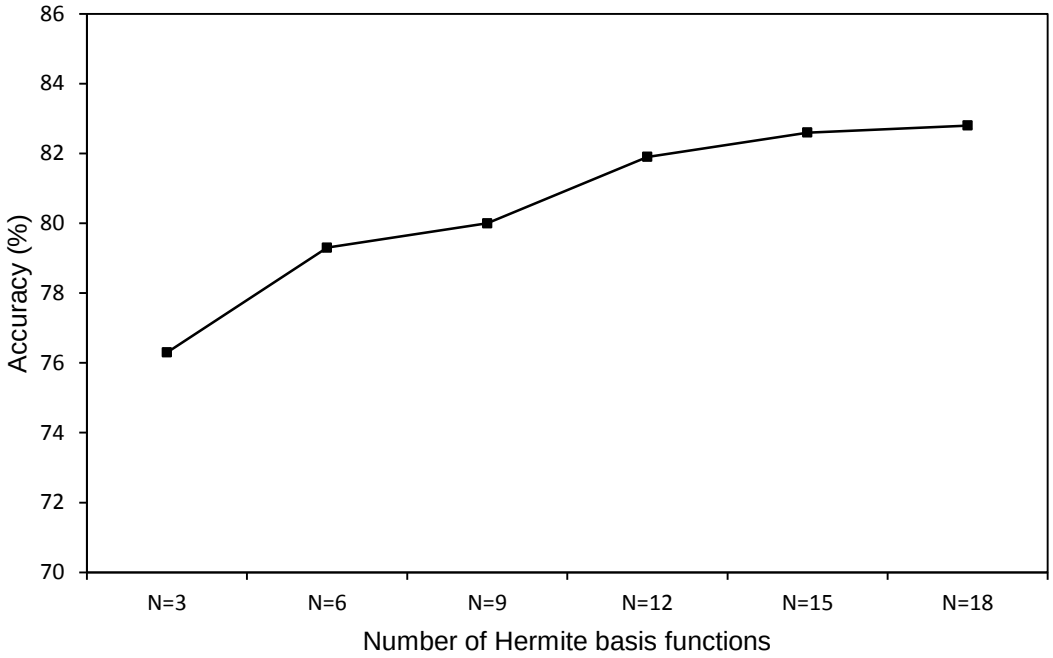

Fig. 5.5 The accuracies calculated for different values of N using the SVM classifier

Table 5.3 provides a comparison between the proposed work and other several studies based on per-recording (per-subject) classification accuracy. However, a higher value of the classification accuracy was achieved in [35] and [50], but their per-recording classification task was different than ours. In these studies, the per-recording classification task was to classify non-borderline recordings (30 recordings of the withheld set) into the apnea and normal recordings. On the other hand, even using all 35 recordings of the withheld set, our proposed algorithm provides comparable performance with the methods existing in the literature for the per-recording classification by achieving an accuracy of more than 97%.

f) Feature selection and classifiers

In this work, we have employed the hill-climb feature selection algorithm to select those features of the feature vector that mostly contribute in the effective classification. Some previous studies for gait pattern classification [134] and sleep apnea detection [37] have applied the feature selection algorithm and shown that fewer features selected from the feature vector are required for the effective classification. Additionally, it was found that performance degrades when the weak features are included in the classification [37]. In our case, after selecting five features, the accuracy degraded as the new features are included, and that can also be seen in Fig. 5.3. In this work, our main objective of employing the hill-climb feature selection approach was to discard the features with the redundancy and noise. Therefore, the feature selection step used in our proposed algorithm is an essential part of the effective classification.

Table 5.3 Comparison of per-recording classification results between the proposed method and some existing algorithms

Reference	Year	Classifier	Accuracy (%)
Marcos *et al.* [131]	2009	KNN, LDA, LR, QDA	87.6
Khandoker *et al.* [37]	2009	SVM	92.9
Alvarez *et al.* [132]	2010	LR	89.7
Morillo *et al.* [133]	2013	Probabilistic Neural Networks (PNN)	93.9
Chen et al. [32]	2015	SVM	92.8
Song *et al.* [43]	2016	HMM+SVM	97.1
Proposed Approach		SVM, LS-SVM	97.14

LDA : Linear Discriminant Analysis; QDA: Quadrature Discriminant Analysis

LR: Linear Regression; HMM: Hidden Markov model

Selection of the best classifiers for a particular problem is necessary for better classification results. For this, we used four different classifiers and compared their classification performances based on the per-segment and per-recording apnea classification. The SVM and its improved version LS-SVM models are widely used for the different pattern recognition and detection problems (including sleep apnea), and some empirical evidence reveals its (SVM) efficient performance in the real-time problems [139]. In addition to that, the KNN and neural networks (NN) are commonly used for various classification problems including the sleep apnea detection [39]. It was found in [39] that, even using lesser number of features, the KNN and NN provide satisfactory classifications performance. Therefore, in this study, our prime motive of using these four classifiers for apnea detection was to determine how well these classifiers perform in the case when the features are derived from the Hermite decomposition based scheme.

g) Selection of parameters

The main goal of the present work is to classify the ECG signals in the normal and sleep apnea patient category. The episodes of sleep apnea will exhibit morphological changes in the QRS complex portion of the ECG signal of a subject. Thus if we expand the QRS complex portion of the ECG signals using the truncated Hermite expansion, the coefficients in the resulting expansion will show the significant change in their values. This spread in the coefficient values is exploited for classification in the proposed technique. For this purpose, we first expand the QRS complex of a normal subject in terms of the truncated Hermite

expansion. This essentially means to find the suitable values of N and σ , and obtain the minimum value of the QRS approximation error when we decompose the QRS complex of the ECG signal in terms of the truncated Hermite expansion. Here, the parameter N as well as width σ will determine the approximation error. The width parameter σ controls the time scaling of the Hermite basis functions. Thus, for a particular value of N and σ , only the approximation error will be minimum. It has been mentioned here that the shape of some lower order Hermite basis function matches very closely with QRS complex part of the ECG signal and hence, for some value of σ the match will be better.

This has been investigated by varying the values of parameters N and σ for the QRS complexes of the ECG signal in the normal subjects of the *Apnea-ECG* dataset. The values of N and σ corresponding to the smallest error are used for the further use of the proposed technique. Using $N=15$ and $\sigma=2.5$ in the Hermite expansion, the approximated QRS complex of the ECG signal closely matches with the original one, and thus the error is smallest.

h) Limitations

The proposed approach for apnea detection is based on the QRS approximation using the lower order Hermite basis functions. In this study, the features are derived from the QRS complexes of ECG signal using the Hermite basis functions. In the real-time scenario, any morphological variations/minimal artifact in the QRS complexes due to the noise (or muscles movement) may result in biasing the estimation of the terms. The appropriate data preprocessing technique or any heuristic approach can be implemented to remove the contaminated segments of ECG to prevent any biasing in the estimations of the terms.

In section 5.2, we investigate the use of the Hermite decomposition of the QRS complexes of single-lead ECG for sleep apnea detection. Table 5.1 and Table 5.2 show the performance parameters computed based on the minute-by-minute (per-segment) classification and per-recording classification, respectively, over testing set using four different types of classifiers. In the proposed methodology, the results demonstrate that fewer features selected from the feature vector can provide satisfactory performance regarding of both the per-segment and per-recording classification of apnea. The average accuracy of the classification using the proposed approach in tenfold cross-validation is obtained above 81% while training the classifiers over a small set of training data. In tenfold cross-validation, it is expected that the average accuracy will also increase when the entire training samples are used for training the classifiers.

5.3 SLEEP APNEA DETECTION BASED ON HRV AND EDR SIGNALS

A comparative analysis of different apnea detection algorithm using single-lead ECG signal is presented in [47], and it was reported that the combine features of both the HRV and EDR signals provided the best classification accuracy. Therefore, our second approach for the detection of sleep apnea is based on the time and frequency domain features extracted from the HRV and EDR signals. Here, the EDR signal is obtained by decomposition each QRS complex of ECG signal in terms of the Hermite basis functions as described in Chapter 4. The extracted features are then used as input to the classifier to classify the ECG segments on the minute-by-minute basis in the apnea and normal categories. Additionally, this section performs classification between the apnea and normal subjects using the time and frequency domain features extracted from the EDR signal (R_{HDSD}) alone to assess its usefulness in the apnea detection problem. Details of the HRV and EDR signals and the features extraction from these signals are provided in Section 5.3.1, and 5.3.2, respectively. Experiment and simulation results are presented in Section 5.3.3.

5.3.1 Extraction of HRV and EDR Signal

a) HRV

Before computing the successive R-R time intervals (HRV), we require to extracting the position of R-peaks in the ECG waveform. The locations of R-peaks in the ECG signal is determined using the Pan-Tompkins algorithm as described in [116].]. A search back post processing algorithm described in [49] is applied to identify and correct the false detected R-peaks. For the tachogram (R-R interval time series), first, the R-R intervals are obtained by calculating the difference between the positions of successive R-peaks of ECG signal. Thereafter, the time series is transformed into an equidistance time series at a sampling frequency of 10 Hz using a cubic spline interpolation.

b) EDR Signal using Hermite Expansion

The EDR technique based on the Hermite basis functions is thoroughly discussed in Section 4.3.2 of Chapter 4. As the EDR signal is required to compute the features for the classification, the EDR technique is briefly described in this section to make it easy to follow the process.

Let L indicate the total number of QRS complexes obtained from an ECG segment. The Hermite approximation of the k^{th} QRS complex $xq_k(t)$ can be expressed as

$$xq_k(t) = \sum_{n=0}^{N-1} c_{n,k}(\sigma)\phi_{n,\sigma}(t) + e_{\sigma,k}(t), \qquad k = 1, 2, \cdots, L.$$

The resulting coefficients $c_{n,k}(\sigma)$ obtained from the decomposition in (5.8) distinguish the QRS complex morphology. Due to the respiration process, morphological changes (change in amplitude, width of the QRS complex, etc.) occur in the ECG signal which in turn will change the expansion coefficients in the Hermite expansion. Therefore, the energy distribution in the individual component of Hermite expansion of the QRS complexes changes with the respiration which affects the variance of Hermite coefficients. Hence, the beat-to-beat measure of the standard deviation of Hermite coefficients can also be used to track the respiratory influence in the QRS complexes of an ECG signal. Let λ_k be the standard deviation value of the coefficients $c_{n,k}(\sigma)$ corresponds to k^{th} QRS complex $x_k(t)$. Now, for L QRS complexes in an ECG segment, a vector $\boldsymbol{\lambda}$ can be formed as

$$\boldsymbol{\lambda} = \{\lambda_1, \lambda_2, \cdots, \lambda_L\}.$$

This vector $\boldsymbol{\lambda}$ itself is the derived respiratory signal using the EDR technique as described in chapter 4 (section 4.3.2). Next, the vector $\boldsymbol{\lambda}$ is resampled at a sampling rate of 10 Hz using a cubic spline interpolation. The resultant signal is further used for the experimental purpose.

5.3.2 Feature Extraction and Classification

The HRV and EDR signals obtained from single-lead ECG, as per the procedure described above, are further processed to extract the features to classify the apnea and normal subjects. It has been proved from studies that the sympathetic activation increases during the apnea episode [42], and the activities of the autonomic nervous system can be understood by the spectral analysis of HRV. In the HRV, high-frequency components evaluate the parasympathetic activity that is related to the respiratory rhythm whereas the low-frequency components are usually related to the sympathetic activities [38]. Thus, the spectral analysis of HRV can provide informative measures for the detection of sleep apnea problem.

On the other hand, it has been reported in previous studies [27], [37] that the occurrence of sleep apnea episodes is associated with the morphological changes in the ECG beats. The EDR signal obtained using the Hermite expansion is also based on tracking the respiratory-induced morphological variations in the QRS complexes of ECG signal. Therefore, any abnormality in the respiratory pattern will also be reflected in the characteristics of derived respiratory signal. This change in the EDR characteristics can be used for apnea detection. In addition to that, it has been mentioned here that the combine features of both the HRV and EDR signals provided the best classification accuracy for the detection of sleep apnea as reported in [47]. Therefore, various time and frequency domain features are extracted

here from both the HRV and EDR signals on the minute-by-minute basis to detect the sleep apnea problem in the patient.

Features: The features extracted from the HRV and the EDR signals are described as follows:

HRV Features

- Mean and standard deviation of the HRV signal.
- Normalized powers of very low frequency (NVLF) band (0.003 – 0.04 Hz), low frequency (NLF) band (0.04 – 0.15 Hz), and high-frequency (NHF) band (0.15 – 0.4 Hz) components of HRV. Here, the total power is computed in the frequency band of 0.003 – 0.4 Hz.
- The ratio of LF to HF powers (LH).
- Average and variance values of the FFT (1024 points) coefficients in the VLF, LF, and HF bands, respectively.
- Variance value of the FFT coefficients in the frequency range of 0.003 – 0.4 Hz.
- Variance values over 3s, 5s, and 10s segment subsections, respectively.
- Variance values (VD_j) and kurtosis values (KD_j) of the detailed coefficients at j^{th} level of the wavelet decomposition using the Daubechies wavelets of order 10. Here, $j = 1, 2, \cdots, 5$.

EDR Features

- Mean and standard deviation of the EDR signal.
- Normalized powers of very low frequency (NVLF) band (0.003 – 0.04 Hz), low frequency (NLF) band (0.04 – 0.15 Hz), and high-frequency (NHF) band (0.15 – 0.4 Hz) components of EDR signal. Here, the total power is computed in the frequency band of 0.003 – 0.4 Hz.
- The ratio of LF to HF powers (LH).
- Average and variance values of the FFT (1024 points) coefficients in the VLF, LF, and HF bands, respectively.
- Variance values over 3s, 5s, and 10s segment subsections, respectively.
- Variance values (VD_j) and kurtosis values (KD_j) of the detailed coefficients at j^{th} level of the wavelet decomposition using the Daubechies wavelets of order 10. Here, $j = 1, 2, \cdots, 5$.

Hence, a total of 51 features (26 features of HRV, and 25 features of EDR signal) are extracted from the HRV and EDR signals on the minute-by-minute basis. The features are then standardized by their z -score ($z = (f_{val} - \mu)/\upsilon$, where f_{val} denotes the value of the

feature, μ and υ denote the mean and standard deviation of the feature, respectively) to reduce the effect of outliers in the features.

Classification: In the classification, our task is to classify the ECG recordings in the apnea and normal categories, and this is also referred as the per-recording classification. The classification between the apnea and normal recordings is carried out based on the AHI value. The AHI value for a recording is determined by computing the average number of estimated minutes with apnea per hour [43]. A recording with the AHI value greater than 5 (threshold value) is diagnosed as the apnea else it is considered as the normal one. In this study, the per-recording classification task is performed using two well-known classifiers, namely the KNN, and the LS-SVM. In the KNN classifier, the class of testing vector is decided using the Euclidian distance with the nearest neighbor value of 100. The Gaussian Radial basis function is used as the kernel function in the LS-SVM classifier. The proposed scheme for sleep apnea detection based on the features extracted from the HRV and EDR signals is also depicted in Fig. 5.6.

5.3.3 Experiment and Simulation Results

This section includes the details of the dataset used in the analysis, data preprocessing steps to get the clean ECG signal and removal of the ECG segments with abnormal amplitude peaks from the recordings. Various parameters used for the performance measurement are also discussed. Next, the classification results for the apnea patient detection are demonstrated.

a) Data

In this study, the *Apnea-ECG* dataset [33], [115], available at PhysioNet, is used to test the performance of the proposed sleep apnea detection technique. Details of the *Apnea-ECG* dataset is provided in section 5.2.3. For our experimental purpose, the released set is utilized for training the classifier whereas the withheld set is used for the independent test.

b) Data Preprocessing

The recordings available in the dataset generally contain the BW noise and some abnormal amplitude peaks which need to be eliminated before the analysis. In this study, the features are extracted from the EDR and HRV. Here, the EDR signal is obtained using the Hermite expansion technique (discussed in Section 5.3.1) which is based on monitoring the respiratory-induced neat-to-beat morphological variation in the QRS complexes of ECG signal. Therefore, any abnormal peak in the QRS complex or miss-detected amplitude peak as R-peak may result in large variation in the values of the Hermite coefficients. This can consequently distort the EDR signal.

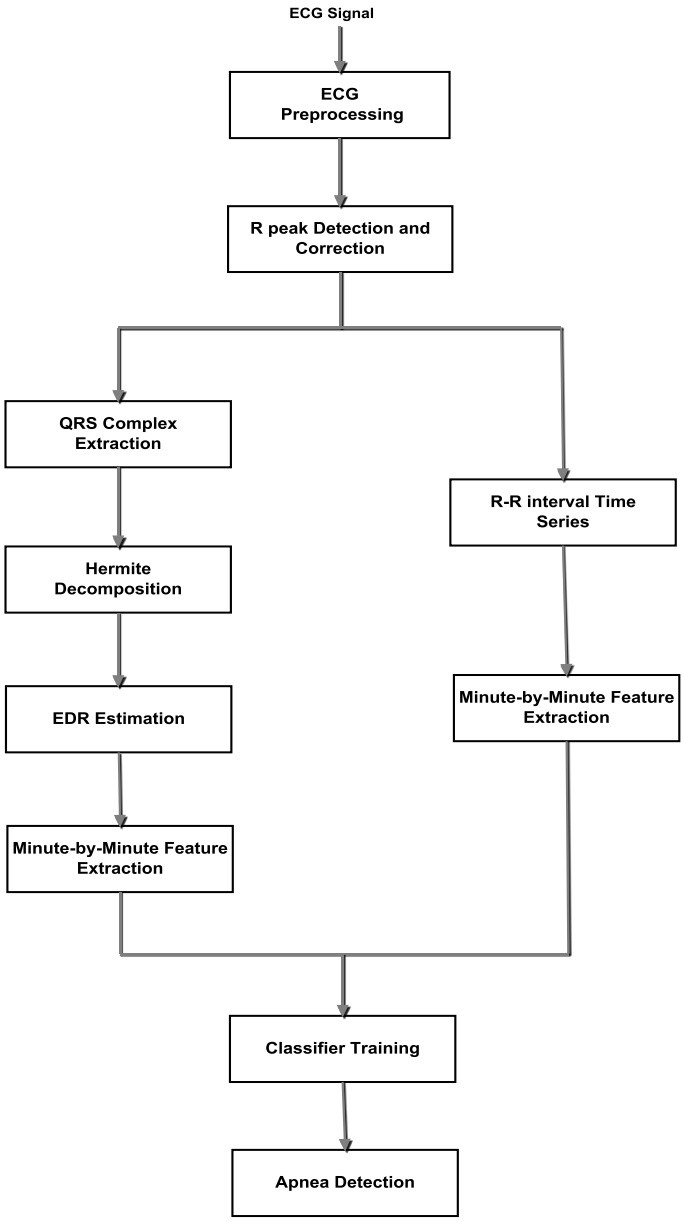

Fig. 5.6 The proposed scheme based on HRV and the EDR signal for detection of the sleep apnea patient using single-lead ECG.

To remove the BW noise, two median filters of widths 200 ms and 600 ms, respectively, are applied in cascade form to extract BW from the ECG [73]. The P and QRS waves are removed using the first median filter of width 200 ms, and the output is again filtered using the second median filter of width 600 ms to remove the T waves. The output of second median filter represents the low-frequency BW, and it is subtracted from the original ECG signal to obtain the BW removed from the ECG signal.

To remove the ECG segments with the abnormal amplitude peaks, a heuristic criterion, as described in Chapter 4, is used here which analyzes each ECG epoch of 60s duration. Using

this criterion, a significant fraction of the ECG segments with abnormal amplitude peaks in the *Apnea-ECG* dataset can be eliminated in the experiment. The main steps of the criterion can be seen in Chapter 4 (Section 4.3.3).

c) Feature Ranking

Feature ranking methods are used to select the most significant features from the feature vector. It is found that the performance of classifier degrades when the weak features are included in the classification [37]. The feature ranking methods rank the features available in the feature vector and arrange them in the order of higher rank to lower rank. The higher ranked features are used for the classification and the lower rank features are excluded from the experiment. Using the feature ranking methods, the computation complexity is reduced without degrading the performance of the classifier. In this work, Wilcoxon method is used to rank the features. The Wilcoxon method ranks the features in the feature vector based on the non-parametric test [137].

d) Training and Testing the Classifiers

For training the classifier, leave-one-out cross-validation technique is applied on the released set of the *Apnea-ECG* data to assess the generalize potential of the classifiers. The cross-validation scheme is widely used to evaluate the classifier performance [129-130]. In this scheme, 34 recordings of the released set are used for training the classifier, and the remaining recording is classified based on the AHI value estimated by computing average number of minutes per hour with apnea. This process is repeated for 35 iterations to make sure that all recordings are utilized as the testing sample. In the independent evaluation, the classifier is trained by the released set and then tested for each recording of the withheld set (35 recordings) on the minute-by-minute basis to estimate the AHI value. Thereafter, the actual AHI and estimated AHI values are compared to decide whether the ECG recording belongs to the apnea category or the normal one based on the threshold level.

e) Results

In the classification, most significant features are selected from the feature vector using the Wilcoxon method. The selected features are used as input to the classifiers. In this work, a total of 36 highly ranked features are selected to classify the apnea and normal subjects. Based on the Wilcoxon method, most of the features (36 features) from the feature vector are selected for the experiment purpose. Therefore, only those features which are excluded from the experiment are mentioned below.

HRV features

- Normalized powers of VLF and HF bands
- Average value of the FFT coefficients in the LF band

- Variance value of the FFT coefficients in the LF band
- Variance values (VD_j), $j = 1, 2, 3, 4$, of the detailed coefficients
- Kurtosis values (KD_j), $j = 2, 3, 4$, of the detailed coefficients

EDR features

- Average value of the FFT coefficients in the VLF band
- Variance value of the FFT coefficients in the LF band
- Variance values (VD_j), $j = 4$, of the detailed coefficients
- Kurtosis values (KD_j), $j = 2$, of the detailed coefficients

These above features are excluded from the experiment, and the remaining 36 features are used to assess the classification performance of KNN and LS-SVM classifiers.

The classification results of both the LS-SVM and KNN classifiers in leave-one-out cross-validation method are shown in Table 5.4. The classification accuracies of both the KNN and LS-SVM classifiers in leave-one-out cross validation method is obtained as 94.3%, and 97.14% respectively. Using LS-SVM classifier, all the normal subjects of the released set are successfully classified. The correlation coefficient is also computed between the estimated AHI and the actual AHI values. Here, the higher value of the correlation is found for the LS-SVM classifier. From the experiments, the LS-SVM is observed to be best performing classifier in leave-one-out cross-validation scheme by achieving higher classification accuracy.

Table 5.4 Leave-one-out cross-validation performance of KNN and LS-SVM classifiers over the released set of *Apnea-ECG* dataset

Classifiers	Sn (%)	Sp (%)	Ac (%)	AUC (%)	Corr.
KNN	95.5	92.3	94.3	93.9	0.69
LS-SVM	95.5	100	**97.14**	97.7	0.65

The independent test results of the KNN and LS-SVM classifiers over the withheld set are presented in Table 5.5. In the independent test, the classification accuracies of the KNN and LS-SVM classifiers are obtained as 97.14% and 100%, respectively. The correlation coefficient computed between the estimated and actual AHI values for the KNN and LS-SVM classifiers are determined as 0.85 and 0.74, respectively. However, the correlation value is obtained higher for the KNN classifier as compared to the LS-SVM, but the LS-SVM model classified all subjects successfully in the categories of apnea and normal.

Table 5.5 Independent test results of the KNN and LS-SVM classifiers over the withheld set of *Apnea-ECG* dataset

Classifiers	*Sn* (%)	*Sp* (%)	*Ac* (%)	*AUC* (%)	Corr.
KNN	100	91.7	97.14	95.8	**0.91**
LS-SVM	100	100	**100**	100	0.71

f) Comparison with existing literature

The performance of the proposed methodology for the detection of apnea problem in the patient is compared with the techniques existing in the literature. Table 5.6 presents a comparison between the proposed work and the existing methods based on the per-recording classification. Although, most of the sleep apnea detection techniques in the literature excluded the borderline recordings [34] from the analysis, but this work investigates all ECG recordings of the *Apnea-ECG* dataset. It can be seen from the comparison shown in Table 5.6 that even including the borderline recordings in the analysis, an accuracy of about 100% achieved using the LS-SVM model. Based on the above results, it can be seen that the proposed methodology outperforms the existing apnea detection techniques.

g) Apnea Patient Classification using EDR features

This section discusses the classification performance of two classifiers (KNN, and LS-SVM) using all 25 features acquired from the EDR signal. The classifications using the EDR features are performed to assess the usefulness of the respiratory signal derived using the Hermite basis functions for the application of sleep apnea detection.

Here, the features extracted from the EDR signal are used for the apnea detection. Independent test results of both the LS-SVM and KNN classifiers are shown in Table 5.7. The LS-SVM is observed to be best performing classifier by achieving the classification accuracy of about 97.14% over the withheld set. In other words, using the EDR features alone, 34 out of 35 recordings of the withheld set are successfully classified using the LS-SVM and KNN classifiers. In the experiment, all the normal subjects are successfully classified using the features extracted from the EDR signal. The classification accuracy obtained using the EDR features is also comparable with existing techniques mentioned in Table 5.6.

This section investigates the time and frequency domain features derived using the EDR signal (obtained using the proposed EDR technique based on the Hermite basis function) for the apnea detection. From the results shown in Table 5.7, it can be observed that the features derived from the EDR signal based on the Hermite expansion can be effectively

Table 5.6 Performance comparison of the HRV and EDR signals based sleep apnea detection approach with several other methods

Reference	Year	Classifier	Accuracy (%)
Macros *et al.* [131]	2009	KNN, LDA, LR, QDA	87.6
Khandoker *et al.* [37]	2009	SVM	92.9
Alvarez *et al.* [132]	2010	LR	89.7
Morillo *et al.* [133]	2013	Probabilistic Neural Networks (PNN)	93.9
Chen et al. [32]	2015	SVM	92.8
Song *et al.* [43]	2016	HMM+SVM	97.1
Sharma *et al.*[*] [158]	2016	SVM, LS-SVM	97.14
Proposed Approach (using HRV and EDR signal)		**LS-SVM**	**100**

***** Apnea detection technique based on the Hermite basis functions as described in Section 5.2

Table 5.7 Independent test results of the KNN and LS-SVM classifiers using EDR features

Classifiers	*Sn*(%)	*Sp*(%)	*Ac*(%)	*AUC*(%)	Corr.
KNN	95.8	100	**97.14**	97.9	**0.81**
LS-SVM	95.8	100	**97.14**	97.9	0.72

applied to discriminate the apnea recording from the normal one. The above results confirm the usefulness of the EDR technique based on the Hermite expansion (described in Chapter 4) to classify the apnea and normal subjects.

5.4 DISCUSSION

This chapter aims to develop an effective approach to detect the sleep apnea problem in the patient. For this purpose, two different methodologies are proposed here to investigate the ECG recording of a subject in order to decide whether the recording belongs to apnea category or the normal one. The development of sleep apnea detection techniques mainly relies on the extraction of those features which contain the information of morphological changes in the QRS complex of ECG signal and variation in the heart rate due to the recurrent pause in the respiration during the sleep. It was reported in [47] that those algorithms which include the features containing information of the morphological variations

of ECG due to apnea perform superior to that one based on the spectral features of HRV. Therefore, our first methodology for sleep apnea detection is based on the concept of tracking the morphological variations in the QRS complexes of ECG signal caused by the event of sleep apnea using the lower order Hermite basis function. To track the morphological variations in ECG, each QRS complex of ECG signal is decomposed using the lower order Hermite basis functions. The coefficients of the decomposition are then used as the features to classify the apnea and normal segments of the *Apnea-ECG* data. The performance of the proposed apnea detection technique is assessed by computing the classification accuracy, sensitivity, specificity, area under the receiver operation characteristic curve (ROC), and the correlation between the estimated AHI and actual AHI values. In the per-recording classification, it is found that the proposed methodology provides comparable accuracy (97.14%) with the methods existing in the literature at reduced computational cost due to the lesser number of features selected for the classification. Further analysis reveals that the classification accuracy also depends on the number of Hermite basis functions selected for the QRS complex approximation. It is also observed that the accuracy is marginally improved when the number of Hermite basis function used in the QRS complex decomposition increased from 15 to 18.

On the other hand, a comparative analysis of different apnea detection algorithm using single-lead ECG signal is presented in [47], and it was reported that the combine features of both the HRV and EDR signals provided the best classification accuracy. Therefore, our second approach for sleep apnea detection is based on the time and frequency domain features extracted from the HRV (RR intervals) and EDR signals. In this approach, RR interval time series is obtained by computing successive time differences between the R peak positions in the ECG signal, whereas the EDR signal is obtained using the Hermite basis function based EDR approach described in Chapter 4. Unlike the previous algorithms which used the RPA method to get the EDR signal, this work utilized the whole QRS complex morphology to track the respiratory influence in the ECG signal using the Hermite basis functions. Moreover, based on the results presented in Chapter 4, the performance of the Hermite basis function based EDR approach is found to be better than the RPA method. Therefore, the features extracted from the HRV and EDR (based on Hermite decomposition) signals are expected to provide better apnea detection performance than the existing methods in the literature. Experiments are conducted over the *Apnea-ECG* dataset to evaluate the performance of the proposed approach. Results demonstrate that the time and frequency domain features extracted from the EDR signal and HRV provided effective classification results. In the per-recording classification, independent test results showed that the 34 out of 35 recordings of the withheld set are successfully classified using the KNN

classifier, whereas the LS-SVM model provided the best classification result with the accuracy of 100%. It has mentioned here that the KNN classifier achieved higher correlation between the estimated AHI and actual AHI values in the independent test. The higher value of correlation indicates that the proposed approach using the KNN classifier can be effectively applied to determine the severity level of sleep apnea problem in the subject. As the LS-SVM model is achieved higher classification accuracy with a lower value of the correlation, the proposed approach using the LS-SVM classifier is observed to be suitable for screening the patient for apnea and normal categories. Moreover, in the independent test, it is found that if the threshold value of AHI is increased to 6, a classification accuracy of about 100% is achieved using the KNN classifier.

In this chapter, the usefulness of the respiratory signal (derived using the Hermite basis function based EDR approach) for apnea detection is also investigated. For this purpose, the EDR features are separately examined to explore their ability to discriminate the apnea patient from the normal one. Independent test results show that even using the EDR features alone, an accuracy of about 97.14% is achieved in the per-recording classification using the KNN and LS-SVM classifiers. Based on the experimental results, it can be stated that the apnea induced variation in the respiratory pattern is also reflected as a change in the EDR signal obtained using the Hermite decomposition. Hence, the EDR signal (R_{HDSD}) can be used to get informative measures of the sleep apnea problem in the patient.

This Chapter also discusses the computational complexity for different classifier used here for the classification of apnea and normal subjects. In SVM, solving the quadratic problem and choosing the support vectors is generally hard. In general, an optimal solution to the SVM problem involves of the order of n^2 dot products, while solving the quadratic problem directly involves inverting the kernel matrix, which has complexity on the order of n^3 (where n is the size of the training set) [164]. In LS-SVM, the computational complexity for solving a linear problem is $O(nl^2)$, (where l is the number of support vectors) [165-166]. The prediction complexity of the LS-SVM classifier is $O(l)$ [166]. On the other hand, the time complexity of the KNN classifier is $O(nd+kn)$, (where d represents the dimension (features) of each sample) [167]. It can be seen from the time complexities of different classifiers, the KNN classifier is computationally less expensive as compared to the SVM, LS-SVM models. In addition to that, as the number of features increases in the classification, the time complexity of the classifier increases. Due to the lesser number of features used for the classification, the apnea detection technique based on the Hermite decomposition is computationally viable as compared to the technique based on the HRV and EDR features.

However, the higher computational cost is acceptable in most of the clinical diagnosis process for effective performance.

The processing time required for individual classifier to classify each recordings (duration: 492 ± 32 min) of *apnea-ECG* data is also computed here. The computations are evaluated on an Intel(R) Core(TM) i5, 2.2 GHz, 8GB RAM, MATLAB R2013a running WINDOWS 7. The time required for classification of a subject into the apnea and normal categories by each classifier is calculated. For all classifiers, the computational time required for the subject classification is measured starting after the feature extraction. In the apnea detection approach based on the Hermite basis functions, the average values of the computational time required for a subject classification using the SVM, LS-SVM, and MLPNN are obtained as 0.37 ± 0.09 s, 0.23 ± 0.06 s, 2.21 ± 0.79 s, 0.20 ± 0.05 respectively. On the other hand, in the apnea detection technique based on HRV and EDR features, the average values of the computational time required for a subject classification using the LS-SVM, and KNN are obtained as 0.29 ± 0.04 s, and 0.22 ± 0.06 s, respectively. It can be seen from above results that the KNN classifier is computationally less expensive as compared to the other classifiers, but it shows the poor performance than that of SVM, LS-SVM, and MLPNN.

In the real-time scenario, even using sophisticated equipment for ECG recording, some artifacts may occur in the ECG waveform due to muscles movements, and body positions. Also, both the proposed methodology for sleep apnea screening uses the morphology of the ECG signal to extract the features for the classification, *i.e.*, the first approach is based on the approximation of QRS complex using the Hermite functions and the second approach uses the respiratory signal derived from the QRS complex morphology. If any minimal artifact presents in the QRS complex of ECG, it can result in large variations in the values of the coefficients of Hermite decomposition. Therefore, the occurrence of any minimal artifact in the QRS complex or miss-detected abnormal amplitude as R-peak can produce bias in the estimating terms. In the first approach, the selected ECG segments for the experiment are manually verified for abnormal artifacts which a time-consuming process. This problem is taken care in the second approach, and a heuristic criterion proposed in Chapter 4 is used. However, this criterion doesn't provide a complete solution, but it can remove a significant part of the ECG segments with the abnormal amplitude peaks from the analysis.

This chapter included two different approaches for the detection of sleep apnea problem, and their performance results are discussed and compared with the existing literature earlier in this chapter. It can be observed from the classification results that the second approach based on the time and frequency domain features provided better performance than the existing methods including out first approach based on the Hermite basis functions. The performance of both the proposed apnea detection approaches is assessed over the *Apnea-*

ECG dataset. Further, investigations over different dataset are required to evaluate the real-time applicability of these two algorithms for the apnea detection.

5.5 CONCLUSION

In this chapter, two different techniques to classify the apnea patient from the normal one using single-lead ECG are proposed. The first technique is based on the use of the Hermite basis functions to extract the features that contain information of the morphological variations in the QRS complexes of ECG caused by the sleep apnea episode. The performance of the proposed apnea detection algorithm is evaluated over the *Apnea-ECG* dataset based on the accuracy, sensitivity, specificity, area under the ROC curve, and the correlation between the actual AHI and estimated AHI values. Independent test results show that 34 out of 35 recordings of the withheld set are successfully classified using the LS-SVM and SVM classifiers at reduced computational cost due to the lesser number of features selected for the classification.

The second approach for apnea patient detection uses the HRV and the respiratory signal derived using Hermite basis functions, for feature extraction. A total of 51 features are extracted from the EDR and HRV signals. Based on the Wilcoxon method, the most significant features in the feature vector are selected and used as input to the classifiers. It is observed from the classification results that, using the selected features of HRV and the EDR signal, all recordings of the withheld set are successfully classified using the LS-SVM model. However, a satisfactory performance is achieved using both the proposed apnea detection techniques, but particularly the features extracted from the HRV and EDR signals provided higher accuracy than the existing literature. In this work, only single-lead ECG signals are used to detect the apnea episode which encourages the development of home-based wearable devices for health monitoring.

CHAPTER – 6

CONCLUSIONS AND FUTURE SCOPE

The ECG signal reveals vital information about our health conditions, and therefore it can be used to investigate various health related issues. Respiration is one of the important physiological events in the patient which needs to be investigated to evaluate the patient deterioration. The use of the conventional equipment for the respiration measurement and detection of sleep apnea problem possess several limitations while using them for long-term monitoring. As a matter of the fact that the respiratory process yields variations in the ECG characteristics, monitoring of the respiration and abnormalities in the respiratory pattern (such as sleep apnea) using single-lead ECG have become interesting areas of research. Though, the researchers are persistently working on investigating the ECG signals for monitoring the respiration and detection of the sleep apnea episodes. But, the development of effective algorithms for accurate estimation of the respiration as well as detection of the sleep apnea problem in the patient using single-lead ECG is desirable for the real-time applications.

In this thesis, our focus was to provide innovative solutions for a reliable estimation of the respiration and detection of sleep apnea problem using single-lead ECG. To get the EDR signal, the ECG signal is processed based on two key ideas: cepstrum filtering of ECG and tracking beat-to-beat variations in the ECG morphology caused by the respiration. On the other hand, the development of sleep apnea detection techniques was mainly based on extracting those features which track the morphological changes in the ECG signal caused by the apnea episodes. In addition to that, the BW noise is a major source of the low-frequency noise in ECG, and it needs to be removed prior to process the ECG signals for the respiration estimation and apnea detection. Therefore, an effective approach based on the HVD for the removal of BW from the ECG signal is also presented in the thesis.

6.1 SUMMARY OF THE SIGNIFICANT FINDINGS

Some of the major findings of the present research work are described as follows.

- The research work undertaken in the thesis is initiated by exploiting the usefulness of the HVD technique for the removal of BW from the ECG signal. The proposed scheme for BW removal is based on the assumption that the BW component in the ECG signal generally has a significant fraction of the total energy of the ECG signal. The simulations are performed over the *MIT-BIH Arrhythmia* dataset. Upon comparing the simulation results,

the performance of the proposed approach is observed to be better than the EMD-MM based technique. Unlike to the HVD, the IMFs in the EMD technique are computed by the spline fitting or some complex empirical algorithm. Therefore, the computational complexity of the EMD technique is higher as compared to the HVD. Based on these aspects, the HVD-based BW removal approach is found to be easy to implement as well as computationally efficient than the EMD technique.

- The next aim of the thesis is focused on deriving the respiratory signal from single-lead ECG. For this purpose, two new EDR techniques based on the homomorphic filtering and the Hermite basis functions are proposed. The main motivation for using the homomorphic filtering as EDR technique stems from the assumption that the ECG signal is generated by the convolution of the electrical signals of heart activities and the transfer function of an LTI system which is influenced by the respiration. Simulations are performed using the *Fantasia* data, and the values of correlation and coherence coefficients for the proposed EDR technique with DFT (R_{DFT}) are observed as 0.73 and 0.89, respectively. Results demonstrate that the EDR based on homomorphic filtering performed better than the RPA and RSA methods, but significant improvement in the performance is not observed when compared to the PCA technique.

- The second EDR approach monitors beat-to-beat variation in the QRS complex of ECG signal due to the respiration using the Hermite basis functions for deriving the respiratory signal. We hypothesize that the respiration, which is a quasi-periodic signal, affects the energy in the QRS complexes and the distribution of energy along each component in the orthogonal signal expansion based on the Hermite basis functions of ECG signal also. The proposed hypothesis is validated through simulation results. Experimental results demonstrate that the overall performance of the proposed EDR technique based on the Hermite basis functions is better than the existing methods by achieving the higher values of correlation and coherence coefficients as 0.693 and 0.846, respectively, for the entire *Fantasia* database.

- Upon comparing the EDR methods based on the error computed between the reference and derived respiratory rates, the least values of the mean absolute error and the relative error are obtained for the EDR methods based on the Hermite expansion as 1.20 bpm and 9.0%, respectively. Also, the EDR signal R_{HDSD} provided a better agreement in the respiratory rates with the higher value of the concordance correlation coefficient (ρ_c = 0.76). Upon investigating the young and elderly subjects of *Fantasia* data separately, the proposed method based on the Hermite decomposition provided satisfactory results for the young subjects but outperformed the existing methods for the elderly subjects.

- Further study is also carried out to evaluate dependency of the performance of the Hermite decomposition based EDR technique on the number of Hermite basis functions used in the expansion. Based on the simulation results, considering the factor of computational complexity, the use of 12 lower order Hermite basis functions is found to be enough for the estimation of the respiratory signal using single-lead ECG.
- The research work is extended to investigate single-lead ECG signal to detect the sleep apnea problem in the patient. To address this problem, an algorithm based on the Hermite basis functions is proposed to classify the apnea and normal subjects. In the proposed technique, the Hermite basis functions are used to decompose each QRS complex of ECG signal. The Hermite coefficients are then used to form the feature vector for the classification of ECG recordings in the apnea and normal categories. In the classification, the most significant features in the feature vector are selected based on the feature selection algorithm. In the classification between the apnea and normal recordings of *Apnea-ECG* dataset, an accuracy of about 97.14 % is achieved using the proposed algorithms based on the Hermite expansion. The performance of the proposed algorithm is observed to be comparable with the existing methods at the reduced computational cost due to the lesser number of features used in the classification.
- The time and frequency domain analysis of the HRV and EDR signals is also carried out to get efficient classification between the apnea and normal populations. For this purpose, an algorithm based on the HRV and EDR signals is proposed to classify the apnea and normal subjects of the *Apnea-ECG* dataset. Here, the EDR signal is obtained from the Hermite expansion of each QRS complex of ECG signal. Selection of the most significant features in the feature vector is carried out using the Wilcoxon method. Independent test results show that all recordings of the withheld set of *Apnea*-ECG data are successfully classified using the LS-SVM model. A satisfactory performance is achieved using both the proposed apnea detection techniques in the thesis, but the features extracted from the HRV and EDR signals provided higher classification accuracy than the existing literature.
- The usefulness of the EDR signal obtained using the Hermite basis functions is also investigated for apnea detection. Using the EDR features alone, an accuracy of about 97.14% is achieved in the independent test performed over the withheld set of *Apnea-ECG* data using the LS-SVM and KNN classifiers. These above results validate the applicability of the EDR approach based on the Hermite basis function for monitoring the respiration during the less controlled cases.

6.2 FUTURE SCOPE FOR RESEARCH

The research work presented in the thesis is carried out starting from the pre-processing of the ECG signal for BW removal to a reliable estimation of the respiration using the ECG signal. The work is extended to address the problem of the detection of sleep apnea in the patient which is associated with the abnormalities in the breathing pattern. However, some effective solutions are provided in this thesis regarding the EDR signal extraction and sleep apnea detection, but a lot more work needs to be done in these areas regarding their implementation in the real-time scenario.

- Deriving the respiration from the noisy ECG signal is still challenging particularly in the case where the QRS complexes of ECG signal are affected by the abrupt changes and motion artifacts. However, a heuristic criterion is proposed in this thesis to remove the ECG segments with the abnormal peaks from the experiments, but it doesn't provide a complete solution to obstruct abnormal amplitude peaks in the ECG recordings. Also, removal of such ECG segments from the experiment can bias the estimating terms particularly in the cases where a long segment of the recording needs to be processed. Thus, an effective approach needs to be developed to process ECG segments with the abnormal amplitude peaks without losing important information of the heart activities.
- Performance results of the EDR techniques show that the RSA method outperforms for the younger subjects. On the other hand, the Hermite basis function based EDR method outperforms for the elderly subjects. Therefore, information fusion of these two EDR signals can provide more accurate results in terms of the respiratory rate estimation for both the younger and elderly populations in the case of constant as well as variable respiratory rates.
- In this thesis, the proposed EDR techniques are investigated on the *Fantasia* dataset. This dataset consists of simultaneously recorded ECG and respiratory signals when the subjects were in resting state. Hence, the proposed EDR algorithms need to be investigated on the ECG recordings collected during less controlled conditions such as jogging, exercise, running, etc.
- In the research work, the performance of the proposed apnea detection techniques is assessed using the *Apnea-ECG* dataset. In the *Apnea-ECG* data, the episodes of apnea and hypopnea are considered as apnea. The future work requires focusing on the classification of apnea and hypopnea events using single-lead ECG signals.

REFERENCES

[1] Gravelyn, T. R., and J. G. Weg, “Respiratory rate as an indicator of acute respiratory dysfunction,” *J. Am. Med. Assoc.*, vol. 244, no. 10, pp.1123–1125, 1980.

[2] Meredith, D. J., D. Clifton, P. Charlton, J. Brooks, C. W. Pugh, and L. Tarassenko, “Photoplethysmographic derivation of respiratory rate: a review of relevant physiology,” *J. Med. Eng. Technol.*, vol. 36, no. 1, pp. 1–7, 2012.

[3] James, N. W., G. M. Adams, and A. F. Wilson, “Determination of anaerobic threshold by ventilatory frequency,” *Int. J. Sports Med.* Vol. 10, no. 3, pp. 192–196, 1989.

[4] G B Moody, R G Mark, A Zoccula, and S Mantero, “Derivation of Respiratory Signals from Multi-Lead ECGs,” *Comput. Cardiol.*, 12, pp. 113-116, 1985.

[5] J Felblinger and C Boesch, “Amplitude demodulation of the electrocardiogram signal (ECG) for respiration monitoring and compensation during MR examinations,” *Magn-Reson-Med*, 38(1):129-136, July 1997.

[6] L G Lindberg, H Ugnell, and P A Oberg, “Monitoring of respiratory and heart rates using a bre-optic sensor,” *Med. Biol. Eng. Comput.*, 30, pp. 533-537, 1992.

[7] C. O’Brien and C. Heneghan, “A comparison of algorithms for estimation of a respiratory signal from the surface electrocardiogram,” *Comput. Biol. Med.*, vol. 37, no. 3, pp. 305-314, 2007.

[8] Y Brans and W Hay, “Physiological monitoring and instrument diagnosis in perinatal and neonatal medicine,” *Cambridge University Press*, 1995.

[9] Task Force AASM, “Sleep-related breathing disorders in adults: recommendations for syndrome definition and measurement techniques in clinical research,” *Sleep*, vol. 22, no. 5, pp. 667-689, Aug. 1999.

[10] N.M. Punjabi, “The epidemiology of adult obstructive sleep apnea,” *Proc Am Thorac Soc,*, 5 (2008), pp. 136–143.

[11] T. Young, P. Peprad, M. Palta, K. M. Hla, L. Finn, B. Morgan, and J. Skatrud, “Population-based study of sleep breathing as a risk factor for hypertension,” *Arch. Intern. Med.*, vol. 157, pp. 1746-1752, 1997.

[12] J. Lazaro, A. Alcaine, D. Romero, E. Gil, P. Laguna, E. Pueyo and R. Bailon, "Electrocardiogram derived respiratory rate from QRS slopes and R-wave angle," *Ann. Biomed. Eng.*, vol. 42, pp. 2072-2083, 2014.

[13] Bailo´n, R, L So¨rnmo, and P Laguna, “ECG-derived respiratory frequency estimation,” in *Advanced Methods and Tools for ECG Data Analysis*, edited by G. Clifford, F. Azuaje, and P. McSharry. Norwood: Artech House Inc., 2006, pp. 215–244.

[14] M. D. Revow, S. J. England, and H O’Beirne, “Robust computer algorithm for detecting breaths in noisy ventilatory waveforms from infants,” *Med. Biol. Eng. Comput.*, 24(6), pp. 609-615, Nov. 1986.

[15] La´zaro, J., E. Gil, R. Bailo´n, A. Minchole´ , and P. Laguna, “Deriving respiration from photoplethysmographic pulse width,” *Med. Biol. Eng. Comput.*, vol. 51, no. 1, pp. 233–242, 2013.

[16] D. Cysarz, R. Zerm, H. Bettermann, M. Frühwirth, M. Moser, M. Kröz, “Comparison of respiratory rates derived from heart rate variability, ECG amplitude, and nasal/oral airflow,” *Ann. Biomed. Eng.*, vol. 36, no. 12, pp. 2085–2094, 2008.

[17] S.-B. Park, Y.-S. Noh, S.-J. Park, H.-R. Yoon, “An improved algorithm for respiration signal extraction from electrocardiogram measured by conductive textile electrodes using instantaneous frequency estimation,” *Med. Biol. Eng. Comput.*, vol. 46, no. 2, pp. 147–158, Feb. 2008.

[18] A. Schäfer, K.W. Kratky, “Estimation of breathing rate from respiratory sinus arrhythmia: comparison of various methods,” *Ann. Biomed. Eng.*, vol. 36, pp. 476–485, 2008.

[19] J.F. Thayer, J.J. Sollers, E. Ruiz-Padial, J. Villa, ”Estimating respiratory frequency from autoregressive spectral analysis of the heart period,” *IEEE Eng. Med. Biol. Mag.*, vol. 21, no. 4, pp. 41–45, Apr. 2002.

[20] Mason, C. L., and L. Tarassenko, “Quantitative assessment of respiratory derivation algorithms,” in: Engineering in Medicine and Biology Society,” *Proceedings of the 23rd Annual International Conference of the IEEE*, Vol. 2, pp. 1998–2001, 2001.

[21] D. Dobrev and I. Daskalov, “Two-electrode telemetric instrument for infant heart rate and apnea monitoring,” *Med. Eng. Phys.*, vol. 20, no. 10, pp. 729–734, Dec. 1998.

[22] B. Raymond, R. M. Cayton, R. A. Bates, and M. Chappell, “Screening for obstructive sleep apnoea based on the electrocardiogram,” Comput. Cardiol., vol. 27, pp. 267–270, 2000.

[23] Pinciroli F., R. Rossi, and L. Vergani, “Detection of electrical axis variation for the extraction of respiratory information,” *Comput. Cardiol.*, vol. 12, pp. 499–502, 1985.

[24] J. Goldberger, N. Bidargaddi, A. Sarela, and M. Karunanithi, “Automatic detection of respiration rate from ambulatory single-lead ECG,” *IEEE Trans. Inform. Technol. Biomed.*, vol. 13, no. 6, pp. 890-896, Nov. 2009.

[25] D. Labate, F. l. Foresta, G. Occhiuto, F. C. Morabito, A. L. Ekuakille, and P. Vergallo, “Emirical mode decomposition vs. wavelet decomposition for the extraction of respiratory signal from single-channel ECG: A comparison,” *IEEE Sensors J.*, vol. 13, no. 7, pp. 2666-2674, July 2013.

[26] P. Langley, E. J. Bowers, and A. Murray, “Principal component analysis as a tool for analyzing beat-to-beat changes in electrocardiogram features: Application to ECG-derived respiration,” *IEEE Trans. Biomed. Eng*., vol. 57, no. 4, pp. 821-829, Apr. 2010.

[27] Devi Widjaja, C. Varon, A. C. Dorado, Johan A. K. Suykens, and S. V. Huffel, “Application of kernel principal component analysis for single-lead-ECG derived respiration,” *IEEE Trans. Biomed. Eng.*, vol. 59, no. 4, pp. 1169-1176, Apr. 2012.

[28] C. Orphanidou, S. Fleming, S.A. Shah, L. Tarassenko, “Data fusion for estimating respiratory rate from a single-lead ECG,” *Biomed. Sig. Process. Control*, vol. 8, no. 1, pp. 98-105, 2013.

[29] L. Mirmohamadsadeghi, J. M. Vesin, “Respiratory rate estimation from the ECG using an instantaneous frequency tracking algorithm,” *Biomed. Sig. Process. Control*, vol. 14, pp. 66-72, 2014.

[30] B. Xie and H. Minn, “Real-time sleep apnea detection by classifier combination,” *IEEE Trans. Inf. Technol. Biomed.*, vol. 16, no. 3, pp. 469-477,2012.

[31] C. Varon, A. Caicedo, D. Testemans, B. Buyse, and S. V. Huffel, “A novel algorithm for the automated detection of sleep apnea from single-lead ECG,” *IEEE Trans. Biomed. Eng.*, vol. 62, no. 9, pp. 2269-2278, Sept. 2015.

[32] L. Chen, X. Zhang, and C. Song, “An Automatic Screening Approach for Obstructive Sleep Apnea Diagnosis based on Single-lead Electrocardiogram,” *IEEE Trans. Autom. Sci. Eng.*, vol. 12, no. 1, pp. 106-115, Jan 2015.

[33] T. Penzel et al, “The apnea-ecg database,” in Proc. *Computers in cardiology*, 2000, pp. 255-258.

[34] P. De Chazal et al, “Automated processing of the single –lead electrocardiogram for the detection of obstructive sleep apnea,” *IEEE Trans. Biomed.* Eng., vol. 50, no. 6, pp. 686-696, Jun 2003.

[35] P. De Chazal et al., “Automatic classification of sleep apnea epochs using the electrocardiogram,” *Comput. Cardiol.*, Cambridge, MA, 2000, pp.745-748.

[36] K. Kesper et al, “ECG signal analysis of the assessment of sleep-disordered breathing and sleep pattern,” *Med. Biol. Eng. Comput.*, vol. 50, no. 2, pp. 135-144, Feb 2012.

[37] A. H. Khandoker et al, “Support vector machines for automated recognition of obstructive sleep apnea syndrome from ECG recordings,” *IEEE Trans. Inf. Technol. B.*, vol. 13, no. 1, pp. 37-48, Jan 2009.

[38] H. M. Al-Angari, A. V. Sahakian, “Use of Sample Entropy Approach to Study Heart Rate Variability in Obstructive Sleep Apnea Syndrome,” *IEEE Trans. Biomed. Eng.*, vo. 54, no. 10, pp. 1900-1904, Oct 2007.

[39] M. O. Mendez et al., “Sleep apnea screening by autoregressive models from a single lead ecg*,” IEEE Trans. Biomed. Eng.*, vol. 56, no. 12, pp. 2838-2850, Dec. 2009.

[40] M. Bsoul et al, “Apnea medassist: real-time sleep apnea monitor using single-lead ecg,” *IEEE Trans. Inf. Technol. B.*, vol. 15, no. 3, pp. 416-427, May 2011.

[41] G. Sannino et al., “An automatic rules extraction approach to support osa events detection in an mhealth system,” *IEEE J. Biomed. Health Inform.*, vol. 18, no. 5, pp. 1518-1524, Mar. 2014.

[42] T. Penzel, “Is heart rate variability the simple solution to diagnose sleep apnoea?,” *Eur. Respir J.,* 2003; 22: 870-871.

[43] C. Song, K. Liu, X. Zhang, L. Chen, and X. Xian, “An Obstructive Sleep Apnea Detection Approach Using a Discriminative Hidden Markov Model from ECG Signals,” *IEEE. Trans. Biomed. Eng.*, vol. 63, (7), pp. 1532-1542, 2016.

[44] J. Bock and D. A. Gough, “Toward prediction of physiological state in sleep apnea,” *IEEE Trans. Biomed. Eng.*, vol. 45, no. 11, pp. 1332–1341, Nov. 1998.

[45] M. Miyata, N. Burioka, H. Suyama, T. Sako, T. Nomura, T. Takeshima, S. Higami, and E. Shimizu, “Non-linear behaviour of respiratory movement in obstructive sleep apnoea syndrome,” *Clin. Physiol. Funct. Imag.*, vol. 22, pp. 320–327, 2002.

[46] M. Miyata, N. Burioka, T. Sako, H. Suyama, Y. Fukuoka, K. Tomita, S. Higami, and E. Shimizu, “A short daytime test using correlation dimension for respiratory movement in OSAHS,” *J. Eur. Respir.*, vol. 23, pp. 885–890, 2004.

[47] T. Penzel et al, “Systematic comparison of different algorithms for apnoea detection based on electrocardiogram recordings,” *Med. Biol. Eng. Comput.*, vol. 40, no. 4, pp. 402–407, Jul 2002.

[48] S. Boudaoud et al, “Corrected integral shape averaging applied to obstructive sleep apnea detection from the electrocardiogram,” *EURASIP J. Adv. Sig. Pr.*, vol. 2007, no. 1, p. 032570, 2007.

[49] P. de Chazal et al, “Automated detection of obstructive sleep apnea at different time scales using the electrocardiogram,” *Physiol. Meas.*, vol. 25, no. 4, p. 967, Aug 2004.

[50] J. N. McNames and A. M. Fraser, “Obstructive sleep apnea classification based on spectrogram patterns in the electrocardiogram,” Computers in Cardiology 2000, Cambridge, MA, 2000, pp. 749-752.

[51] Guilleminault C, Connolly S, Winkle R, Melvin K, Tilkian A, “Cyclical variation of the heart rate in sleep apnea syndrome. Mechanisms and usefulness of 24 h electrocardiography as a screening technique,” *Lancet*, 1:126–131,1984.

[52] Narkiewicz K, Somers VK, “Sympathetic nerve activity in obstructive sleep apnoea,” *Acta Physiol Scand,* 2003; 177: 385–390.

[53] Dingli K, Assimakopoulos T, Wraith PK, Fietze I, Witt C, Douglas NJ, “Spectral oscillations of RR intervals in sleep apnoea/hypopnoea syndrome patients,” *Eur Respir J.*, 2003; 22: 943–950.

[54] S. Gupta, B. C. Valery, A. R. Corral, A. Shamsuzzaman, V. K. Somers, and G. S. Pressman, “Association between QRS Duration and Obstructive Sleep Apnea,” *J Clin Sleep Med*, vol. 8, no. 6, pp. 649-654, 2012.

[55] Hayano J, Yasuma F, Okada A, Mukai S, Fujinami T, “Respiratory sinus arrhythmia. A phenomenon improving pulmonary gas exchange and circulatory efficiency,” *Circulation*, 1996; 94:842–847.

[56] De Burgh Daly M. Interactions between respiration and circulation. In: Cherniack NS, Widdicombe JG, eds. Handbook of Physiology, Section 3: The Respiratory System, Vol II: Control of Breathing, Part 2. Bethesda, *Md: American Physiological Society*; 1986:529-594.

[57] Shykoff BE, Naqvi SSJ, Menon AS, Slutsky AS, “Respiratory sinus arrhythmia in dogs: effects of phasic afferents and chemo stimulation,” *J Clin Invest.*, 1991; 87:1621-1627.

[58] Horner RL, Brooks D, Kozar LF, Gan K, Phillipson EA, “Respiratory-related heart rate variability persists during central apnea in dogs: mechanisms and implications,” *J Appl Physiol*, 1995; 78:2003-2013.

[59] Fouad FM, Tarazi RC, Ferrario CM, Fighaly S, Alicandri C, “Assessment of parasympathetic control of heart rate by a noninvasive method,” *Am J Physiol.*, 1984; 246:H838-H842.

[60] Hayano J, Sakakibara Y, Yamada A, Yamada M, Mukai S, Fujinami T, Yokoyama K, Watanabe Y, Takata K, “Accuracy of assessment of cardiac vagal tone by heart rate variability in normal subjects,” *Am J Cardiol.*, 1991; 67:199-204.

[61] van Ravenswaaij-Arts CMA, Kollee LAA, Hopman JCW, Stoelinga GBA, van Geijn HP, “Heart rate variability,” *Ann Intern Med*, 1993; 118:436-447.

[62] Appel ML, Berger RD, Saul JP, Smith JM, Cohen RJ, “Beat to beat variability in cardiovascular variables: noise or music?,” *J Am Coll Cardiol*, 1989; 14:1139-1148.

[63] Malliani A, Pagani M, Lombardi F, Cerutti S, “Cardiovascular neural regulation explored in the frequency domain,” *Circulation*, 1991; 84:482-492.

[64] Saul JP, Berger RD, Chen MH, Cohen RJ, “Transfer function analysis of autonomic regulation, II: respiratory sinus arrhythmia,” *Am J Physiol*, 1989; 256:H153-H161.

[65] Saul JP, Berger RD, Albrecht P, Stein SP, Chen MH, Cohen RJ, “Transfer function analysis of the circulation: unique insights into cardiovascular regulation,” *Am J Physiol*, 1991; 261:H1231-H1245.

[66] Blanco-Velasco, M.; Weng, B.; Barner, K.E, “ECG signal denoising and baseline wander correction based on the empirical mode decomposition,” *Comput. Biol. Med.,* 2008, 38, 1–13.

[67] Coast, Douglas A., et al. "An approach to cardiac arrhythmia analysis using hidden Markov models," *IEEE Trans. biomed. Eng.*, 37.9 (1990): 826-836.

[68] S. H. Oguz, M. H. Asyali, “A morphology based algorithm for baseline wander elimination in ECG records,” *Proceedings of the 1992 International Conference Biomedical Engineering*, Auguest 1992, Instanbul, Turkey, pp. 157-160.

[69] Van Alsté JA, van Eck W, Herrmann OE, “ECG Baseline wander reduction using linear phase,” *Comput Biomed Res*, 1986, 19: 417-427.

[70] Laguna P, Jane R, Caminal P, “Adaptive filtering of ECG baseline wander,” *14th Annu Int Conf IEEE Eng Med Biol Soc,* 1992, 2, 508–509.

[71] Thakor NV, Zhu VS, “Application of adaptive filtering to ECG analysis: noise cancellation and arrhythmia detection,” *IEEE Trans Biomed. Eng.*, 38:785–793, 1991.

[72] O. Sayadi and M. B. Shamsollahi, “Multiadaptive bionic wavelet transform: Application to ECG denoising and baseline wandering reduction,” *EURASIP J. Adv. Signal Process.*, vol. 2007, pp. 1–11, 2007.

[73] F. Portet, “P wave detector with PP rhythm tracking: evaluation in different arrhythmia contexts,” *Physiol. Meas.*, vol. 29, no. 1, pp. 141-155, 2008.

[74] Ziarani AK, Konrad A, “A Nonlinear Adaptive Method of Elimination of Power Line Interference in ECG Signals,” *IEEE Trans Biomed. Eng.*, 2002, 49: 540–547.

[75] “American National Standard for Ambulatory Electrocardiographs,” Association for the Advancement of Medical Instrumentation, *ANSI/AAMI*, EC38-1994, 1994.

[76] T. Young, P. Peprad, M. Palta, K. M. Hla, L. Finn, B. Morgan, and J. Skatrud, “Population-based study of sleep breathing as a risk factor for hypertension,” *Arch. Intern. Med.*, vol. 157, pp. 1746-1752, 1997.

[77] V.X. Afonso, W.J. Tompkins, T.Q. Nguyen, K. Michler, S. Luo, “Comparing stress ECG enhancement algorithms,” *IEEE Eng. Med. Biol. Mag.,* 15 (3) (1996), 37–44.

[78] J.M. Leski, N. Henzel, “ECG baseline wander and powerline interference reduction using nonlinear filter bank,” *Signal Process*, 35 (4) (2004), 781–793.

[79] S. Iravanian, L. Tung, “A novel algorithm for cardiac biosignal filtering based on filtered residue method,” *IEEE Trans. Biomed. Eng.*, 49 (11) (2002), 1310–1317.

[80] J.M. Leski, “Robust weighted averaging,” *IEEE Trans. Biomed. Eng.*, 49 (8) (2002) 796–804.

[81] P.E. Tikkanen, “Nonlinear wavelet and wavelet packet denoising of electrocardiogram signal,” *Biol. Cybern.*, 80 (4) (1999), 259–267.

[82] C.Y.-F. Ho, B.W.-K. Ling, T.P.-L. Wong, A.Y.-P. Chan, P.K.-S. Tam, “Fuzzy multi-wavelet denoising on ECG signal,” *Electron. Lett.*, 39 (16) (2003), 1163–1164.

[83] E. Ercelebi, “Electrocardiogram signals de-noising using lifting-based discrete wavelet transform,” *Comput. Biol. Med.*, 34 (6) (2004), 479–493.

[84] S. Poornachandra, N. Kumaravel, “Hyper-trim shrinkage for denoising of ECG signal,” *Digital Signal Process,* 15 (3) (2005), 317–327.

[85] V. Almenar, A. Albiol, “A new adaptive scheme for ECG enhancement,” *Signal Process*, 75 (3) (1999), 253–263.

[86] J.S. Paul, M.R.S. Reddy, J. Kumar, “Data processing of stress ECG using discrete cosine transform,” *Comput. Biol. Med.*, 28 (6) (1998), 639–658.

[87] A.K. Barros, A. Mansour, N. Ohnishi, “Removing artifacts from electrocardiographic signals using independent components analysis,” *Neurocomputing*, 22 (1998), 173–186.

[88] Sun, P et al., "An improved morphological approach to background normalization of ECG signals," *IEEE Trans Biomed. Eng.*, 50.1 (2003), 117-121.

[89] T.Y. Ji, Z. Lu, Q.H. Wu, and Z. Ji, "Baseline normalization of ECG signals using empirical mode decomposition and mathematical morphology," *Electron. Lett.*, vol.44, no.2, pp.82-83, 2008.

[90] J.A. Van Alste, T.S. Schilder, “Removal of base-line wander and power-line interference of the ECG by an efficient FIR filter with a reduced number of taps,” *IEEE Trans. Biomed. Eng.*, 32 (1985), 1052–1060.

[91] S. Hargittai, “Efficient and fast ECG baseline wander reduction without distortion of important clinical information,” *Comput. Cardiol.*, 35 (2008), 841–844.

[92] J.R. Gradwohl, E.W. Pottala, M.R. Horton, J.J. Bailey, “Comparison of two methods for removing baseline wander in the ECG,” *Comput. Cardiol.*, pp. 493–496, 1998.

[93] Z. Zhidong, L. Juan, “Baseline wander removal of ECG signals using empirical mode decomposition and adaptive filter,” in *Proceedings of International Conference on Bioinformatics and Biomedical Engineering*, June 2010, pp. 1–3.

[94] M. Dai, S.L. Lian, “Removal of baseline wander from dynamic electrocardiogram signals,” in *Proceedings of 2nd International Congress on Image and Signal Processing*, October 2009, pp. 1–4.

[95] M. A. Mneimneh, E. E. Yaz, M. T. Johnson, and R. J. Povinelli, “An adaptive kalman filter for removing baseline wandering in ECG signals,” in Proc. *Comput. Cardiol.*, pp. 253-256, 2006.

[96] Agrawal, Sakshi, and Anubha Gupta, "Fractal and EMD based removal of baseline wander and powerline interference from ECG signals," *Comput. Biol. Med.*, 43.11 (2013): 1889-1899.

[97] Y. Lian, and Y. JH, “The reduction of noises in ECG signal using a frequency response masking based FIR filter,” *IEEE Int. Workshop on Biomed. Circ. Sys.*, vol. 2, pp. 17-20, 2004.

[98] Haung NE, Shen Z, Long SR, Wu ML, Shih HH, et al., “The Empirical Mode Decomposition and Hilbert Spectrum for Nonlinear and Non-stationary Time Series Analysis,” *Proc. R. Soc. London Ser.*, A 454:903-95, 1998a.

[99] D.H. Zhang, “Wavelet approach for ECG baseline wander correction and noise reduction,” in *Proceedings of 27th Annual IEEE International Conference of Engineering in Medicine and Biology Society*, September 2005, pp. 1212–1215.

[100] T. Jing-tian, Z. Qing, T. Yan, L. Bin, Z. Xiao-kai, “Hilbert-Huang Transform for ECG De-Noising,” in *Proceedings of 1st International Conference on Bioinformatics and Biomedical Engineering*, July 2007, pp. 664–667.

[101] G. Berntson, J. Cacioppo, and K. Quigley, “Respiratory sinus arrhythmia: Autonomic origins, physiological mechanisms, and psychophysiological implications,” *Psychophysiology*, vol. 30, no. 2, pp. 183–196, 1993.

[102] D. Widjaja, “Cardiorespiratory dynamics: algorithms and application to mental stress monitoring,” PhD thesis, Faculty of Engineering, KU Leuven, 2015.

[103] G. Hahn, I. Ŝipinková, F. Baisch, and G. Hellige, “Changes in the thoracic impedance distribution under different ventilatory conditions*,” Physiol Meas.*, vol. 16, no. 3A, pp. A161-A173, Aug. 1995.

[104] R. Pallas-Areny, J. Colominas-Balague, and F. J. Rosell, “The effect of respiration-induced heart movements on the ECG,” *IEEE Trans. Biomed. Eng.*, vol. 36, no. 6, pp. 585-590, Jun. 1989.

[105] Narkiewicz K, Somers VK, “Sympathetic nerve activity in obstructive sleep apnoea,” *Acta Physiol Scand*, 2003; 177: 385–390.

[106] Dingli K, Assimakopoulos T, Wraith PK, Fietze I, Witt C, Douglas NJ, “Spectral oscillations of RR intervals in sleep apnoea/hypopnoea syndrome patients,” *Eur Respir J*, 2003; 22, pp. 943–950.

[107] Task force of the European Society of Cardiology and the North American Society of Pacing and Electrophysiology, “Heart rate variability. Standards of measurement, physiological interpretation, and clinical use,” *Circulation*, 1996; 93, pp. 1043–1065.

[108] L. Bacharova, E. Triantafyllou, C. Vazaios, I. Tomeckova, I. Paranicova, and R. Tkacova, “The effect of obstructive sleep apnea on QRS complex morphology,” *J Electrocardiol*, 2015, 45, pp. 164-170.

[109] Feldman, M, “Time-varying vibration decomposition and analysis based on the Hilbert transform,” *J. Sound Vib.*, 2006, 295, 3–5, pp. 518–530.

[110] S. Braun, M. Feldman, “Decomposition of non-stationary signals into varying time scales: Some aspects of the EMD and HVD methods,” *Mech. Syst.d Signal Process*., 25 (2011), pp. 2608–2630.

[111] Moody, G. B., Mark R. G., “The Impact of the MIT-BIH Arrhythmia Database,” *IEEE Eng. Med. Biol. Mag.*, 20 (3), 45-50, 2001.

[112] Alan V. Oppenheim, Ronald W. Schafer, “Homomorphic analysis of speech,” *IEEE Trans. Audio Electroacoust,*, vol. AU-16, no. 2, pp. 221-226, June 1968.

[113] Alan V. Oppenheim, Ronald W. Schafer, and Thomas G. Stockham, “Nonlinear filtering of multiplied and convolved signals,” *IEEE Trans. Audio Electroacoust.*, vol. AU-16, No. 3, pp. 437-466, Sept. 1968.

[114] I. S. N. Murthy, M. R. Rangaraj, K. J. Udupa and A. K. Goyal, “Homomorphic analysis and modeling of ECG signals,” *IEEE Trans. Biomed. Eng.*, vol. BME-26, no. 6, pp. 830-844, June 1979.

[115] A. L. Goldberger, L. A. N. Amaral, L. Glass, J. M. Hausdorff, P. C. Ivanov, R. G. Mark, J. E. Mietus, G. B. Moody, C. K. Peng, and H. E. Stanley, “Physiobank, physiotoolkit, and physionet: components of new research resource for complex physiologic signals,” *Circulation*, vol. 101, no. 23, pp. e215-e220, 2000.

[116] J. Pan, and W. J. Tompkins, “A Real-Time QRS Detection Algorithm,” *IEEE Trans. Biomed. Eng.*, vol. 32, no. 3, March 1985.

[117] M. Lagerholm, C. Peterson, G. Braccini, L. Edenbrandt, and L. Sornmo, “Clustering ECG complexes using Hermite functions and self-organizing maps,” *IEEE Trans. Biomed. Eng.*, vol. 47, pp. 838–848, July 2000.

[118] H. Haraldsson , L. Edenbrandt, and M. Ohlsson, "Detecting acute myocardial infarction in the 12-lead ECG using Hermite expansions and neural networks", *Artif. Intell. Med.*, vol. 32, pp.127 -136, 2004.

[119] T. H. Linh, S. Stanislaw, and M. Stodolski, “On-Line Heart Beat Recognition Using Hermite Polynomials and Neuro-Fuzzy Network,” *IEEE Trans. Instrum. Meas.*, vol. 52, no. 4, pp. 1224-1231, 2003.

[120] Lin, L. I., “A concordance correlation coefficient to evaluate reproducibility,” *Biometrics*, 45, pp. 255–268, 1989.

[121] J. Coleman, “Complications of snoring, upper airway resistance syndrome, and obstructive sleep apnea syndrome in adults,” *Otolaryngol. Clin. North Amer.*, vol. 32, pp. 223-234, 1999.

[122] F. J. Neito, T. B. Young, B. K. Lind, E. Shahar, J. M. Samet, S. Redline, R. B. D’Agostino, A. B. Newman, M. D. Lebowitz, and T. G. Pickering, “Association of sleep disordered brathing, sleep apnea, and hypertension in a large community-based study,” *J. Amer. Med. Assoc.*, vol. 283, pp. 1829-1836, 2000.

[123] J. Suykens and J. Vandewalle, "Least Squares Support Vector Machine Classifiers," *Neural Process. Lett.*, vol. 9, no. 3, pp. 293-300, 1999.

[124] C.M. Bishop, Neural Networks for Pattern Recognition, Oxford University Press, Walton Street, Oxford, 1995.

[125] C. H. Wan, L. H. Lee, R. Rajkumar and D. Isa, "A hybrid text classification approach with low dependency on parameter by integrating K-nearest neighbor and support vector machine*", Expert Syst. Appl.*, vol. 39, no. 15, pp. 11880 -11888, 2012.

[126] U. Orhan, M. Hekim, and M. Ozer, “EEG signals classification using the K-means clustering and a multilayer perceptron neural network model,” *Expert Syst. Appl.*, 38 (2011), pp. 13475-13481.

[127] G. Cybenco, “Approximation by superposition of a sigmoidal function,” *Math. Control Signals Syst.*, 2 (1989), pp. 303–314.

[128] K. Hornik, M. Stinchcombe, H. White, “Multilayer feed forward networks are universal approximators,” *Neural Netw.*, 2 (1989), pp. 359–366.

[129] B. D. Ripley, Pattern Recognition and Neural Networks. Cambridge, U.K.: Cambridge Univ. Press, 1996.

[130] R. Kohavi, “A study of cross validation and bootstrap for accuracy estimation and model selection,” in *Proc. 14th Int. Joint Conf. Artificial Intelligence*, 1995, pp. 1137–1143.

[131] J. V. Marcos et al., “Assessment of four statistical pattern recognition techniques to assist in obstructive sleep apnea diagnosis from nocturnal oximetry,” *Med. Eng. Phys.*, vol. 31, no. 8, pp. 971–978, Oct. 2009.

[132] D. Alvarez et al., “Multivariate analysis of blood oxygen saturation recordings in obstructive sleep apnea diagnosis,” *IEEE Trans. Biomed*. Eng., vol. 57, no. 12, pp. 2816–2824, Jul. 2010.

[133] D. S. Morillo and N. Gross, “Probabilistic neural network approach for the detection of SAHS from overnight pulse oximetry,” *Med. Biol. Eng. Comput*., vol. 51, no. 3, pp. 305–315, Nov. 2013.

[134] R. K. Begg, M. Palaniswami, and B. Owen, “Support vector machines for automated gait classification,” *IEEE Trans. Biomed. Eng*., vol. 52, no. 5, pp. 828-838, May 2005.

[135] C. M. Travieso et al., “Building a Cepstrum-HMM kernel for Apnea identification,” *Neurocomputing*, vol. 132, pp. 159-165, May 2014.

[136] T. Hastie, R. Tibshirani, and J. J. H. Friedman, The Elements of Statistical Learning. New York, NY, USA: Springer, 2001, vol. 1.

[137] Derryberry, D. R., Schou, S. B., & Conover, W. J., “Teaching rank based tests by emphasizing structural similarities to corresponding parametric tests,” *Journal of Statistics Education*, 18(1), pp. 1–19, 2010.

[138] Silverthorn, D., Johnson, B., Ober, W., Garrison, C., and Silverthorn, A., “Human Physiology: An Integrated Approach,” Pearson Education, 2013.

[139] Thibodeau GA, Patton KT. Anatomy & physiology, ed 5, St Louis, 2003, Mosby.

[140] Heart, Wikipedia [Online]. Available: https://en.wikipedia.org/wiki/Heart.

[141] Einthoven’s triangle, Available: https://en.wikipedia.org/wiki/Einthoven’s_triangle.

[142] J. M. Robinson, ECG Interpretation Made Incredibly Easy, 5th ed., Lippincott Williams & Wilkins, China, 2011.

[143] Malliani, A., Pagani, M., Lombardi, F., and Cerutti S., “Cardiovascular neural regulation explored in the frequency domain,” *Circulation*, 84, 2 (1991), 482–492.

[144] Vaishnav, S., Stevenson, R., Marchant, B., Lagi, K., Ranjadayalan, K., and Timmis, A. D., “Relation between heart rate variability early after acute myocardial infarction and long-term mortality,” *Am J Cardiol*, 73, 9 (1994), 653–657.

[145] Kleiger, R. E., Miller, J. P., Bigger Jr, J. T., and Moss, A. J., “Decreased heart rate variability and its association with increased mortality after acute myocardial infarction,” *Am J Cardiol*, 59, 4 (1987), 256–262.

[146] Acharya, U. R., Joseph, K. P., Kannathal, N., Lim, C. M., and Suri, J. S., “Heart rate variability: a review,” Medical and Biological Engineering and Computing, 44, 12 (2006), 1031–1051.

[147] Task Force of The European Society of Cardiology and The North American Society of Pacing and Electrophysiology, “Heart rate variability: Standards of measurement, physiological interpretation, and clinical use,” *Eur Heart J*, 17, 3 (1996), 354–381.

[148] Reyes del Paso, G. A., Langewitz, W., Mulder, L. J., Roon, A., and Duschek, S., “The utility of low frequency heart rate variability as an index of sympathetic cardiac tone: a review with emphasis on a reanalysis of previous studies,” *Psychophysiology*, 50, 5 (2013), 477–487.

[149] García-González, M., Vázquez-Seisdedos, C., and Pallàs- Areny, R., “Variations in breathing patterns increase low frequency contents in HRV spectra,” *Physiol. Meas.*, 21, 3 (2000), 417– 423.

[150] Julien, C., “The enigma of Mayer waves: facts and models,” *Cardiovasc Res*, 70, 1 (2006), 12–21.

[151] Eckberg, D. L., “Sympathovagal balance: a critical appraisal,” *Circulation*, 96, 9 (1997), 3224–3232.

[152] Yildiz, M., and Ider, Y., “Model based and experimental investigation of respiratory effect on the HRV power spectrum,” *Physiol. Meas.*, 27, 10 (2006), 973–988.

[153] Berntson, G., Cacioppo, J., and Quigley, K., “Respiratory sinus arrhythmia: Autonomic origins, physiological mechanisms, and psychophysiological implications,” *Psychophysiology*, 30, 2 (1993), 183–196.

[154] Berntson, G. G., Bigger Jr, J. T., Eckberg, D. L., Grossman, P., Kaufmann, P. G., Malik, M., Nagaraja, H. N., Porges, S. W., Saul, J. P., Stone, P. H., and Van Der

Molen, M. W., “Heart rate variability: Origins, methods, and interpretive caveats,” *Psychophysiology*, 34, 6 (1997), 623–648.

[155] R. W. Schafer and L. R. Rabiner, “A digital signal processing approach to interpolation,” *Proc. IEEE*, vol. 61, pp. 692–702, 1973.

[156] Hemant Sharma, and K. K. Sharma, "Baseline wander removal of ECG signals using Hilbert vibration decomposition," *Electron. Lett.,* 51, no. 6 (2015), pp. 447-449.

[157] Hemant Sharma, K. K. Sharma, and Om Lata Bhagat, "Respiratory rate extraction from single-lead ECG using homomorphic filtering," *Comput. Biol. Med.,* 59 (2015): 80-86.

[158] Hemant Sharma, K. K. Sharma, “An algorithm for sleep apnea detection from single-lead ECG using Hermite Basis functions,” *Comput. Biol. Med.,* vol. 77, pp. 116-124, 2016.

[159] Schmidt, Marcus, et al. "ECG derived respiration: comparison of time-domain approaches and application to altered breathing patterns of patients with schizophrenia." *Physiological Measurement* 38.4 (2017): 601.

[160] Charlton, P.H., Bonnici, T., Tarassenko, L., Clifton, D.A., Beale, R. and Watkinson, P.J., “An assessment of algorithms to estimate respiratory rate from the electrocardiogram and photoplethysmogram,” *Physiol. Meas.*, *37*(4), p.610, 2016.

[161] P. Charlton, T. Bonnici, L. Tarassenko, J. Alastruey, D. A Clifton, R. Beale, and P. J Watkinson, “Extraction of respiratory signals from the electrocardiogram and photoplethysmogram: technical and physiological determinants,” *Physiol. Meas.*, vol. 38, pp. 669-690, 2017.

[162] Penzel, Thomas, et al. "Modulations of Heart Rate, ECG, and Cardio-Respiratory Coupling Observed in Polysomnography." *Frontiers in physiology* 7 (2016).

[163] Orphanidou, Christina. "Derivation of respiration rate from ambulatory ECG and PPG using Ensemble Empirical Mode Decomposition: Comparison and fusion." *Computers in biology and medicine* 81 (2017): 45-54.

[164] Bordes, Antoine, et al, "Fast kernel classifiers with online and active learning," *Journal of Machine Learning Research,* 6, Sep (2005): 1579-1619.

[165] Suykens, Johan AK, et al, "Weighted least squares support vector machines: robustness and sparse approximation," *Neurocomputing,* 48.1 (2002): 85-105.

[166] Jiao, Licheng, Liefeng Bo, and Ling Wang, "Fast sparse approximation for least squares support vector machine," *IEEE Trans. Neural Netw.,* 18.3 (2007): 685-697.

[167] Lecture notes “K Nearest Neighbor”, Available at:
http://www.csd.uwo.ca/courses/CS9840a/Lecture2_knn.pdf

PUBLICATIONS FROM THE WORK

Based on the research carried out, following papers have been published/accepted/submitted for publication in various journals and conferences:

International Journals – Published

1. Hemant Sharma, and K. K. Sharma, "Baseline wander removal of ECG signals using Hilbert vibration decomposition," *Electronics Letters,* 51, no. 6 (2015): 447-449.
2. Hemant Sharma, K. K. Sharma, and Om Lata Bhagat, "Respiratory rate extraction from single-lead ECG using homomorphic filtering," *Computers in Biology and Medicine, Elsevier*, 59 (2015): 80-86.
3. Hemant Sharma, K. K. Sharma, “An algorithm for sleep apnea detection from single-lead ECG using Hermite Basis functions,” *Computers in Biology and Medicine, Elsevier*, vol. 77, pp. 116-124, 2016.

International Journals - Under Revision

4. Hemant Sharma, K. K. Sharma, “ECG-derived respiration using Hermite expansion,” *Biomedical Signal Processing and Control, Elsevier*, (*revision submitted*).

International Conferences – Published/ Accepted for Publication

5. Hemant Sharma, K. K. Sharma, “Application of Iterated Hilbert Transform for Deriving Respiratory Signal from Single-lead ECG,” in *India International Conference on Information Processing, IEEE*, New Delhi, 2016.

International Journals - Under Preparation

6. Hemant Sharma, K. K. Sharma, “Sleep apnea screening based on HRV and ECG-derived respiration,” is under preparation.